# OPTICAL STUDIES OF SOME IMPACT PHENOMENA AND SURFACE HARDNESS MEASUREMENTS

Thesis presented for the degree of

Doctor of Philosophy

in the

University of London

by

V.R.HOWES

April 1955

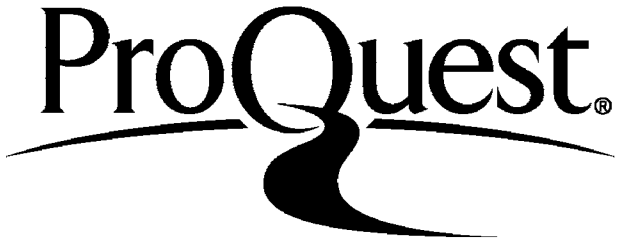

## ABSTRACT

An introduction to the phenomena of pressure crack figures is given with special reference to static-impact figures produced on glass and diamond. The optical techniques and the apparatus used are described, including the Interferometric technique used for the detection and measurement of the surface distortions for crack figures obtained first on glass, and then on diamond. The spherical impactors used were of steel (for glass), tungsten carbide and diamond (mainly for diamond).

A study is made of the fracture strength properties of ten different types of optical glass and the results are compared with other properties of the glasses, including measurements of their surface hardnesses obtained by an abrading method described in the Appendix.

Orientated crack figures have been produced on three different faces of diamond, the shapes being hexagonal on the octahedral and the dodecahedral faces, and square on the cubic face. For the octahedral and a cubic face, the development of these figures is studied as the load is gradually increased; and the mechanism of the crack formation and the accompanying cracking effects within the body of the crystal are discussed in terms of easy cleavage and shattering, respectively. It is found that the octahedral face is definitely the least resistant to fracture by this method, the cubic face appearing

to be most resistant: also the critical stresses involved are found to be considerably less than a theoretically calculated value which indicates some form of flaw distribution over the surface analogous to the Griffith cracks for glass.

It has also been seen that the octahedral face of diamond can be cracked in this way by using Tungsten Carbide or Sapphire balls, although in the latter case the tip of the ball was shattered by the occurrence of multiple slip.

Both for glass and diamond, the observations obtained from the interferograms of the surface distortions is considered to offer strong evidence for the existence of micro plastic flow. No signs of micro slip could be detected in the studies on diamond except possibly in connection with the crystallographic shattering which occurred internally for one test on the octahedral stone.

CONTENTS : CHAPTERS

CONTENTS : SECTIONS

# CHAPTER I

# INTRODUCTION

## 1.1 Hardness

Ring cracks were first produced on glass in elastic deformation experiments, based upon the theory of Hertz (1881), where the elastic limit was reached - and the onset of fracture was used by Hertz in a definition of hardness.

The definitions of Hardness are many and varied involving a large number of different physical properties, but those involving mechanical properties can be separated into two groups; namely Fracture Hardness and Deformation Hardness. The concept of Hardness was first dealt with by mineralogists, and they were most interested in the first of these, where the surface of the material may be broken because the stresses set up exceed the breaking stress under the conditions of the test. The first type of test employed was the ability of one material to scratch another (the point of loading moving so that the point of rupture becomes a scratch), and by this method Mohs (1722) classified many materials using ten minerals as standard; these were numbered one (talc) to ten (diamond), and were chosen so that each would scratch all those below it in the scale.

The most common type of test in the Deformation Hardness group is the Static Indentation test. Used most commonly on metals, these tests have been discussed by O'Neill (1934), who maintains that recoverable elastic deformations should be

included when hardness measurements are based on an indentation technique. However, the definition given by Hertz treats hardness as essentially related to the irreversible phenomena occurring when the elastic limit of the material is exceeded in any part of the applied stress system.

The latter definition is certainly the most satisfactory for brittle materials where the irreversibility occurs suddenly in the form of fracture. It is however to be noted that in recent years, micro indentation tests involving plastic deformation, have been done by Taylor (1949) on several minerals and on a selection of optical glasses.

Lastly, there are some cases where it is unimportant for practical purposes whether microscopic fractures or simple deformation takes place. The mechanical wear properties of surfaces of materials are usually measured by Abrasive Hardness. This type of hardness measurement is more of an empirical nature and there are consequently many types of tests. Two are to be mentioned here, the Grinding hardness of materials as measured by the amount removed from the surface per unit time under specified experimental conditions. This method has been used on different optical glasses by Willott (1950) and on the different faces of diamond by Wilks (1952) who used a micro method. The other method of measuring the abrasion hardness is by measuring optically the effect on the surface of a material upon which has been dropped quantities of an abrasive under specified experimental conditions. This method has been

used on metal surfaces by Chalmers (1941), and on different plastics and glass by Starkie (1942): using this method with an improvement in the optical measurement technique, the author gives in the Appendix results obtained for a selection of well known optical glasses. This type of test gives an indication of the surface hardness properties of materials.

## 1.2 Theory of Hertz

The Theory of the elastic deformation of two bodies in contact, given by Hertz in 1881, is fundamental to the whole problem of fracturing of brittle materials under pressure with a spherical impactor.

He considers the general case where, by neglecting small quantities of higher order, the surfaces of the bodies near the point of contact can be represented by two homogeneous quadratic functions. His method is inductive, beginning with a definition of a function which can be regarded, referring to the theory of potential, as the potential of an infinitely flattened ellipsoid which would just fill the surface of pressure.

The results of his work will be considered here simply for the special case when one of the surfaces is a sphere of r radius and the other is a plane. If the sphere is subject to a normal load P, its centre will approach the plane by a distance x, and it will be in contact with the plane in a circle of radius a where these quantities are given by

$$x = \left[ \frac{9}{16} \frac{P^2}{r} \left( \frac{1 - \sigma_1^2}{E_1} + \frac{1 - \sigma_2^2}{E_2} \right)^2 \right]^{1/3}$$

$$a = \left[\frac{3}{4} P \left(\frac{1-\sigma_1^2}{E_1} + \frac{1-\sigma_2^2}{E_2}\right)\right]^{1/3}$$

where E and $\sigma$ are the Youngs modulus and the Poisson ratio, the suffices referring to the two materials involved. The average pressure applied and the maximum pressure at the centre of the circle of contact are given by:-

$$p = \frac{P}{\pi a^2} \quad \text{and} \quad p_o = \frac{3}{2}\frac{P}{\pi a^2} \quad \text{respectively.}$$

Timoshenko (1934) derives the value of the maximum shearing stress, which is below the centre of the circle of contact, as 0.31 $p_o$ (for $\sigma \sim 0.3$); the maximum tensile stress (MTS) is at the perimeter of the circle of contact and is given by

$$(\text{MTS}) = \frac{1-2\sigma}{3} p_o$$

It is the shear stress which causes the onset of plastic deformation by which an indentation is made in the material, whereas in the case of brittle materials it is by tensile stress that fracture or cracking occurs. The tensile stresses, within the stress system in the body having the plane face, decreases least rapidly, from the maximum value around the perimeter of the area of contact, in a direction downwards from the surface and away from the region of contact, along a cone surface. The ring cracks occurring on glass surfaces are the surface

manifestation of the 'Hertzian cone crack' penetrating into the glass.

Hertz, from his theoretical work, gave as a definition of hardness that it was to be measured by the normal pressure which must act at the centre of a circular surface of pressure in order that in some point of the body the stress may reach the limit consistent with perfect elasticity.

1.3 Survey of the phenomena on glass

Auerbach (1902) made the first thorough investigation of the validity of Hertz's Theory. He did a series of experiments on the contact of spherical glass lenses with a plane surface, using the technique of observing, through a microscope, the contact area between the faces as the load was increased. He found that in the elastic deformations occurring there was agreement with the theory: for one value of the lens radius ( $r$ ), the value of $P/a^3$ was constant. However, in an extension of the experiments for the breaking of glass, by increasing the load until a ring crack formed, he found that the theoretical results were not fulfilled: in the tests, the glass breaking under uniform tensile stress, the value of $P_o$ should be constant where the value of $r$ was varied, but this was found not to be the case.

Preston (1926) discussed the formation of ring cracks theoretically concluding firstly, in general agreement with Auerbach that the cracks were formed by tensile stress only acting at the surface of the glass, and secondly, that the

apparent failure of the Hertz theory was due to the breaking of the glass from nuclei or weak points on the surface, which accounted for the dependance of strength on the scale of the experiment as found in the results of Auerbach, but not recognised by him. As Haward (1949) summaries this conclusion 'According to this view the whole phemonenon is simply a particular aspect of a strength-area relation.'

Such a relation was investigated by Bailey (1939), who proposed a theory relating to the measured strength of a glass specimen to the area of the surface under stress, based upon bending tests on glass rods, also by Preston (1945), who estimated the maximum tensile stress, according to the Hertzian formula, which was required to fracture glass in contact with loaded balls of differing diameter. His results show that the critical stress increases considerably as the size of the ball decreases, until for very small diameter balls fracture strengths are obtained comparable to that of glass fibres.

The concept of weak points and an area-strength relationship is based fundamentally upon the classical work of Griffith (1920) who put forward a flaw theory for the strength of glass in the massive and fibrous states. He postulated that the theoretical tensile strength (derived from the heat of vaporization) is very much greater than that found in practice because of a distribution of flaws (or Griffith cracks) for the glass. Using Inglis' calculation (1913) of the stress distribution around an elliptical hole in a stressed plate, by regarding the crack as a very flat elliptical hole Griffith

derived the length of the hypothetical cracks necessary to reduce the theoretical strength of glass to the experimental value. He went on to obtain for a thin glass plate, by considerations of potential energy involving the surface energy, the equation:-

$$T_c = \sqrt{\frac{2\alpha E}{\pi C}} \qquad \text{(see Orowan 1948-9)}$$

where $T_c$ is the critical value of applied tensile stress for fracture to occur, and $\alpha$, E and C are respectively the specific surface energy, the Youngs modulus, and the length of the surface Griffith cracks. Griffith verified his equation experimentaly, and further support was obtained from experiments on the effects of edge and surface treatment.

Optical studies of ring crack phenomena on glass have been carried out by Raman (1920 and 1926) and by Tolansky and Howes (1954). Raman's work was on percussion marks obtained dynamically by impacting a glass plate with steel balls. He has photographed the silhouette of the Hertzian cone going into the glass from the surface by observing through the side face of the block of glass, and also shows a plan photograph of the ring crack in which circular interference fringes can be seen in the Hertzian cone crack. In the later paper he has studied the accompanying surface distortion for these percussion ring cracks interferometrically, and has shown that there is a smooth pile up to the crack from the outisde, of approximately 2.5 microns in height; a sudden

discontinuity occurring at the crack itself to a flat depressed area within the crack. This depression is 'a mystery', but Raman mentions the possibility that 'at the instant the crack starts part of the material which has shifted its position outwards under the intense compressive forces remains outside and is unable to return.'

The second reference is to the publication of the work described in Chapter 4 of this Thesis. A quantitative study of the distortions for static ring cracks was made. The height displacements above the undisturbed level were found to be of the order of 1000 A units, thus being 25 times less than those found by Raman for percussion ring cracks (the interferometric method of making quantitative measurements was very much more accurate).

## 1.4 Survey of the phenomena on crystals

Both pressure figures and percussion figures have been produced and studied on Quartz by Schubnikow and Zinserling (1932). They take the form of rounded distinctive shapes for the different faces of the crystal and can be used to detect different faces in a similar way as etch figures are used. The mechanism by which the cracking takes place is that of twinning.

Schuler and Dimpker (1935) did some experiments on the strength of hard crystals. They used spheres and ball ended cones of varying radii, doing static impact tests with them on plates of the same material to find the critical loads for

initial mutual cracking and for final mutual smashing. They obtained a proportionality between the critical pressures and the radii of curvature of the impactor in both cases for synthetic sapphire, this being contrary to the Hertz Theory (where the relation should be $P_c \propto r^2$ ). A photograph is shown of an initial crack on the sapphire plate, and also there is a picture of a crack figure produced on a quartz plate. Their technique did not allow for the measuring of the areas of contact so that no stress determination was possible. They carried out a single test on a diamond plate using a diamond ball ended cone of radius 0.18 mm. at the tip. The initial cracking here occurred at 25 kgm. load, the appearance they describe as being similar to that of the crack on the quartz. At 14.4 kgm. the tip of the cone broke off symmetrically - this value being about ten times greater than the equivalent value for sapphire using an impactor of the same radius. The authors also mention that slip lines occurred on the synthetic sapphire at initial cracking, which was in complete contrast to the diamond test, where no signs of slip were evident whatsoever.

Percussion marks have long been known as familiar features on the faces of diamonds found in coastal deposits. Williams (1932) states that the cracks generally appear on the surface of the diamond as halfmoons, although in many cases the fracture takes the form of a complete circle, the cracks penetrating for a considerable depth. He says that they appear only when the boulders and associated diamonds have been battered about on some ocean shore line; however

in a recent paper, Tolansky and Halperin (1954) have shown that natural hexagon features on the natural octahedral face of diamonds from mines have exactly similar surface distortion characteristics, detected interferometrically, as were found by Tolansky and Howes (1954) for ring cracks on glass - this leading to the conclusion that the features were in fact percussion or pressure figures on the face of the diamonds.

Finally experimentally, a full investigation of the artificial production of static pressure crack figures on the three different crystallographic faces of diamonds has been carried out by Tolansky and Howes (1955); this being the publication of the work described in Chapters 6, 7 and 8 of this Thesis.

From the theoretical point of view, Orowan (1948-9) states that a detailed calculation has shown that the cleavage type of crack, occurring for a crystal with cleavage planes such as diamond gives the same fracture condition, with only slightly different values of the numerical factors, as the elliptical crack of Griffith.Smekal (1927) proposed that, in the case of crystals; the discrepancy between the molecular cohesion and the observed strength would be a consequence, not of accidental flaws, but of a universal 'block structure' of crystalline matter; however subsequently an overwhelming amount of evidence accumulated against this hypothesis.

In the light of modern crystallographic theory, it may well be that the flaws of Griffith, in the case of crystals, are

occurrences of vacant-sites in the crystal lattice or possibly the manifestation of sessile dislocation within the crystal structure or on the surface.

1.5 Diamond properties and structure.

Diamond is the hardest material known, the homopolar forces holding the carbon atoms together being very strong. It occurs in Octahedral, Cubic and Dodecahedral forms and is classified in the cubic system. It has the lowest compressibility of all substances and has a very small Thermal expansion. Up to the present, diamonds have been classified into two types: Robertson, Fox and Martin (1934) showed that a majority of diamonds exhibited optical birefringence and infra-red activity in the region of 8 $\mu$ of the spectrum; these were also opaque to ultra-violet light below 3000 A, and this was taken to define type I. Type II diamonds are comparatively rare, and are transparent to ultra-violet down to 2300 A, having also no absorption in the infra-red region of 8 $\mu$ .

The structure of diamond as determined by X-rays (Bragg and Bragg 1913) consists of two interpenetrating face-centred cubic lattices as seen in Fig.1, where the planes shown by A's are (111) planes: the length of the edge of the lattice cube is 3.56 A. Fig.2 shows the structure with the (111) planes horizontal, the scaffolding of the cubic cell having been dispensed with:the length of the C-C bond is 1.54 A. Harkins (1942) has calculated the energy necessary to break the C-C bond as $6.22 \times 10^{-12}$ ergs, and from deductions involving this

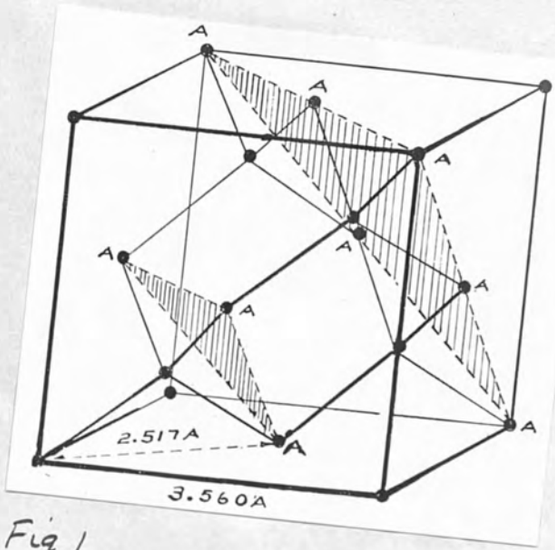


Fig 1

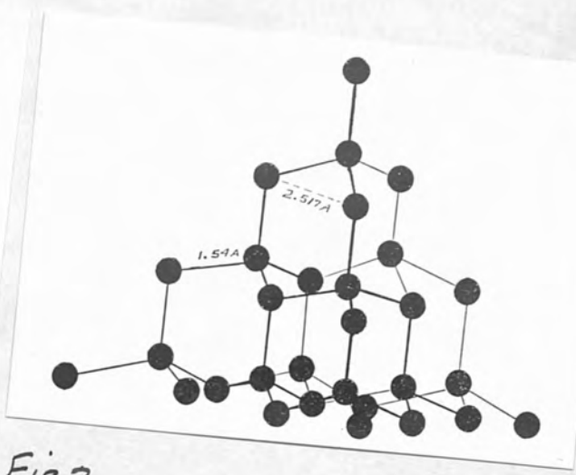


Fig 2

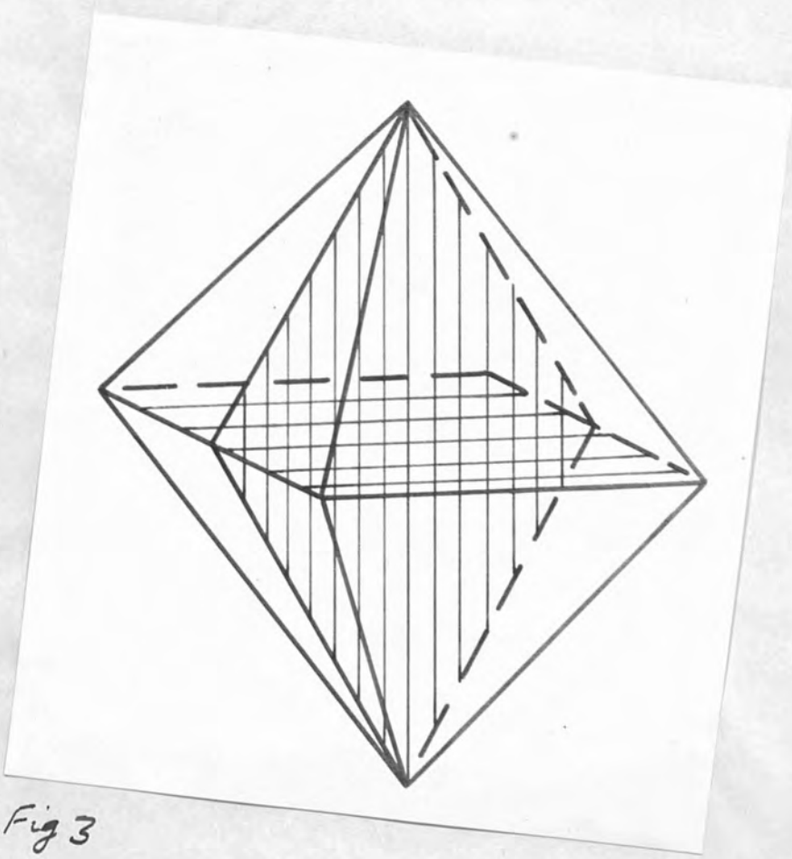

Fig 3

Ramaseshan (1946) has shown theoretically that cleavage will occur far easier in the (111) plane than in any other crystallographic direction. He lists the possible cleavage planes in order of probability with the dodecahedral (110) plane in the middle and the (100) cubic plane at the bottom. The relative probabilities are experimentally justified.

The elastic constants of diamond have been found experimentally by Bhagavantam and Bhimasenachar (1945) as $C_{11} = 9.5$ , $C_{12} = 3.9$ , $C_{44} = 4.3 \times 10^{12}$ dynes / sq.cm. and agree well in the theoretically deduced values. The only measurement of hardness available for diamond is that found by abrasion, for which the octahedral face is found most resistant, and the cubic face least - which is in strong contrast to the results of the static impact experiments described in this thesis, where it is seen that the octahedral face is definitely the least resistant.

The growth mechanism of diamond is still in doubt. No evidence whatsoever has been found for spiral growth on diamond, and it seems most probable that growth in layers occurs. This view is upheld by Champion's results (1953) on investigating the conduction pulse properties of diamonds by irradiating them with $\alpha$ and $\beta$ particles, also by the results of etching investigations by Omar, Pandya and Tolansky (1954), and Pandya and Tolansky (1954). Finally, all evidence from surface studies on natural octahedral faces points to this type of mechanism.

## 1.6 The Theoretical Fracture Strength of Diamond

By making considerable assumptions, it is possible to calculate a very approximate theoretical value for the critical average pressures, which should be required to form static pressure figures on the different diamond surfaces by a mechanism of cleavage along (111) planes. The resulting values will be no more than of the right order, but at least they will give an interesting comparison with the experimental values of critical average pressure found in this research.

The energy required to break a C-C bond is $6.22 \times 10^{-12}$ ergs. as already quoted, and Ramaseshan used this to calculate the necessary cleavage energy per unit area for different planes. For the (111) plane this is found to be 11330 ergs./sq.cm. Orowan (1948-9) has shown that where fracture begins, the critical fracture stress is given by $\sigma_c^2 = \frac{2Ee}{a}$ where E is the Youngs modulus, a is the atomic spacing, and e is the surface energy of the surfaces of fracture; for diamond, E is of the order of $10^{13}$ dynes /sq.cm. and a is 1.54 A, for a cleavage fracture the quantity e is equivalent to the cleavage energy, 11330 ergs/sq.cm. for a (111) plane. Thus the (111) cleavage stress for diamond may be calculated as $3.8 \times 10^{12}$ dynes/sq.cm.

If we assume that the Hertzian stress-field for a ball pressing down on an isotropic material holds for an anisotropic crystal under similar pressure, then the maximum tensile stress which will occur at the perimeter of the area

of contact, will act parallel to the undisturbed surface, and will have the value given by the equation (MTS) = $\frac{1-2\nu}{3} p_o$ where $\nu$ is Poissons Ratio and $p_o$ is the pressure at the centre of the area of contact, and, again by the Hertz theory, is equal to $\frac{3}{2} p$ where $p$ is the average pressure applied. For diamond, assuming Poisson's Ratio to be approximately 0.3, this gives (MTS) $\sim 0.2\, p$ .

By considering the critical values when fracture occurs, and remembering that it occurs not in the direction normal to the surface where the stress is maximum, but along (111) planes inclined to the surface; then by applying Sohncke's Law, it is seen that the cleavage energy, $\sigma_c = (\text{MTS})_c \sin^2\theta$ so $\sigma_c = 0.2\, p_c \sin^2\theta$ — so that the theoretical critical average stress $p_c = \frac{19 \times 10^{12}}{\sin^2\theta}$ dynes /sq.cm. where $\theta$ is the angle of inclination of the (111) plane to the particular diamond face concerned.

Thus for Octahedral faces where $\theta = 70^\circ 32'$ the calculated approximate value of $p_c$ is $21 \times 10^{12}$ dynes/sq.cm ; for the cubic face ($\theta = 54^\circ 44'$), $p_c$ - is $29 \times 10^{12}$ dynes/sq.cm; and for the dodecahedral face where there are two sets of intersecting (111) planes, $p_c = 19 \times 10^{12}$ dynes/sq.cm., considering the set for which $\theta$ is largest, i.e., $90^\circ$ (the other value of $\theta$ is $35^\circ\ 16'$).

These are larger than the experimental values as would be expected, and show that cracking should be more easily initiated on the octahedral face than on the cubic

face - which is found to be so; the case of the dodecahedral surface pressure crack figure is complicated by the presence of secondary (111) cleavage occurring along the two odd sides of the hexagonal crack figure.

## 1.7 Definitions

Some terms used may need defining first where special meanings are involved. The term impact, as used, does not imply dynamic experiments, but includes both types of tests referred to as static and dynamic impact tests. The equivalent of ring cracks on glass, for diamond are called pressure crack figures, and whenever the term 'pile up' is used this is not in the same literal sense as the pile up phenomena of metal indentations, but just means that material which has been disrupted so that it is permanently raised above the surface level.

The 'Real' critical average stress is the load at first crack divided by the circular area of contact at this load, and the 'nominal' critical average stress is the maximum load applied divided by the largest surface crack area.

Finally, the Girdle and Two-point planes referred to in the text are technological terms for crystallographic planes illustrated in Fig.3 : the former is the horizontal shaded plane and the latter is the shaded plane which is vertical.

# CHAPTER II

# EXPERIMENTAL AND MICROSCOPIC TECHNIQUES

## 2.1 Static and Dynamic Testing

In all the static impact experiments carried out, a Penetrascope portable hardness tester has been used to apply the pressure. This is a commercial instrument operated by a hydraulic thrust unit capable of applying loads from 1 to 30 kgm. Operation is normally by hand - the load being increased continuously from 800 up to the required value, and read directly from a dial gauge. The specimen to be impacted can be studied for suitable positioning by a microscope attachment to the instrument. The load is removed by the reverse procedure to how it is applied, there being no method by instantaneous release.

In the experiments on glass, to be described, some dynamic tests were done. Here the procedure was very simple: a $\frac{1}{4}$" steel ball was used and was dropped from rest down a vertical glass tube of length 80 cms. and having a clearance of just $\frac{1}{4}$". Various heights were tried, but 80 cm. was found to give a well formed ring crack without the specimens being shattered.

No dynamic tests were done on diamond because of the danger of shattering, the stones being relatively thin and the force required to produce cracks being great.

The impacting surfaces in all tests were spherical

As mentioned above, a $\frac{1}{4}$" steel ball was used in the dynamic tests. In the static experiments, the Penetrascope could be fitted with any impactor with suitable mounting. The bulk of the experiments were done using a specially prepared diamond hemisphere - a mounted cylinder of diamond with a hemispherical ball end of diameter 0.78 mm. The largest pressure cracks formed with this impactor were small enough for this ball ended cylinder to be considered as a sphere. Other impactors used were mounted spherical balls of steel $\frac{1}{4}$" diameter; and of sapphire and tungsten carbide - 1 mm. diameter in each case.

## 2.2 Technique of Observation during Tests

During the course of the early initial experiments of forming ring cracks in glass it was soon seen that it would be of great advantage to the study of the mechanism of pressure cracking if observations could be made of the region of contact between impactor and specimen during the application of the load from zero up to cracking point and, in some cases, beyond. The nature and development of cracking features could thus be followed and the load increased or released appropriately. The expectation was fully justified when it was clearly seen that in all but extreme cases, the Hertzian cracks i.e., those cracks developing on the surface of the specimen around the circle of contact and penetrating into the body of the specimen became invisible to normal observation on release of load - the Newtons rings interference fringes

formed in these circles disappearing one by one as load was gradually reduced to zero.

To achieve this aim, the complete stage of the Vickers' inverted-type projection microscope was removed and replaced by the Penetrascope instrument, already described, on its own stage. Thus, as the impactor in the Penetrascope pressed down on the specimen from above, the contact region could be observed through the microscope from below: the specimens of course, have to be transparent and the two faces must be smooth, flat and parallel to each other. For later experiments this arrangement was adapted to be motor driven. Impact phenomena is dependant upon rate of application of load as well as the period of application, so it was thought an improvement to have the rate of load increase independant of the operator. The complete arrangement for testing can be seen in Fig.4 where a slow-motor reversible drive is seen mounted vertically above the Penetrascope with an easy coupling device.

It must be noted that although the adaptation gives a constant drive to the Penetrascope its design is such that the rate of real load increase is dependant to some extent on the elastic deformation properties of the impactor and the specimen. This is because with a hydraulic system, it has to be driven further to attain the same load when elastic deformation occurs readily, than when the combination of specimen and impactor is elastically highly resistant.

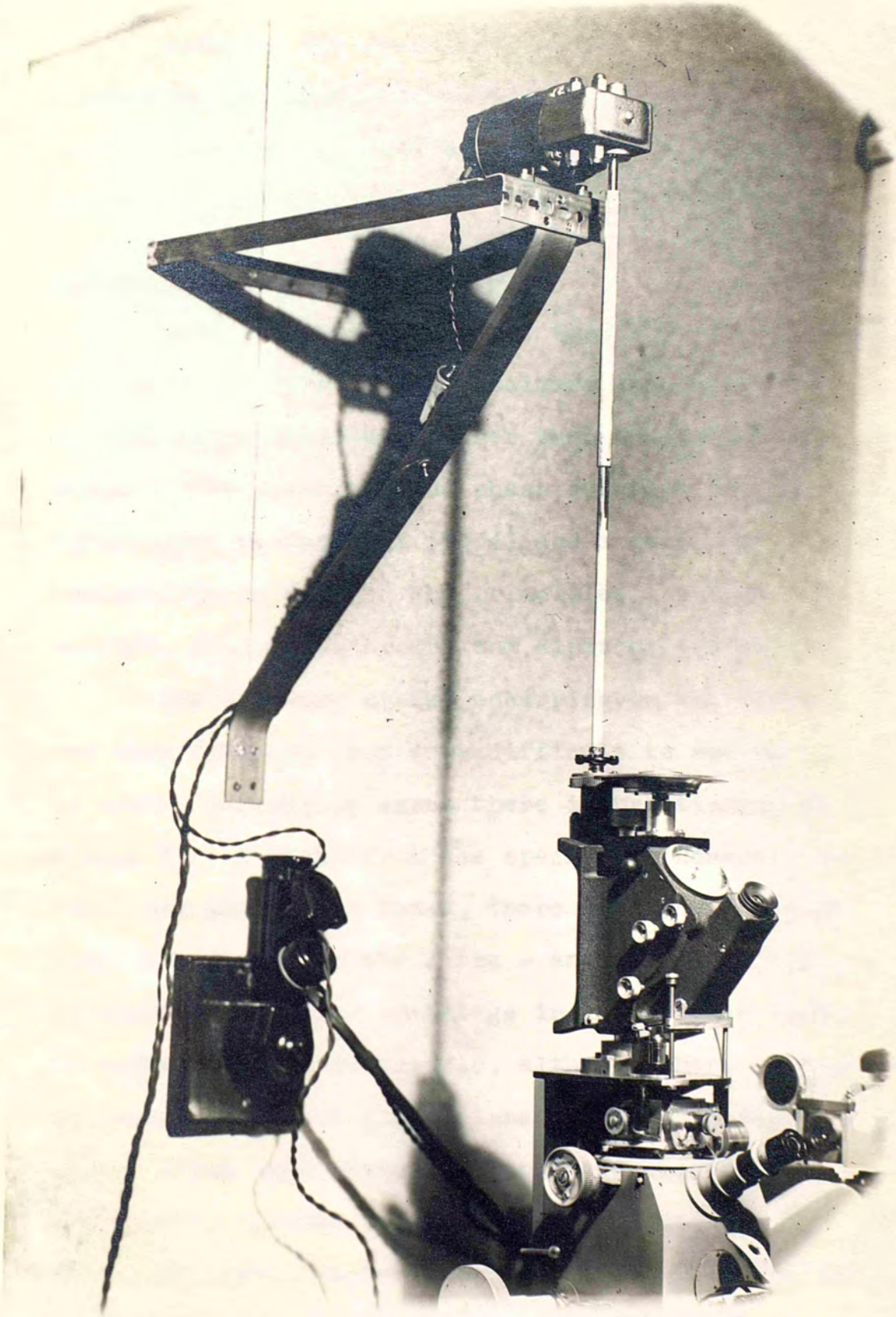

Fig 4

However, the arrangement does allow for exactly repeatable experiments, and the measured rates of increase in load are between 0.47 kgms/s. for Tungsten Carbide against glass and 0.55 kgm/sec. for diamond on diamond.

## 2.3 Phase Contrast Microscopy

This is now a well known technique for increasing the visibility of microscopic specimens which have variations in refraction or thickness rather than in transparency and colour. The principles of phase contrast microscopy were first given by Zernicke (1934) and a good account of the application as well as the principles involved is given by Bennett, Jupink, Osterburg and Richards (1951).

The pressure cracks occurring on the diamond surfaces are very fine and thus very difficult to see on the surface by normal microscopy since there is practically no amplitude change in the light from the specimen. However, due to the small air gap in the crack, there is a phase change in the light emerging from the crack - and this is a typical example of where there is an advantage in using phase contrast microscopy. This is because, although there is a defraction pattern in the back focal plane of the objective for an object which only gives rise to phase changes, the light of the central maximum is in advance in phase by $\lambda/4$ to the defracted light, so that the interference in the image plane responsible for the formation of a contrasted image is unable

to take place, the resulting image being nearly invisible. By using the phase contrast technique the phases of the direct and diffracted light are adjusted by retarding the central beam either by $\lambda/4$ so that the phases are the same (negative phase contrast) or by $3\lambda/4$ so that the phases differ by $\lambda/2$ (positive phase contrast); in either case interference occurs in the image plane to give a visible image.

The apparatus used was the Cooke Troughton and Simms phase contrast equipment for incident illumination fitted on to a Vickers' projection microscope. A diagrammatic scheme of the arrangement is shown in Fig.5. The annular diaphragm D serves as an entrance pupil to the optical system, the light source is focussed on this by the condenser lens C. The field lens and objective form a real image $D_1$ of D after the light has been reflected from the specimen surface and gone through the objective once more. Image $D_1$ is the exit pupil and it is here that the phase plate is positioned.

In this equipment, the microscope objective lens, the beam splitter and the phase plate are mounted in one unit, the objective. The principal of positive phase contrast is used, with a single phase plate having an absorption of 80 %. There are suitable adjustments for getting the surface of the specimen perpendicular to the optical axis of the microscope, and for superimposing the image of the annular diaphragm exactly on the phase plate annulus. To make the most of the increased visibility, high contrast Kodak B 20

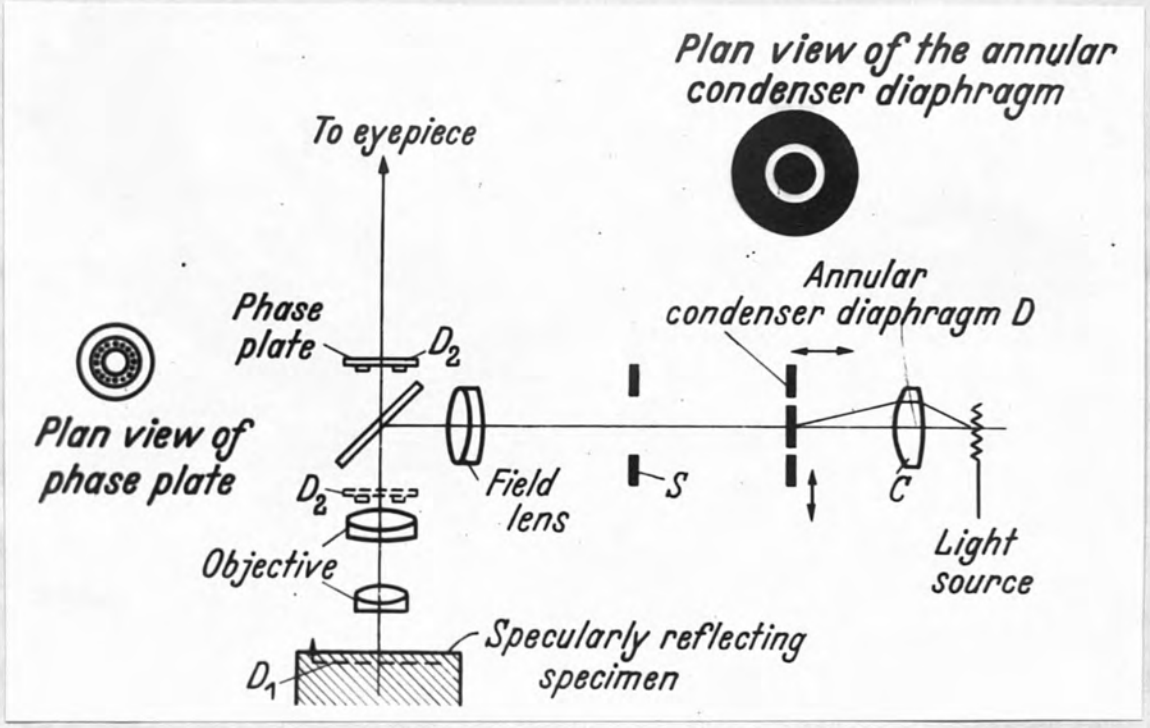
Plan view of the annular condenser diaphragm
To eyepiece
Annular condenser diaphragm D
Phase plate
$D_2$
Plan view of phase plate
$D_2$
Field lens
S
C
Light source
Objective
Specularly reflecting specimen
$D_1$

Fig 5

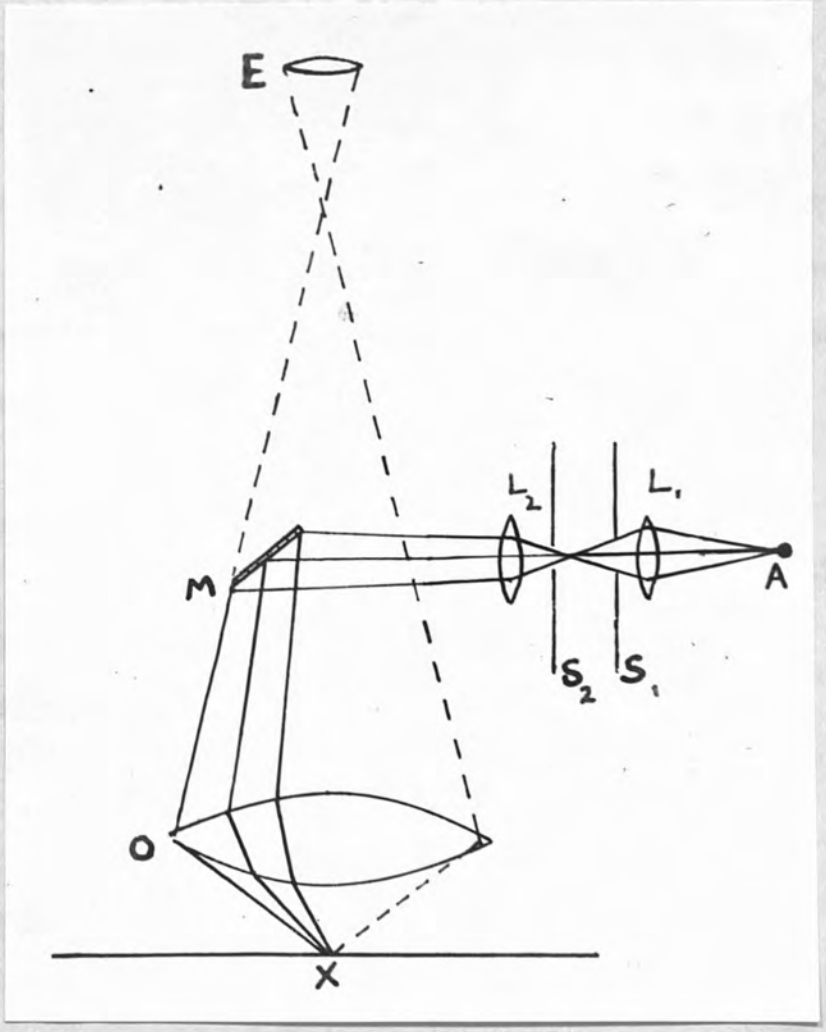
E
$L_2$
$L_1$
M
A
$S_2$
$S_1$
O
X

Fig 6

plates were used together with a contrasty developer Kodak D 8.

In practice there are two further advantages of this technique, the first is that best contrast is obtained when the specimen surface is exactly in focus whereas in bright field microscopy defocussing is used to observe specimens of low contrast which means a reduction in clarity. Secondly, the phase contrast microscope is operated at full aperture so that there is practically no decrease in resolution. A limitation of the method is that, for a rough surface, some of the incident light is scattered from the specimen instead of being specularly reflected, this tends to give a blurred image of the diaphragm in the back focal plane, so that exact superposition on the phase-plate annulus is no longer possible, and the contrast efficiency is consequently reduced. However, all the surfaces of specimens in the investigations to be described, were necessarily flat and smooth.

## 2.4 Light Profile Microscopy

In some of the work done on ring cracks on glass, the Light Profile Microscope Technique developed by Tolansky (1951) has been used. This is a complementary technique to Multiple Beam Interferometry, which is discussed in the next chapter, in topographical investigations. It is a development of the light-cut procedure of Schmaltz (1936) This was rather a clumsy method and had several disadvantages

which were overcome with the development of the Light Profile. Here, any microscope can be used by making a minor adaptation and having a universal illuminator: the necessary arrangement can be seen schematically in Fig.6. A is a monochromatic source which is necessary because off-centre illumination entials severe chromatism. $L_1$ is the condensing lens and $S_1$ a diaphragm. $S_2$ is the field iris in the universal illuminator, as near as possible to which the profile is fitted - this consists of a mounted thin wire or a scratch on a disc of glass or, very conveniently, the edge of a coverslip. The metal tongue of the illuminator M gives the off-centre illumination. The procedure is very simple. The surface to be studied X is first focussed in the microscope, of which E is the eyepiece. Then the profile is adjusted until its image, projected by the objective lens O, is exactly in focus i.e., the image is in the plane of the surface of the specimen. Because of the inclination of the incident illumination any light displacements are profiled into lateral displacements of the line image as seen through the microscope. The resulting profile magnification is $M' = \frac{M \tan i}{\mu}$ where $i$ is the angle of incidence of the illuminating pencil of light, $\mu$ is the refractive index of the medium surrounding the surface, and M is the microscope magnification. For practical purposes the Profile constant $\frac{M'}{M}$ is obtained by empirical calibration, standardizing by interferometric measurements. It was conveniently found that, for the 2 mm. oil immersion

objective used, this constant is 1 so that microscope magnification and profile magnification are equal. Magnification up to about × 2000 can be used, and the accuracy of measurements is of the order of 1000 Å when this objective is used.

The reason for the use of this technique in some of the investigations, is the limiting feature of multiple beam interferometry, in that high resolution in depth is achieved effectively at the expense of resolution in extension, so that fine lateral detail cannot always be detected by this method. It is seen above that the light profile technique although not giving the height-displacement accuracy of high dispersion fringes, gives very high lateral magnification in conjunction with considerable vertical magnification - such power in both directions simultaneously are of considerable value. However, the technique was adopted only where height displacements were large enough to give significant displacements of the profile.

## 2.5 Polarized Light Technique

In attempting to observe the internal disturbances caused in the diamond crystals impacted on the various faces, it was found that the contrast was very considerably increased by using polarized light, and having the analyser crossed with the polarizer - a familiar technique in metallography and in crystallography for detecting strains. The stones were viewed

in transmission and the undisturbed regions are dark; what is seen is effectively a strain pattern, but it is very complicated, irregular and in three dimensions. However, the technique is excellent for showing up fine crack lines and multiple conchoidal fracturing which occur, beyond the surface crack figure in the body of the crystals, and several photographs where this method has been employed can be seen in the present work.

# CHAPTER III

# INTERFEROMETRIC TECHNIQUES

## 3.1 Introduction

The established technique of multiple beam interferometry developed by Tolansky (1944,1945,1946), has been extensively used in the research for the quantitative measurements of the inherent surface distortions accompanying the production of pressure crack figures on glass and diamond. A full account and discussion of this technique has been given by Tolansky (1948) and a review of the subject is given by Kuhn (1951).

Most of the observations were carried out using the reflection system, because in this method it is easier to identify the phenomena on the surface, and both techniques of Fizean fringes and Fringes of equal chromatic order, have been used.

The accuracy of the method is inherently high and the distortions under investigation lie within the range most suitable for its application.

## 3.2 Summary of the Theory

For an interferometer consisting of two parallel surfaces, having transmission and reflection coefficients of intensity T and R respectively, which are separated by a dielectric of thickness t and refractive index $\mu$, the intensity distribution in the transmitted system is given

by the Airy formula:-

$$I = \frac{T^2}{(1-R)^2} \cdot \frac{1}{1 + \frac{4R}{(1-R)^2} \sin^2 \frac{\delta}{2}}$$

where $\delta = \frac{2\pi}{\lambda} 2\mu t \cos\theta$ is the constant phase lag between successive beams, $\theta$ being the angle of incidence.

For a slight inclination between the two surfaces so that they form a wedge of a small angle, the Airy summation should apply with the modification that there will be a progressively varying phase lag for each beam of the reflected light: when this supplementary phase lag obtains a value in the order of $\pi$ (so that the corresponding path difference is $\lambda/2$ ) there will be a tendency to destory the condition for the formation of sharp interference fringes. Brossel (1947) has shown that in this case the path difference between the first and n th beam is approximately ($2nt - \frac{4}{3} n^3 \varphi^2 t$ ) where $\varphi$ is the small wedge angle. The theoretical limiting condition in multiple beam interferometry for the transmission system is thus seen to be that the supplementary path difference $(4/3\, n^3 \varphi^2 t)$ due to the wedge angle, must be less than $\lambda/2$ .

For a given reflectivity, the critical values of $\varphi$ and t for the above condition can be found, and the experimental conditions varied accordingly. In topographical studies the wedge angle is usually fixed, the gap being then the only variable; in practice it is found that this must be of the order of a few wavelengths of light at the most, otherwise the fringe definition suffers considerably.

The corresponding treatment for a reflection system is more complex. The theory of reflection fringes has been given by Hamy (1906) and Holden (1949), the complication arising from the fact that the first reflected beam has a phase change, with respect to the second beam, which is quite different from that between any other two successive beams. For silver films of reflectivity over 80%, it is found that the intensity distribution in the reflected and transmitted systems are approximately complementary, although the experimental conditions for good reflection fringes are more critical than in transmission.

Finally it is to be noted that localized multiple beam fringes obey the equation:-

$$n\lambda = 2\mu t \cos\theta$$

where n is the order of interference and is an integer, $\lambda$ is the wavelength of the light, $\mu$ is the refractive index of the material between the interferometer plates, t is the thickness of the gap and $\theta$ is the angle of incidence - this is normally always kept constant and equal to zero. If $\lambda$ is also constant, then Fizeau fringes of equal thickness are obtained; whereas if $\lambda$ is allowed to vary, the value of $\lambda/t$ is constant for each fringe giving the fringes of equal chromatic order as termed by Tolansky.

## 3.3 Fizeau Fringes

The experimental arrangement for observing these

fringes in reflection is shown in Fig.7. A metallurgical microscope is adapted so that the image of the light source is formed in the back focal plane 1, of the objective O, thus the light emerges from the objective lens parallel, and is incident upon the interferometer X normally. The fringes localized at the interferometer gap are observed through the microscope.

The experimental conditions for the production of highly sharpened multiple-beam Fizean fringes can be summarized thus:-

(1) The surfaces must be coated with a highly reflecting film having minimum absorption.

(2) These films must contour the surfaces exactly and be highly uniform in thickness.

(3) Monochromatic light, or at most a few widely spaced monochromatic wavelengths should be used.

(4) The interfering surfaces must be separated by not more than a few wavelengths of light.

(5) A parallel beam of light should be used.

(6) The incidence should be normal.

For the Fizean system, it has been seen already that each fringe is a fringe of equal thickness. Also since the incidence is always kept normal and the gap is in practice invariably an air gap, then the height displacement between successive contour fringes is $\lambda/2$ . A mercury source is normally used, a Wratten 77 A filter transmitting the

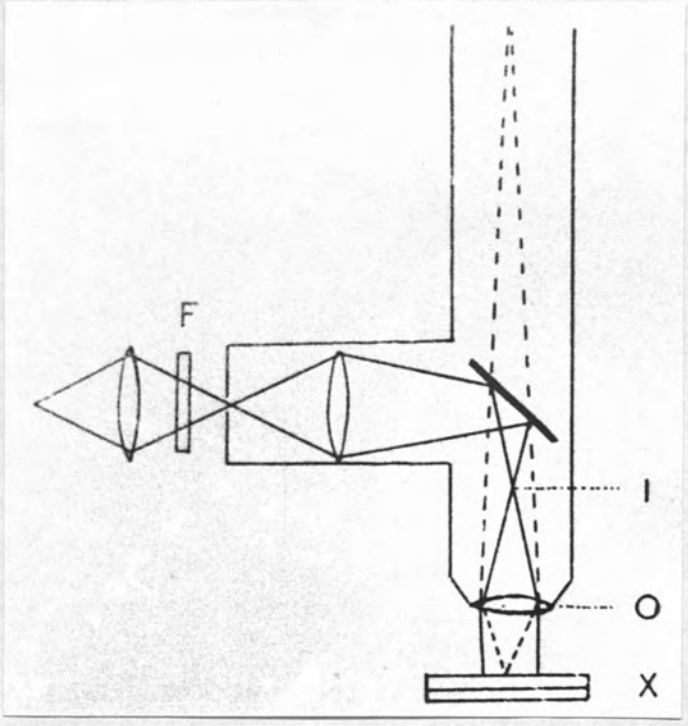


Fig 7

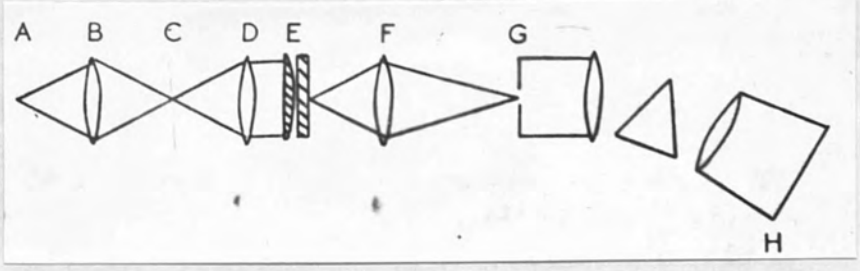


Fig 8

solitary 5461A spectrum line. Any displacement of a fringe is measured as a fraction of the distance between adjacent fringes, thus giving the height displacement as a fraction of 2730 A units.

3.4 Fringes of Equal Chromatic Order

Where Fizeau fringes cross a feature on the surface under observation, the consequent pattern is not a true linear profile of the height distortion, but is a complex, resulting both from the shape of the feature and from the surface topography. For securing a true topographical section the white light fringes of equal chromatic order are distinctly advantageous. The difference is well illustrated in a comparison of Figs.9 and 10.

The experimental arrangement for the production of this type of fringe pattern in transmission is shown in Fig.8; A is a white light source which illuminates the aperture C by means of condensor lens B, lens D producing parallel light which is incident normally on the interferometer E. The lens F now projects an image of the localized fringe pattern onto the slit G of the spectrograph H. The slit is used to select a line section of the pattern, from which the light passes through and forms a spectrum. Taking $\mu = 1$ and $\theta = 90^{\circ}$ then the equation governing the formation of the fringes is

$$n\lambda = 2t \quad \text{or} \quad t = \frac{n}{2}\lambda$$

thus for any one fringe produced, $t/\lambda$ is constant, and a slight increase in the interferometer gap t will produce a consequent increase in the wavelength given by:-

$$\delta t = \frac{n}{2} \delta\lambda$$

Hence, if in the spectrum, any one fringe deviates towards the red (i.e. $\lambda$ increasing), this means that the gap is increasing or that there is a 'hollow' or 'valley' in the surface under examination with reference to an optically flat second surface. Since each fringe order corresponds to the same line section, the shape of all the fringes is the same but their magnification varies according to the variation of the chromatic dispersion of the spectrograph used.

From the equation $\delta t = n/2 \, \delta\lambda$ it is seen that to measure a height displacement on the surface it is necessary to know the order of a particular fringe and the quantitative variations of $\lambda$ along it. The latter can be obtained from the dispersion calibration of the spectrograph, by referring to the variations in distance of the fringe from standard spectrographic lines - these being superimposed on the fringe pattern from a mercury source. The order of a particular fringe can be determined by considering the fringe and an adjacent fringe, for which

$$n\lambda_1 = (n+1)\lambda_2$$

whence

$$n = \frac{\lambda_2}{\lambda_1 - \lambda_2}$$

the values of $\lambda_1$ and $\lambda_2$ being obtained again from the dispersion calibration of the spectrograph.

In this way fringe displacements can be converted into surface measurements so that a line section profile is obtained for each fringe pattern. The use of very high dispersion of the fringe patterns allows real magnifications in height of about 250,000 to be attained. For the photographs of these fringe patterns shown only the lateral magnifications (the magnification of the line section chosen) is given, as the vertical magnification changes with the chromatic dispersion of the spectrum. For all photographs of this type calibration diagrams are given where necessary.

It is to be noted that in the photographs of these fringes of equal chromatic order, the fringe dispersion is very much higher in some than in others: this can be judged (where no spectrum lines are visible) by the fact that the distance between the yellow doublet and the green lines of the mercury spectrum (a difference of 320 A) is approximately equal to half the width of the spectra as seen in the photographs.

# CHAPTER IV

# OPTICAL STUDY OF RING CRACKS ON GLASS

## 4.1 Introduction

The phenomenon of ring cracks on glass surfaces has been known for many years and the literature is discussed in Chapter 1. Here the investigation is carried a stage further in a study of the micro-distortions of the surface in the region of a ring crack formed by static impact, and, in the next chapter, the variation of the phenomena for a selection of ten well known types of optical glass. The height displacements for statically produced ring cracks are in the order of 1000 A and profiles of sections through a diameter are obtained with an accuracy of more than 50 A.

For the initial study of the surface distortions, static impacts were made with both the diamond ball of 0.78 mm. diameter mounted in the Penetrascope instrument, and a similarly mounted Tungsten Carbide ball of 1 mm. diameter. Loads were applied gradually by hand, and it was found for the few glasses studied here that a load range of 2 to 4 kgm. was sufficient for the production of primary cracks. Included in this first set of experiments, was a single dynamic test done for comparison with the static tests. Here a $\frac{1}{4}$" steel sphere was used, being dropped vertically on to the glass surface; it was found by experiment that for a drop height of 80 cm. a primary ring crack could be formed on the particular glass investigated without further excessive

damage occurring due to shatter.

In all tests, the glass surfaces were silvered by evaporation, after the impacts had been made, and matched against a silvered flat for the production of multiple beam interference fringes by which surface distortions were detected and measured.

4.2 The surface distortions for Primary Ring Cracks

The first surface to be studied was that of a disc of Extra Light Flint (ELF) glass of thickness 1.5 mm. A ring crack was formed on this by the Tungsten Carbide ball with a load of 3 kgm, and by microscopic examination it was seen to be a single completed primary ring-crack. Fig.9 shows the Fizean fringe picture with a fringe passing across a diameter of this crack, the dispersion is such that a fringe displacement towards the top of the photograph represents an elevation on the surface. It is seen that, on approaching from the left towards the ring crack from the undisturbed level, the surface exhibits a smooth regular rise up to a height of 400 A; on reaching the crack there is an abrupt drop to zero level on the inside. It is notable that the whole of the disc circumscribed by the crack is at zero level, (i.e., the level of the undisturbed region away from the crack), the main disturbances being localized round the perimeter region. On the right of the ring crack, the disturbance is seen to be of a similar nature but much greater in amount. This asymmetry in the amounts of the displacements

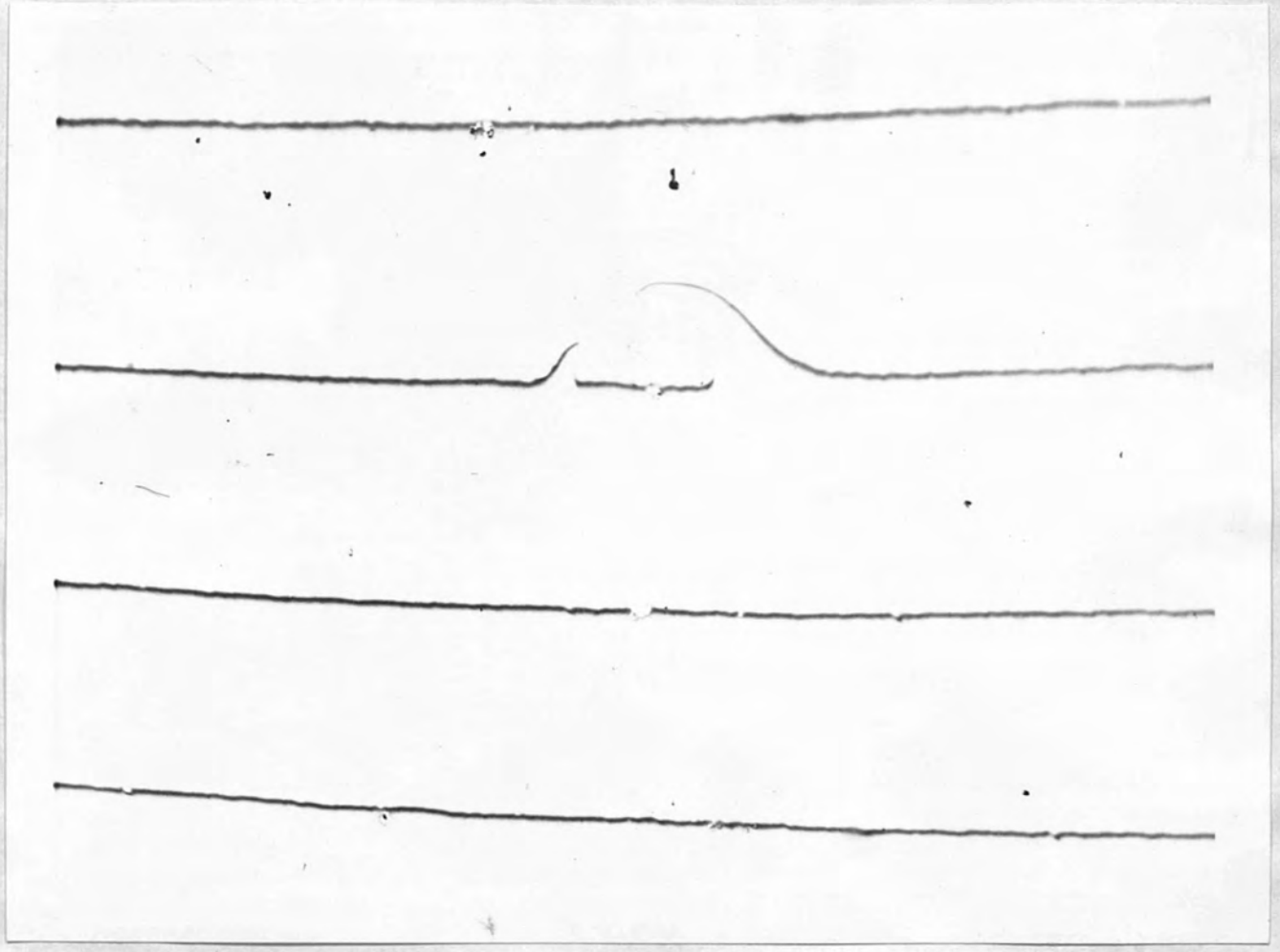

Fig 9 x 135

on the two sides is interesting in that it occurs in the majority of cases, as can be seen by examining the fringe patterns given in this work for a number of ring cracks produced on different glasses; the striking thing is, that microscopic examination alone is quite incapable of detecting this asymmetry, the cracks appearing in most cases as just dark, perfectly circular, lines on the surface. Indeed, the whole of the disturbance in level clearly seen in Fig.9, has not previously been detected for ring cracks produced by gradual static loading, although Raman (1926) detected similar disturbances, but on a much larger scale, around percussion ring cracks on blocks of glass (the height displacements, which he measured by Newtons Rings fringes, were of the order of 2$\mu$ as compared with 0.1$\mu$ in this investigation).

The Fizeau fringes are not linear profiles, and there is considerable advantage in using fringes of equal chromatic order, as has been discussed in the previous chapter. The white light fringe pattern for the same ring crack as above, is seen in Fig.10, where the magnification is greater than before. Each fringe is a true profile section, and a small number of fringes are included to give an idea of the dispersion - the spectrum line being for the 5461 A green line of mercury. The remainder of the interferograms, showing the surface distortions for different impacts on different types of glass, are of this type, and the photo-

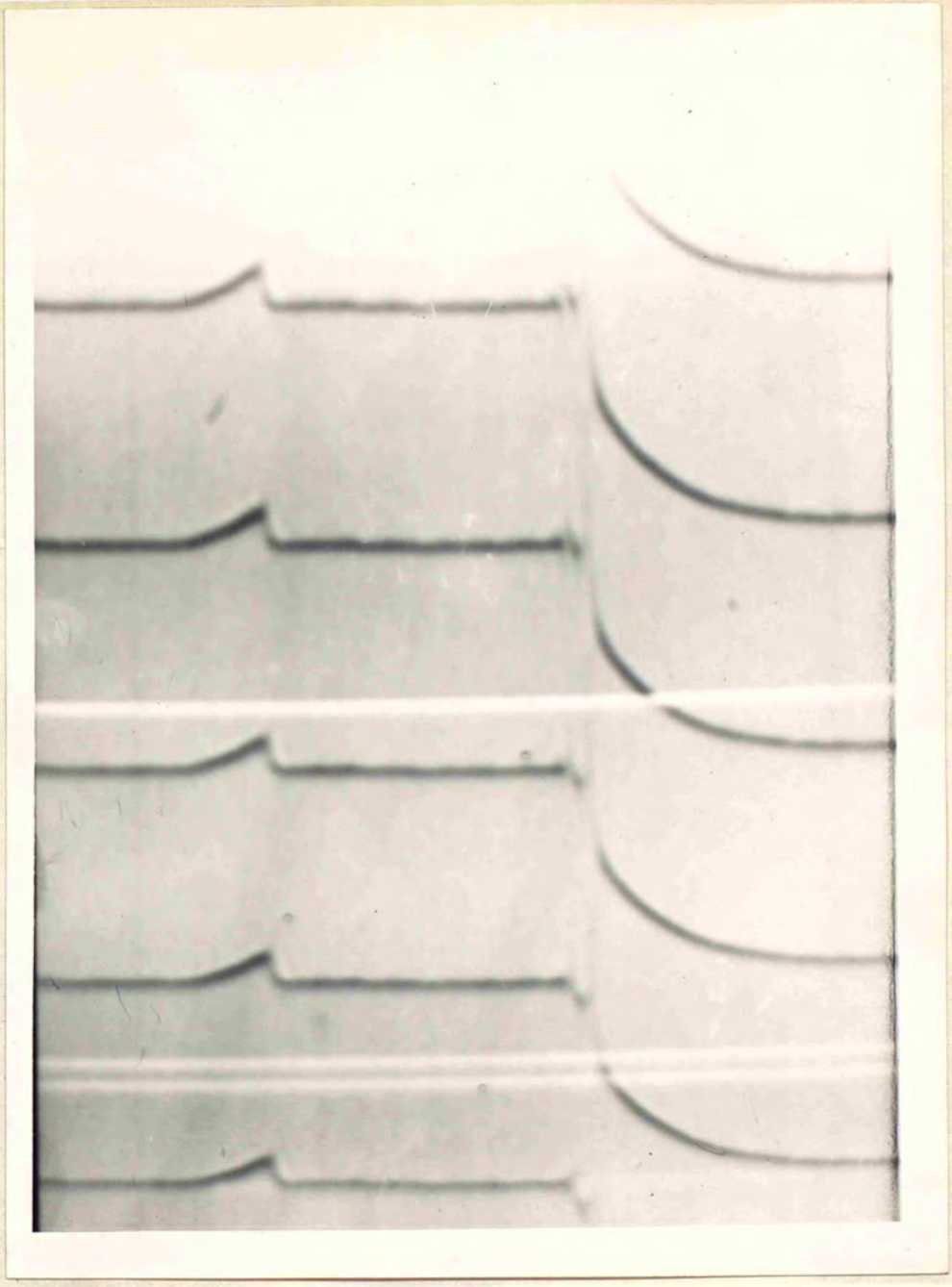

Fig 10 x 320

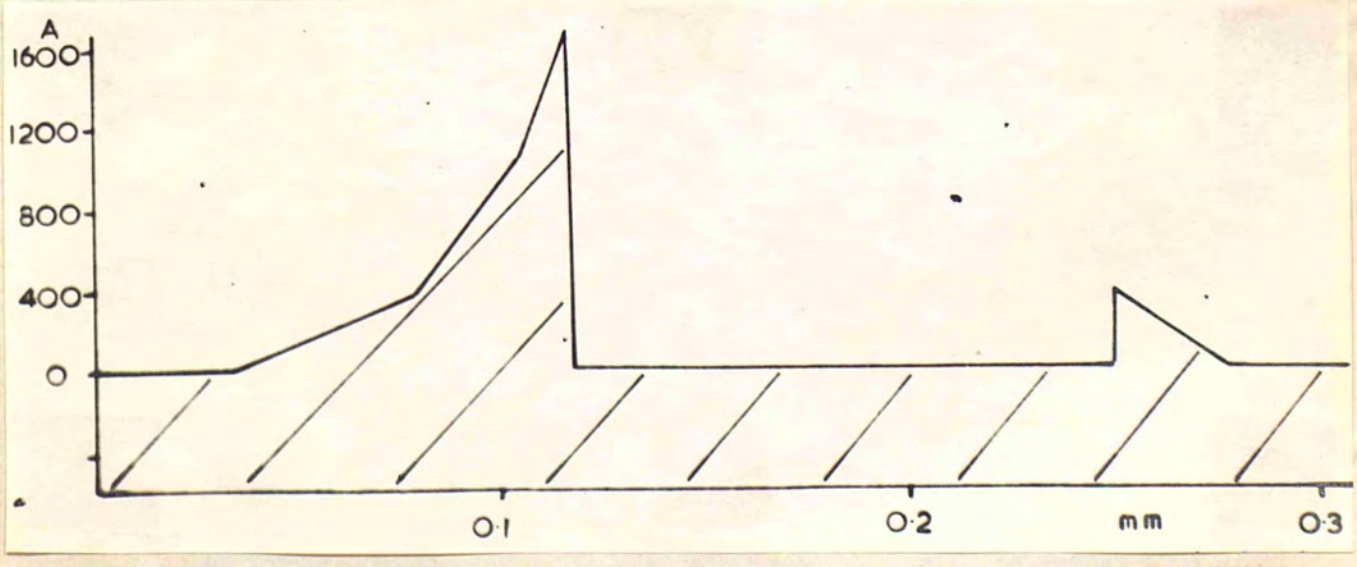


Fig 11

graphs are arranged with the chromatic dispersion vertical so as to give a direct impression of the associated surface displacements. For any one interferogram, a calibration has to be done allowing for the chromatic dispersion of the spectrograph used, so that for each fringe pattern there is a corresponding scale drawing giving an exact vertical section through the respective ring crack; this is shown in Fig.11 for the fringes of Fig.10.

## 4.3 Surface Distortions for Multiple Ring Cracks

In further experiments, where greater stress was applied, multiple ring cracks were produced consisting of two or three concentric circular cracks. In these tests the diamond ball was used, having a smaller radius, on blocks of various glasses approximately half an inch thick. Characteristics of the surface distortion for multiple cracks are illustrated in Figs.12, 13 and 14 showing the white light fringe patterns passing over diameters of cracks produced on blocks of Boro Silicate Crown (BSC) and Light Flint (LF) glasses respectively, the load applied being 4 kgm. in each case. In the calibration of Fig.12, drawn to scale in Fig.15, it is seen that three major cracks have occurred and the characteristic sloping up from the outside and sudden drop on the inside is repeated for each crack; there is evidence, on the right hand side, of a fourth minor crack which has not completed its full circle. Another important difference here is that the central area although still being perfectly flat,

has been depressed by as much as 200 A below the undisturbed outside region. This is a common occurrence for multiple cracks, both on glass and on diamond; it was also found by Raman to occur for percussion ring cracks. In Fig.16 the calibrations are given of both Fig.13 and Fig.14: the top scaled drawing (D) was for one impact on LF glass which produced one complete ring crack and a half formed second crack, a stage between the formation of primary and multiple cracks. The central portion is here seen to be flat but very slightly slanting. This was a new observation and the test was repeated on the same glass: the second diagram (E) representing the fringe patterns of Fig.14 is the resulting calibration. Although the load was approximately the same in this test, the cracking has been more pronounced, and this has produced a central area, flat, but having a very distinct slope. The slopes of these two sections of the central disc are 1 and 20 seconds of arc respectively, and in both cases the slope is such that the larger drop below zero, corresponds with the larger mass of glass displaced above the zero level.

The diameters of the ring cracks can be seen in the scale drawings, and thus an idea of the area of extent ascertained. By assuming approximate symmetry, the order of the volumes displaced above zero level at the formation of multiple ring cracks can be found from these calibrations of the fringe pattern. It has been calculated as being of the order of $10^{-9}$ cc. ( several calculations were made for

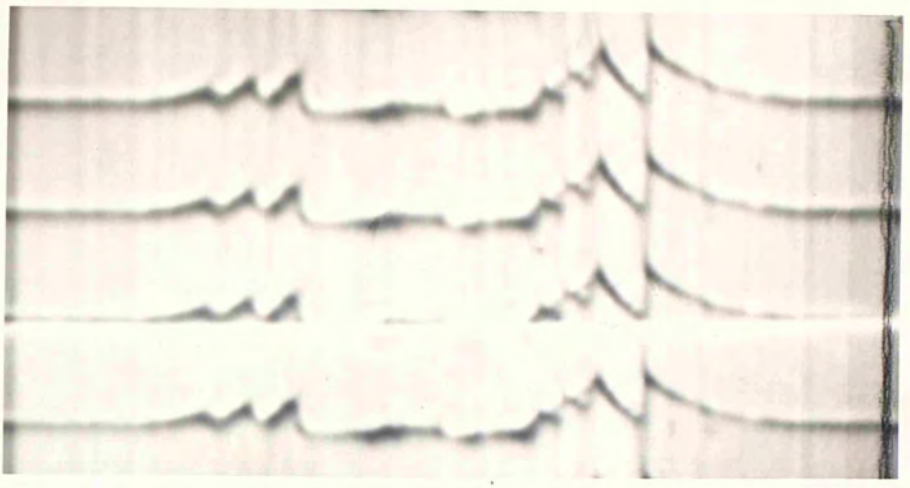

Fig 12 x320

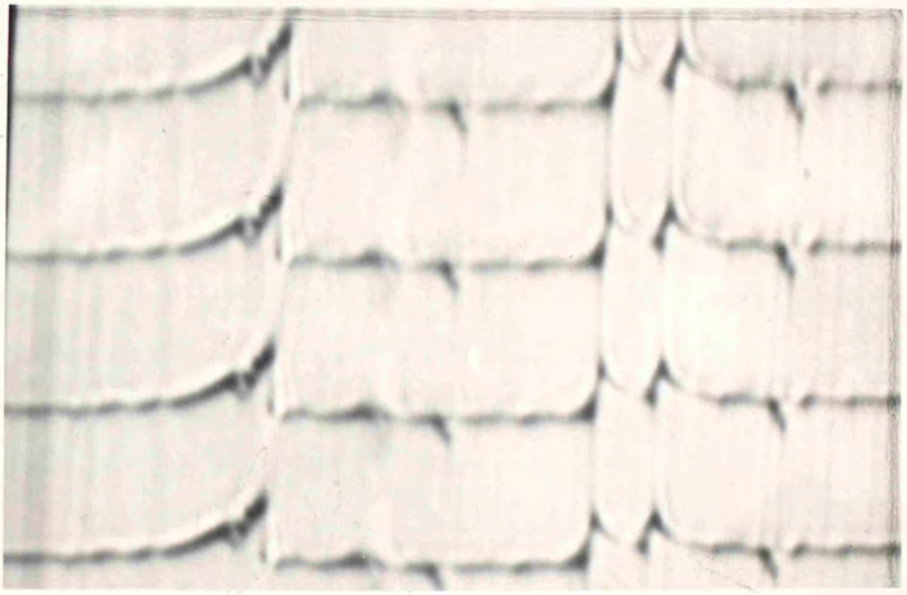

Fig 13 x320

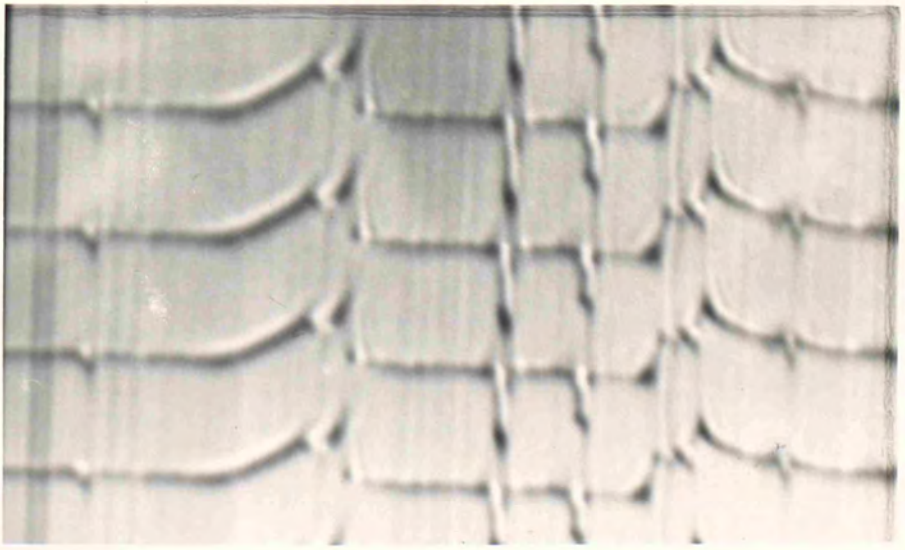

Fig 14 x320

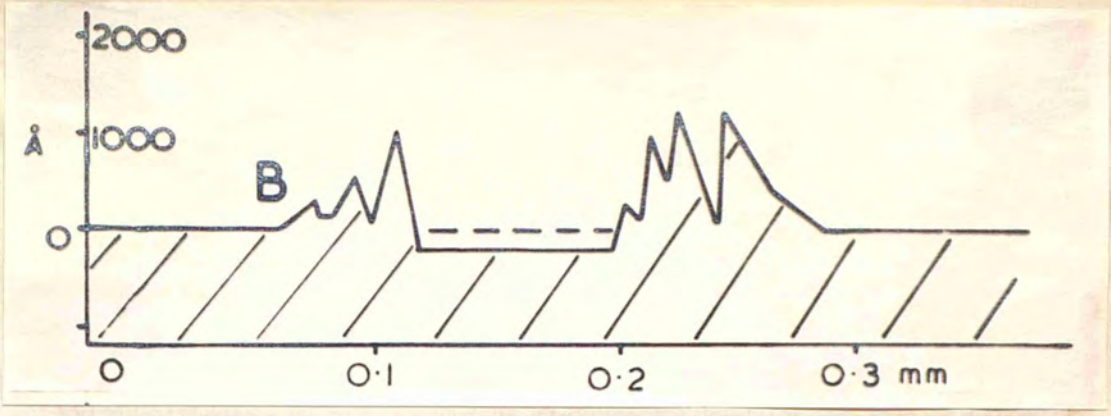


Fig 15

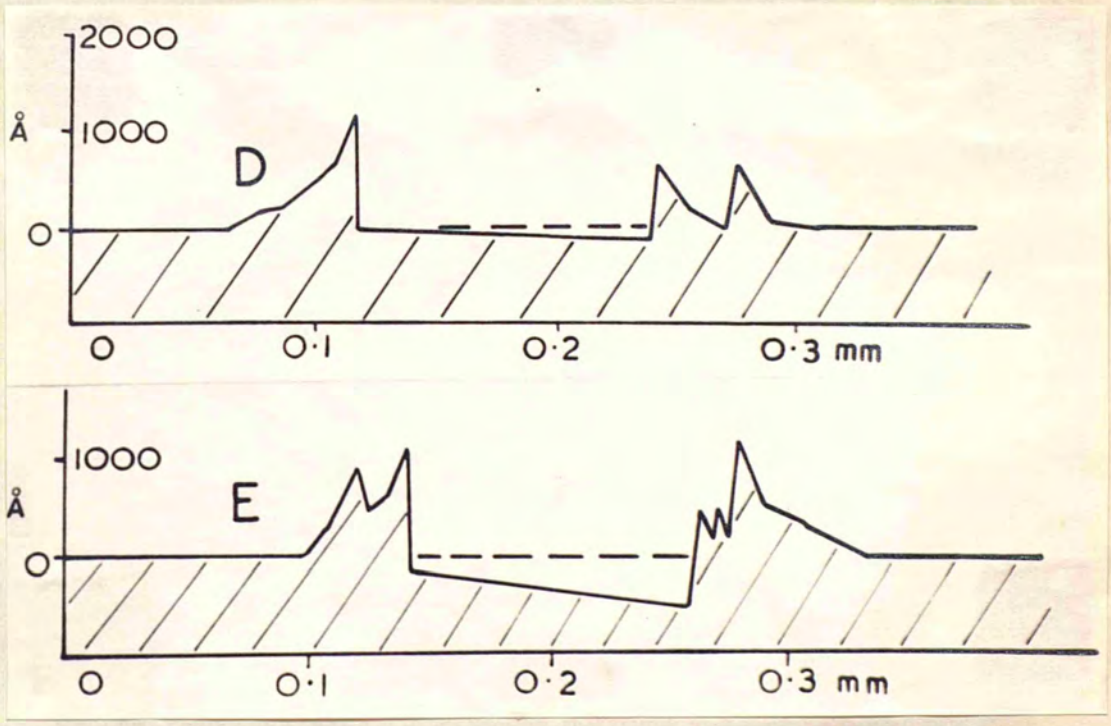


Fig 16

X60

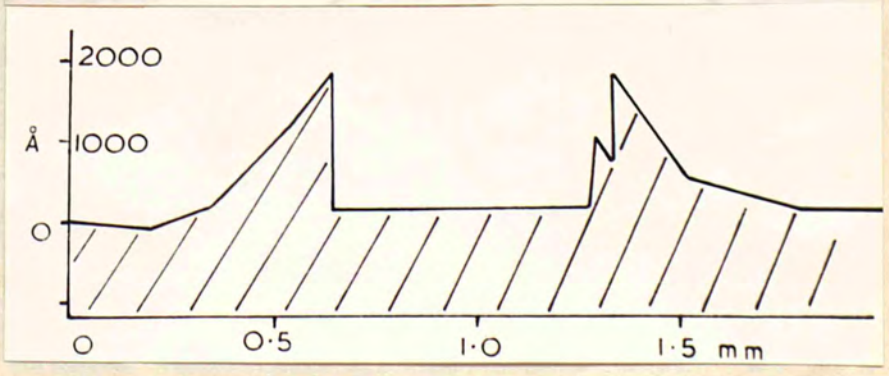


Fig 17

the different ring crack patterns obtained and the value varied between 0.8 and 1.2 x $10^{-9}$ cc).

4.4 The Dynamic Test

This was carried out, as previously described, on a block of Double Extra Dense Flint (DEDF) glass, which is relatively soft. A complete primary ring crack was just formed without shatter, the block being half an inch thick. The corresponding fringe pattern obtained for a section across a diameter is shown in Fig.17 together with its calibration. The characteristics closely resemble those found for the static impacts; but it is to be noted that although approximately four times as great in horizontal extent, there is not an exact sealing up of the pattern, the height displacement being only about 1.5 times as large.

Finally, for this last ring crack, since its height displacements were greater than in the other tests, the light-profile technique was applied. Although this is limited in its height resolution, there is the advantage over interferometric observations of having very high lateral resolution, an oil immersion 2 mm. objective being used. Because of the high lateral magnification only a segment of a ring crack can be observed at a time, since the complete ring extends beyond the field of view. Fig.18 shows a light profile crossing the ring crack of the dynamic test at a region of the crack corresponding to that seen on the right of Fig.17 (calibration). In the profile photograph the main

ring crack is seen in the centre, and there are two subsidiary cracks one on either side (of which only one has been detected in the fringe pattern photograph). The three cracks are separated by about 25$\mu$ between each, and the centre of the ring crack figure is beyond the left side of the photograph. In this photograph the vertical profile magnification and the horizontal lateral magnification are the same. The profile coming from the right just resolves the displacement at the first crack, the gradual smooth rise up on approaching the main crack is quite evident but in addition to the former interferogram data a new point is now revealed. What appears to be an abrupt drop on the inside of the crack in the interferometric study is seen to be otherwise:there is a definite slope of the profile from the crack down to the inside surface. Whether in fact, the surface does slope, or whether this is a mean effective surface produced by the lodgement of very fine de bais, is difficult to settle. The most probable explanation is that, what is seen is an artificial 'lip' to the crack due to conchoidal chipping on the inside edge of the ring crack which has been compressed as the crack formed, while the outside edge has been pulled away.

## 4.5 Development to fracture of Ring Cracks on Glass

The series of experiments to be described in the next Chapter were carried out with the Penetrascope on the Vickers Projection microscope as shown in Fig.4 so that the impact

was being observed as made. In several of the tests, the glass discs fractured from the ring crack into two or more pieces.

The development of a ring crack to fracture for a disc of Light Barium Crown (LBC) glass is shown in the series of photographs in Figs. 19, 20, 21, 22 and 23: the first shows the Newton Rings fringes obtained between the 1 mm. diameter Tungsten Carbide impactor and the glass surface, the second shows similar fringes but with a 'dark spot' over the area of contact for a load of 1·5 kgms. Fig.21 shows the primary ring crack which formed at 4.3 kgm. under an average stress over the area of contact of 225 kgm/sq mm. It is a perfect circle, and the Hertzian cone going into the material is indicated by the three interference fringes which can be seen concentric with the crack, and which are due to interference of reflected light between the two faces in the crack as it goes into the body of the glass. By a load of 7.1 kgm. this cracking had increased as seen in Fig.22; also the ring crack had become multiple. Immediately after this, fracture occurred suddenly and the load instantly dropped to 4.0 kgm - Fig.23 shows the appearance. When the load was completely removed, it was found that the disc had broken into several pieces and a few splinters.

The interference fringes within the crack seen in Figs. 21 and 22 occurred very often with the initiation of a ring crack at a fairly high load; but it was always observed

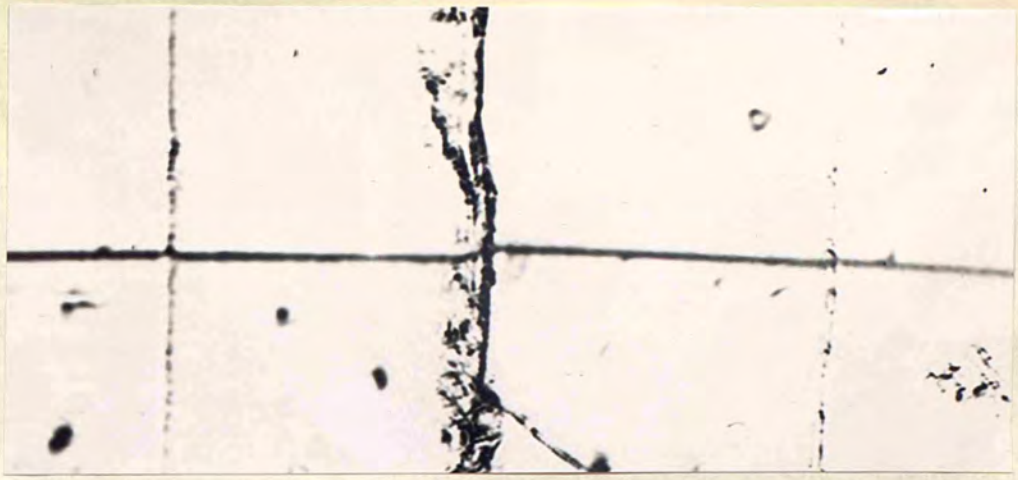

Fig 18 x 1850

Fig 19 x 275

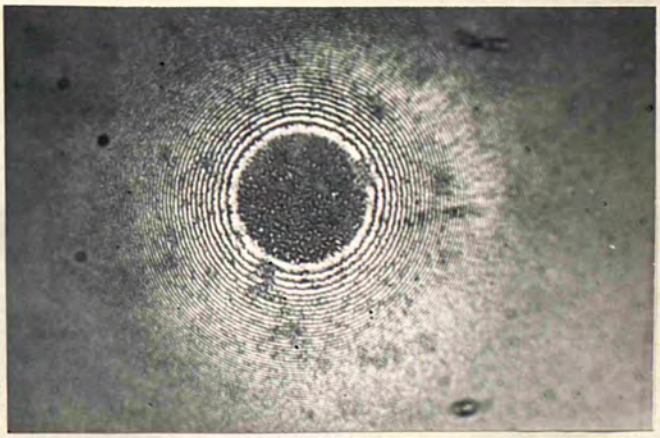

Fig 20 x 165

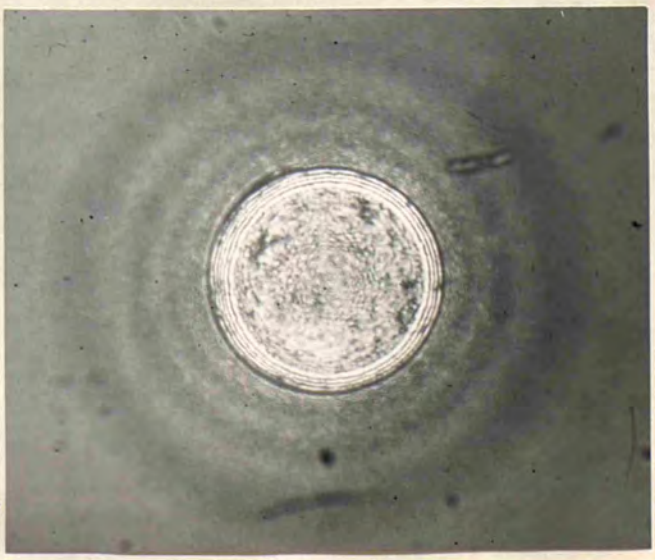

Fig 21 x 165

Fig 22 x 165

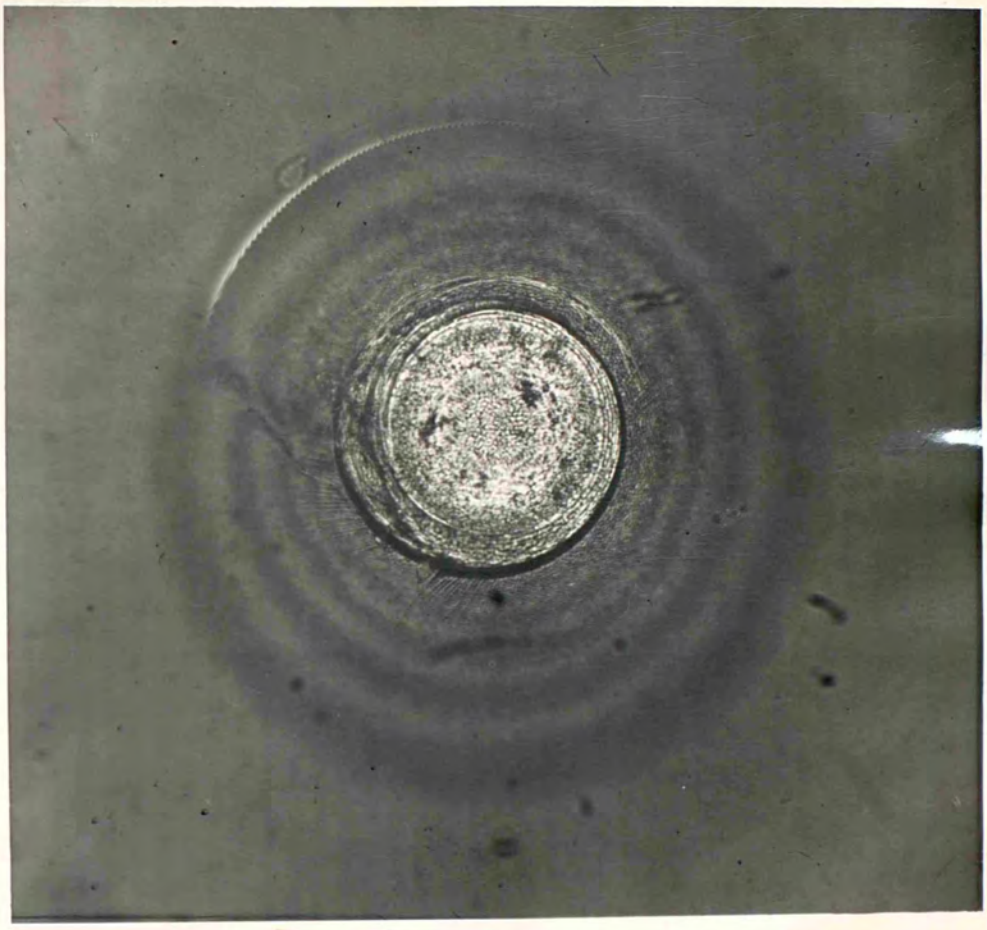

Fig 23 x 165

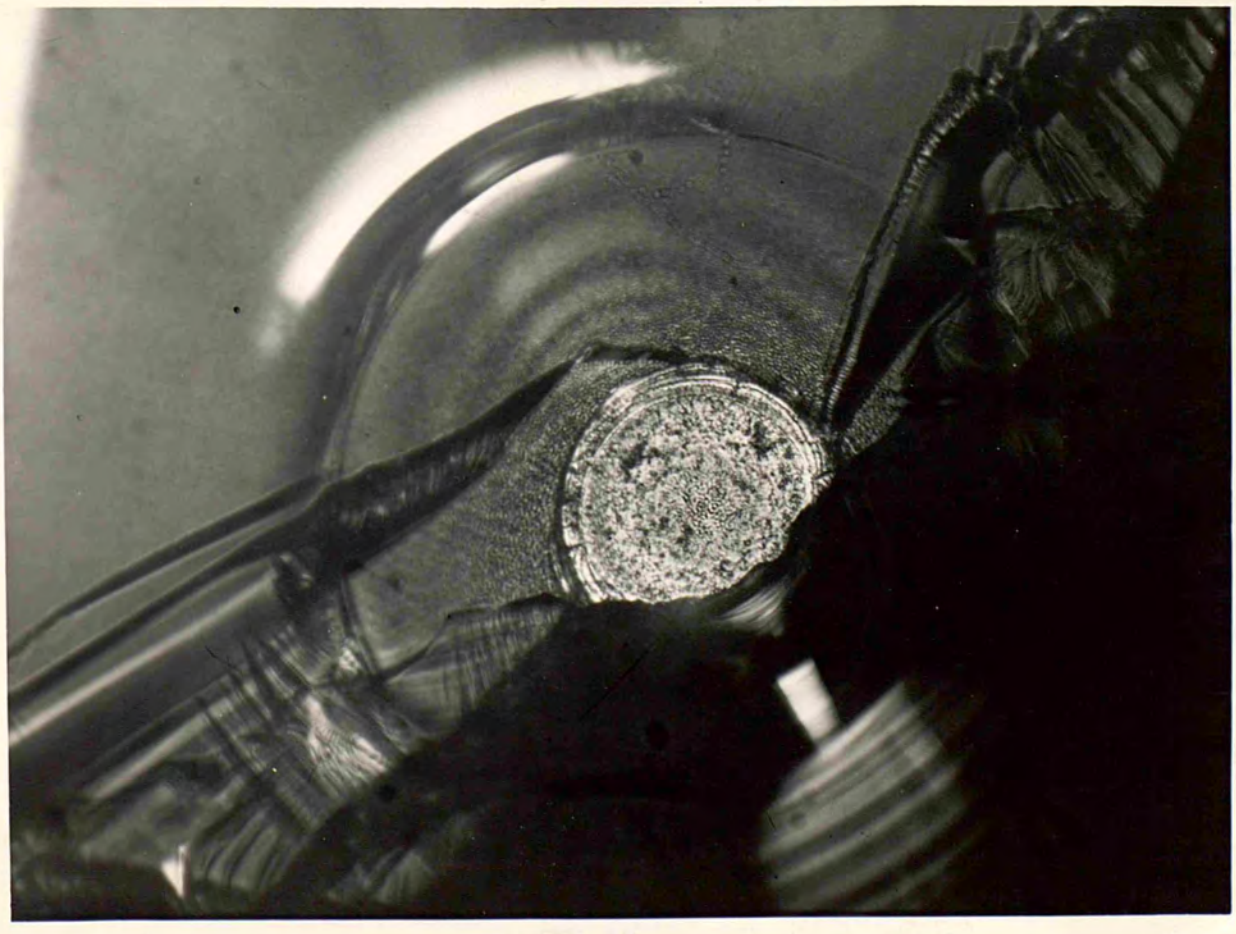

that - if the disc did not fracture - when the load was removed, the fringes shrink towards the centre and disappeared as the load was gradually reduced to zero, indicating that the crack is closing up. This differs from Raman's observations (1920) for dynamic percussion marks, where such interference fringes can clearly be seen inside the crack when the glass block is observed after the test. To verify that the Hertzian cone crack still existed after it became invisible, a typical ring crack was viewed from the side. The crack was made on a piece of plate glass with a clean flat-faced edge to it, near the edge. Afterwards the piece of glass was stood on end and its edge microscopically examined by transmitted light. Fig.24 shows that ring crack as it was here seen (Raman (1920) was the first to show such photographs). The curving surface of the Hertzian cone reflects incident light away so that the crack outline is dark when observed in transmission.

## 4.6 The Study of Fracture faces produced

A short investigation was made of the nature of the fracture faces formed when a disc fractured from a ring crack. A disc was chosen where a ring crack had formed and had then developed into a clean fracture of the glass into just two pieces. The regions of the two pieces with the ring crack on them can be seen in Fig.25. The fracture face of the piece shown in the top of this photograph is seen in Fig.26, and Fig.27 shows the other corresponding fracture face. Both photographs are taken just of the region near to the surface

Fig 24 x 135

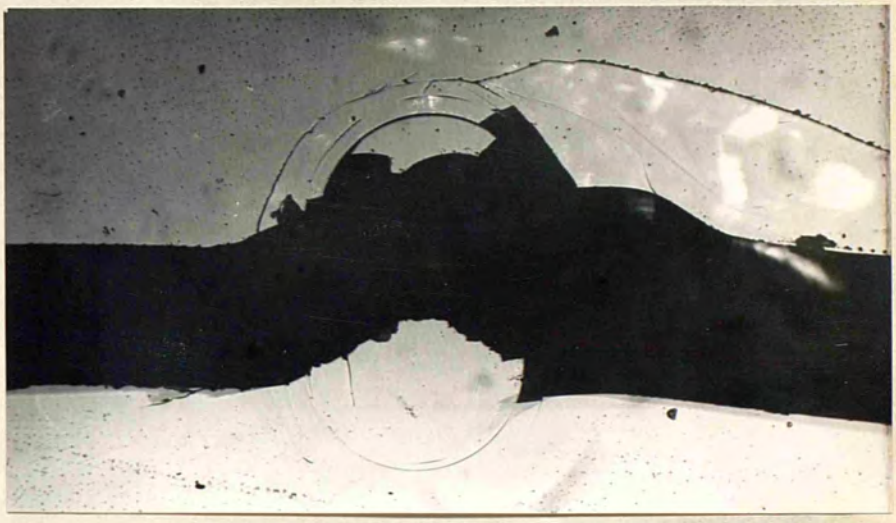

Fig 25 x 65

Fig 26 x 15

Fig 27 x 15

ring crack, and it must be mentioned that fracturing did not occur perpendicular to the disc faces. The fracture developed from the Hertzian cone crack already present, thus breaking the disc into two pieces having complicated conchoidal faces, one convex and the other concave, in the vicinity of the ring crack, but the curvature becoming less pronounced towards the outer regions of the fracture surfaces. It can be seen in the two photographs of these surfaces that immediately below the ring crack their exists a breakage front of mirrorlike smoothness, beyond this on either side are curving concentric tracks spreading away from the ring crack. It is also seen that considerable disruption has occurred directly opposite the ring crack at the other face of the disc: it is believed that this is initiated at the reflexion of the elastic shock-wave, which passes through the thickness of the disc immediately fracture begins.

The curving tracks are also thought to be the result of elastic shock waves occurring in a similar manner to the circular arc lines seen and used by Smekal (1953) on pre-stressed fractured glass rods - being the interaction of the fracture 'break fronts' and the transverse elastic shock waves spreading from the initiation point (Smekal used these line tracks to determine the velocity of fracture, knowing the velocity of elastic waves in glass). It is noteable that there is a correspondence between the dispositions of these lines on the two faces, which can be clearly seen for

example on the left side of Fig.26 and the right side of Fig.27; here the first line, from the central region below the ring crack, has a trailing edge, the second is single, the third is a doublet, the fourth develops into three at the bottom and so on in similarity.

This actual fracture is an example of the true strength relationship well known in glass phenomena. The ring crack was initiated at 20 kgm. by a $\frac{1}{4}$" steel spherical impactor, the load was then increased up to the maximum of 30 kgm. but it was several seconds after this that fracture occurred.

## 4.7 Visibility of Ring Cracks in Glass

During the testing already described it was very often noticed that after a fine primary crack had been produced at a low load, as the load was slowly released the crack completely closed up becoming quite invisible: after the tests these cracks could not be found by microscopic examination of the surface. If the required critical load for initiation was high so that the stress release was large on cracking, or if multiplicity developed, then the produced ring crack did not disappear and was subsequently quite easy to find in the surface. To check that this was merely due to closing up of the two surfaces and not to any actual joining up, an etching test was made. A steel ball of $\frac{1}{4}$" diameter was impacted on a glass disc until a ring crack was just initiated, eight tests were made and the

respective critical loads were 25 kgm, 19 kgm, 20 kgm. 14 kgm. 17 kgm, 18 kgm. 26 kgm. and 21 kgm, the increase in load being stopped as soon as the crack appeared and then reduced to zero. Afterwards the disc was examined and only two figures could be seen on its surface, the first and the seventh ring cracks. The specimen was then etched in 50% Hydrofluoric Acid for 15 hours and observed microscopically once more, Fig.28 shows the etched surface and all eight ring cracks are here visible being made so by preferential etching at the existing crack on the surface.

This is of particular interest with respect to diamond where it is often found that in the first stages of etching natural octahedral faces the first small etch pits occur in 'contiguous chains of very small pits distributed in a specifically oscilitated manner usually based on a hexagon pattern' (Omar, Pandya and Tolansky 1954). It is then concluded by the author that this is due to preferential etching around natural hexagonal pressure figures, similar to those found by Tolansky and Halperin (1954(, which before etching have been invisible to direct optical observation. This conclusion is fully substantiated by the above experiment for ring cracks on glass.

## 4.8 Discussion

The study of the surface distortions accompanying ring cracks on glass indicates that there is a micro-plastic flow

Fig 28 x 6

of the material around the perimeter of the crack, and the depression of the central area within the crack, which is to be found in most cases of multiple ring cracks, reinforces this evidence

The surface distortion shown up by the interferograms across the various ring cracks indicates that there is a distinct volume of glass raised up above the level surface; this is believed to be accounted for by the volume of the surrounding crack in the material, together with the volume amount of the central area depression, where this occurs. Where it does occur, the cracks are always multiple - the corresponding displaced volumes being correspondingly greater.

The mechanism of the actual cracking is seen to be dependant on the stress release. Where this is small, cracking occurring at a low value of applied load, the mechanism of the production of the Hertzian cone crack into the bulk of the material is seen to be reversable - the crack closing up as the load is released. If the stress release is large at cracking the process is irreversible and the crack remains. However this applies only to the crack line appearing on the surface as it has been clearly seen that the cone crack shown up by interference fringes while specimen is under load, always closed up for the static tests carried out. The reason for the visibility of the surface crack is probably due to the permanent plastic deformation at the surface referred to above, which occurs when the strain release is sufficient; while

the deformation on either side of the cone crack down in the material is still elastic, so that on reduction of the load the two sides will recover although they cannot join. That they do not join is well illustrated by the etching test.

It is also seen that if cracking does not occur until there is considerable stress applied, there is increased danger of the ring crack, finally formed, developing suddenly into complete fracture of the specimen. Then this does happen it is violent and shock waves are evident by the line tracks observed on the fracture faces.

In spite of the much larger scale of the distortions obtained by Raman for percussion marks, it is seen that for dynamic tests, the surface distortions are of the same order as for the static tests when the force used in each case is that which is just sufficient to produce a primary ring crack (i.e., when the scale of the experiments is the same).

# CHAPTER V

# INVESTIGATION OF THE FRACTURE STRENGTHS OF TEN DIFFERENT GLASSES

## 5.1 Introduction

Following from the experiments described in the last chapter, an investigation into the ring crack phenomena was undertaken for 10 different types of glass. These are listed below together with the respective letters, in brackets, by which reference is made to particular glasses throughout this Chapter.

Medium Barium Crown (MBC)

Borosilicate Crown (BSC)

Hard Crown (HC)

Zinc Crown (ZC)

Barium Flint (BF)

Light Flint (LF)

Extra Light Flint (ELF)

Telescope Flint (TF)

Dense Flint (DF)

Double Extra Dense Flint (DEDF)

The specimens of these glasses were in the form of discs of approximately 1.5 mm. thickness, which were well polished, flat on both sides and parallel faced. Approximately 15 separate tests were done on each specimen in order to allow for the well known scatter characteristics of quantitative measurements on glass. For these tests, the impactor, mounted in the

mechanically driven Penetrascope instrument, was a 1 mm. diameter Tungsten Carbide sphere. The applied loads, which were increased gradually from zero at a constant rate of $\frac{1}{2}$ kgm/sec (see Chapter 2) until a primary ring crack was initiated, were in the range of 1 - 12.5 kgm.

The chemical compositions of the different glasses are given in Table 1, and comparisons are made between details seen in the table, the results of the impact tests, and other physical properties of the different glasses.

## 5.2 Experimental Results

As soon as a primary ring crack was initiated, in each test, the increase in load was stopped, and the diameter of the circle of contact was measured by means of an eyepiece graticule. The load was noted and then reduced to zero, the next test being done well away from the region of the first test so that the series of tests on the same disc were quite independent of each other. The results of this series of tests are given in Table 2, but it is to be remembered that the stress values obtained are dependent upon the thickness of the specimens impacted and thus (because of the elastic bending of the relatively thin discs used in this study by microscope), are only significant for the 1.5 mm. disc specimens; it is for this reason that the order in which the 11 specimens occur is more interesting in terms of strength comparisons than the actual stress values obtained for each specimen. In the table each square gives the values for

TABLE 1

TABLE OF GLASSES

PERCENTAGE COMPOSITION

| Glass Type | Silica | Lime | Soda | Potash | Alumina | Boric Oxide | Antimony Oxide | Arsenic | Barium Oxide | Lead Oxide | Zinc Oxide |
|---|---|---|---|---|---|---|---|---|---|---|---|
| MBC.572577 | 47.9 | | 3.2 | 3.6 | 0.5 | 8.4 | 0.1 | 0.3 | 24.5 | 1.6 | 9.9 |
| BSC.510644 | 71.8 | | 4.0 | 15.4 | 0.6 | 7.5 | 0.4 | | | | 0.3 |
| HC.517606 | 73.5 | 9.3 | 8.8 | 6.2 | 0.1 | 1.2 | | 0.7 | 0.2 | | |
| ZC.508612 | 64.8 | | 7.9 | 0.4 | 4.4 | 11.7 | | 0.5 | | | 10.3 |
| BF.605438 | 46.1 | | 2.5 | 4.9 | 0.1 | | 0.8 | 0.5 | 16.7 | 22.3 | 6.4 |
| LF.575426 | 55.1 | | 5.1 | 3.9 | 0.1 | 1.6 | | 0.5 | 0.6 | 32.9 | 0.2 |
| DF.620362 | 45.4 | 0.3 | | 6.65 | 0.2 | | | 0.25 | | 47.2 | |
| TF.525511 | 70.0 | | 12.9 | 0.5 | 0.9 | | 6.1 | | | 9.6 | |
| ELF.542474 | 63.2 | | | 12.1 | 0.1 | | | 0.2 | 1.7 | 22.7 | |
| DEDF.748278 | 31.9 | | | 1.7 | 0.04 | | | 0.1 | | 66.3 | |

TABLE 2

| Glass | 1 | 2 | 3 | 4 | 5 | 6 | 7 | 8 | 9 | 10 | 11 | 12 | 13 | 14 | 15 | 16 | 17 | Average | Standard Deviation For Stress |
|---|---|---|---|---|---|---|---|---|---|---|---|---|---|---|---|---|---|---|---|
| | 2.1 | 1.8 | 4.2 | 7.1 | 2.0 | 1.2 | 1.3 | 2.2 | 7.1 | 2.0 | 4 | | | | | | | 3.2 | |
| MBC | 20 | 18.5 | 24.5 | 28 | 20 | 17.5 | 18 | 20.5 | 29.5 | 20 | 25 | | | | | | | 22 | |
| | 216 | 217 | 289 | 374 | 206 | 162 | 166 | 216 | 336 | 206 | 277 | | | | | | | 240 | ± 60 |
| BSC | 1.7 | 4.0 | 2.5 | 3.3 | 2.1 | 5.8 | 8.2 | 2.8 | 6.8 | 6.3 | 2.4 | | | | | | | 4.5 | |
| | 19 | 24.5 | 21 | 23 | 20 | 27 | 31.5 | 22 | 28 | 28 | 21 | 31 | | | | | | 25 | |
| | 194 | 275 | 234 | 258 | 217 | 328 | 341 | 239 | 358 | 332 | 225 | 344 | ±57 | | | | | 280 | ± 50 |
| | 2.2 | 7.3 | 1.2 | 1.8 | 5.1 | 2.9 | 1.2 | 2.2 | 4.0 | 7.9 | 6.9 | 5.4 | 5.4 | | | | | 4.1 | |
| HC | 21 | 29.5 | 18 | 19.5 | 26 | 22 | 17.5 | 21 | 24 | 30.5 | 29 | 27 | 27 | | | | | 24 | |
| | 206 | 346 | 153 | 195 | 312 | 243 | 162 | 206 | 287 | 351 | 338 | 306 | 312 | | | | | 265 | ± 70 |
| | 3.8 | 8.0 | 1.4 | 1.2 | 1.3 | 3.2 | 7.6 | 2.3 | 6.2 | 4.7 | | | | | | | | 4.0 | |
| ZC | 25 | 31.5 | 20 | 19 | 19 | 24 | 31 | 21.5 | 29 | 26 | | | | | | | | 24.5 | |
| | 251 | 332 | 144 | 137 | 148 | 230 | 326 | 205 | 304 | 287 | | | | | | | | 235 | ± 70 |
| | 7.0 | 1.0 | 4.1 | 3.5 | 1.2 | 2.8 | 3.8 | 6.0 | 7.4 | 3.6 | 2.2 | 4.2 | 3.3 | 3.3 | 6.7 | 1.8 | 4.9 | 4.0 | |
| BF | 30.0 | 17.5 | 26 | 25 | 19 | 24 | 25 | 30.5 | 33.5 | 25 | 20 | 28 | 24.5 | 24.5 | 31.5 | 20 | 27 | 25.5 | |
| | 321 | 135 | 251 | 231 | 137 | 201 | 251 | 266 | 272 | 238 | 227 | 221 | 227 | 227 | 270 | 186 | 277 | 230 | ± 40 |
| | 3.5 | 5.9 | 2.6 | 1.2 | 4.9 | 1.2 | 2.3 | 1.1 | 2.4 | 1.2 | 5.4 | 2.0 | 5.8 | 6.6 | 2.0 | | | 3.2 | |
| LF | 24.5 | 29 | 23 | 18 | 27 | 18.5 | 22 | 18.5 | 23 | 18.5 | 29 | 21.5 | 30 | 31 | 21 | | | 24 | |
| | 241 | 290 | 203 | 153 | 277 | 145 | 196 | 132 | 187 | 145 | 265 | 178 | 266 | 284 | 187 | | | 220 | ± 50 |
| | 11.1 | 4.8 | 3.9 | 5.3 | 5.2 | 3.2 | 2.5 | 3.8 | 3.0 | 3.1 | 9.2 | 9.0 | 4.3 | | | | | 5.3 | |
| ELF | 36.0 | 28 | 26 | 29.5 | 29 | 25 | 23 | 26 | 24 | 24.5 | 34 | 34 | 27 | | | | | 28 | |
| | 354 | 262 | 238 | 251 | 255 | 211 | 195 | 232 | 215 | 213 | 329 | 321 | 243 | | | | | 255 | ± 50 |
| | 4.1 | 6.9 | 2.8 | 4.7 | 10 | 12.4 | 10.9 | 6.8 | 7.2 | 3.0 | 5.5 | 11.1 | 2.5 | | | | | 6.8 | |
| TF | 27 | 31.5 | 28.9 | 27.5 | 34.5 | 38.5 | 35 | 31 | 32 | 24.5 | 30 | 37 | 23 | | | | | 30.5 | |
| | 231 | 287 | 209 | 256 | 347 | 334 | 368 | 292 | 290 | 207 | 252 | 334 | 195 | | | | | 275 | ± 50 |
| | 5.0 | 2.9 | 2.8 | 1.0 | 2.7 | 5.8 | 2.0 | 1.2 | 3 | 1 | 2.75 | 2.9 | 1.5 | 1.5 | 1.2 | 4.0 | 3.1 | 2.6 | |
| DF | 29 | 24 | 24 | 18 | 24.5 | 30 | 22 | 19 | 25 | 18 | 24 | 24 | 20.5 | 21 | 18.5 | 27 | 25 | 23 | |
| | 245 | 208 | 201 | 127 | 186 | 249 | 170 | 137 | 198 | 127 | 197 | 208 | 147 | 147 | 145 | 226 | 204 | 185 | ± 40 |
| | 1.2 | 1.2 | 1.5 | 2.0 | 1.8 | 1.5 | 1.8 | 1.2 | 1.1 | 1.1 | 1.2 | 1.1 | 1.05 | 1.9 | 3.4 | | | 1.5 | |
| DEDF | 20 | 20.5 | 21.5 | 24 | 23 | 21.5 | 22.5 | 20 | 19.5 | 19.5 | 20 | 19.5 | 19 | 22 | 26.5 | | | 21.5 | |
| | 124 | 118 | 134 | 143 | 140 | 134 | 140 | 124 | 119 | 119 | 124 | 119 | 120 | 162 | 200 | | | 135 | ± 20 |

one test, at the top is the critical load in kgm., then there is the area of contact in divisions of the eyepiece graticule used, and at the bottom is the calculated average stress over this area at which cracking is initiated in, kgm/sq mm. In the last column but one is given the average values of the three quantities. The experimental error in determining the stresses is in the order of 5% which amounts on average to about 10 kgm/sq mm. It is seen that a great deal of scatter occurs in these results in spite of the high degree of control in the experimental procedure, this however is very common in any quantitative measurements on glass and 'such variations are invariably large and are inherent in glass' (Haward 1949). In such cases it is standard practice to give the standard deviation for the results, and in the last column these are given for the stress values determined for each glass. The sequence of the different glasses in order of critical average stress values is given in column A of Table 3, the glass with the greatest value being at the top.

Apart from the strength information gained in these tests, it is also interesting to note that they give an indication of the elastic properties of the different glasses also (this is a secondary consideration of this investigation and is dealt with here only qualitatively). If for each set of results a graph is drawn of 2 ac (diameter of the area of contact) against the corresponding value of pc (critical stress), then for each glass a different straight line is obtained as shown in Fig.29; where the thick parts of each line show the region

where the experimental points lie and the thin parts are the extrapolations of these lines to the region of the origin of the graph. The straight lines are to be expected, from the Hertz Theory for elastic deformation only (see Chapter 1), since the critical values at cracking are just the last of the series of values for the preceding elastic deformation; thus even if in subsequent tests cracking occurs later, the values will still obey the elastic theory. Accepting the above explanation of the straight lines, these should then pass through the origin; that they do not is probably on account of a constant zero error in the values of 2 ac due to the presence of a Newtons Rings dark spot existing between ball and surface even before there is contact and consequent stress. However, the lines should definitely all pass through one point even if this is indeterminant theoretically. They do not pass through one point, and the only explanation of this is that there have been errors in plotting of the straight lines due to the large scatter existing in the experimental results (each set of results was considered separately, the best possible straight line being drawn in each case, independantly), unfortunately this cannot be corrected since the position of the true origin is unknown.

From the Hertz Theory, using the same ball impactor in all the tests, the slope of the straight lines considered gives a measure $\left(\frac{1-\sigma^2}{E}\right)$ for each glass (see Chapter 1)

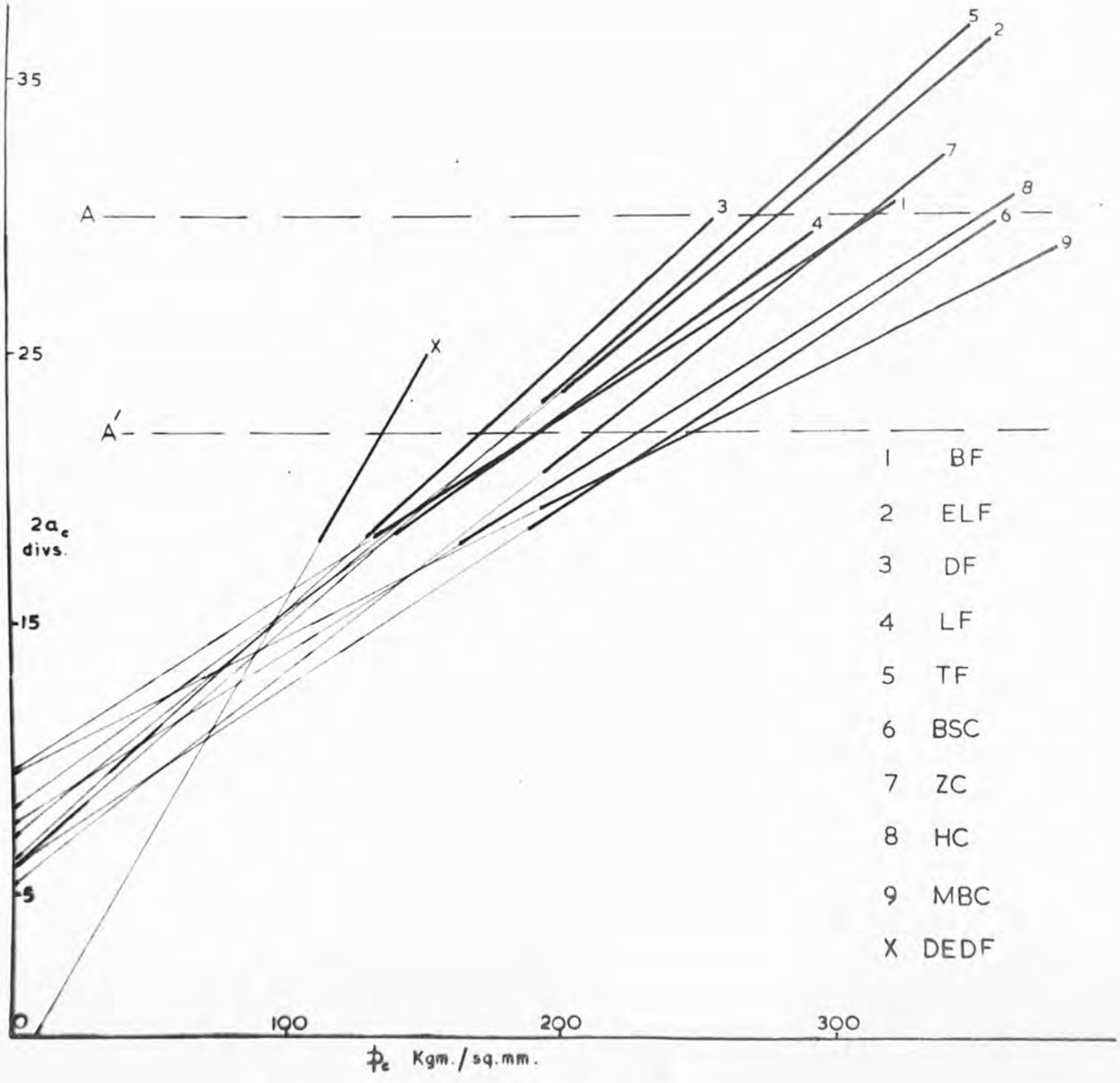
35
25
15
5
0
A
A'
2a_c divs.
100
200
300
P_c Kgm./sq.mm.
1 BF
2 ELF
3 DF
4 LF
5 TF
6 BSC
7 ZC
8 HC
9 MBC
X DEDF

Fig 29

From the graph, the most accurate determination of the order in which the values of the slopes occur, is obtained from the order in which the straight lines occur across the graph, the line farthest on the right having the least slope. This order is the same over a very large portion of the range of values for which cracking occurs for the glasses (between the lines A and A' on the graph) and is seen in column B of Table 3. where glass MBC, being the most resistant at any chosen area and thus farthest to the right, is at the top - the slope of the line being least.

The reason why this method of obtaining the order of the slopes is more accurate than a straight forward ordering of the numerical values of each slope is because of the inevitable errors in drawing each line through its points, due to the large scatter of the latter. Since all the lines should pass through one point then the order in which they occur is a measure of the true slopes, whereas the lines themselves, although occurring in this order, may have erroneous slopes due to the finite angle of error obtaining to the drawing of a line through experimental points which have a considerable amount of scatter.

It is seen that the sequences in column A and B of Table 3 are not the same: differences and comparisons will be discussed in the next section

5.3 Comparison with other Properties for the Glasses.

This is confined to the differences in relative position of the types of glass in tables giving the order of the glasses for several different physical qualities: the actual values of these quantities are not considered.

Since the formation of ring cracks is one way of investigating the strength or fracture resistance of glasses, the other qualities discussed are concerned with strength or hardness. The relative positions in each case are given in the columns of Table 3 the details of which are given below.

A. The fracture strengths from ring crack criteria. Gives the sequence of the averages of the critical average stresses necessary for the initiation of ring cracks on the glasses, obtained from the experiments already described. The glass with the greatest value is at the top.

B. The elastic qualities of the glasses, derived from the straight line graphs just described. The order in which the lines occur in the graph from right to left gives the inverse order of the magnitude of the respective slopes; the inverse of the slope value is a measure of $\left(\frac{E}{1-\sigma^2}\right)$ where E is Youngs Modulus and $\sigma$ is Poisson Ratio, for each glass. The glass with the largest value of $\left(\frac{E}{1-\sigma^2}\right)$ is at the top.

C. The sequence of glasses for values of Youngs modulus. The actual values of E in kgm/sq.mm. are 7580, 7540, 7230, 6210 and 5490 for glasses MBC, BSC, HC, LF and DEDF respectively. These values were supplied by Chance Brothers Ltd. in a

TABLE 3

| A | B | C | D | E | F | G |
|---|---|---|---|---|---|---|
| BSC | MBC | MBC | MBC | BSC | HC | HC |
| TF | BSC | BSC | BSC | HC | ZC | BSC |
| HC | HC | HC | HC | TF | TF | TF |
| ELF | ZC | | ZC | ZC | BSC | ZC |
| MBC | BF | | BF | MBC | ELF | ELF |
| ZC | LF | LF | LF | ELF | LF | LF |
| BF | ELF | | DF | BF | MBC | MBC |
| LF | TF | | TF | LF | BF | BF |
| DF | DF | | ELF | DF | DF | DF |
| DEDF | DEDF | DEDF | DEDF | DEDF | DEDF | DEDF |

private communication, and are the only values available out of the glasses under investigation. The glass with the highest value is at the top of the column.

D. The micro indentation hardness for the glasses. The Vickers Diamond Pyramid hardness values were obtained by Taylor (1949) using a micro hardness tester, the indentor of which was a normal diamond pyramid. The actual values are in Taylor's paper the order is given here with the 'hard est' glass at the top.

E. The surface hardness for the glasses. This is a statistical hardness measurement achieved by abrading the surface of the glass with falling carborundium particles and measuring the resulting effect. This method, described fully in the Appendix to this Thesis, has been devised by the author. The glass with the highest surface hardness value is at the top of the column.

F. The Grinding hardnesses for the glasses. These values were obtained by Willott (1950) and are given in his paper. They are derived from the amount of glass ground away in equal timesfor each glass. At the top is the glass having the largest 'grinding hardness'.

G. Percentage amounts of Silica present in each glass - the actual values are given in Table 1 showing the chemical composition of the glasses. The glass with the greatest amount of silica present is at the top.

## 5.4 Discussion

The following information is obtained from comparisons made in Table 3 for the ten different glasses investigated.

(1) There is evidence of a relation between the silica content of the glass and the Grinding hardness as found by Willott (columns G and F). The surface hardness order also conforms roughly with that of the silica content. From these three columns it would seem that the wear properties of any glass definitely depend upon the amount of silica in its composition.

(2) There is a better relation between sequences for surface hardness and Grinding hardness (columns E and F) than between sequences for the former and Vickers indentation hardness (column D). This illustrates that the surface hardness measurements are for an abrasive action of chipping the glass away, rather than a plastic deformation action.

(3) That fracture rather than deformation takes place in the surface hardness measurements is strongly indicated by the relation seen between this order and the order for the average critical stresses (columns A and E) which gives the order of fracture strengths.

(4) It is strikingly obvious that Taylors indentation hardness measurements are distinctly related to the elastic properties of the glasses (columns B and D) The sequences for the values derived from the micro plastic deformation and for the values of $\left(\frac{E}{1-\sigma^2}\right)$, as obtained from the graph

of Fig.29 are almost exactly the same. It is also to be noted that the order of the five values for the Youngs modulus is the same as that found in column B for the sequence pertaining to the values of $\left(\frac{E}{1-\sigma^2}\right)$ .

(5) There are several distinctive features in the properties of the different glasses. The elastic properties and the indentation hardness of MBC glass are greater than for any other glass, yet its fracture strength and surface hardness values are quite low compared with other glasses, being approximately in the middle of the sequences for these properties (columns A and E). The amount of silica this glass contains is also relatively low. Conversely the fracture strengths and the surface hardnesses of TF and ELF glasses are relatively high, while it is seen that for both of these the values of $\frac{E}{(1-\sigma^2)}$ and the indentation hardness are low compared with values for the other glasses (columns B and D). In this case the silica content is high.

(6) There are several glasses for which the relative positions in the sequences are the same for <u>all</u> of the different properties considered. These positions are low for DEDF, DF and LF glasses, and are high for BSC and HC glasses. It can be generally stated that, with the exception of Telescope Flint and Borosilicate Crown glasses, the crown glasses have greater values of the different properties considered than the Flint glasses.

# CHAPTER VI

# OPTICAL STUDY OF PRESSURE FIGURES ON THE OCTAHEDRAL FACE OF DIAMOND

## 6.1 Introduction

This work follows on directly from the investigation of ring cracks on glass by Tolansky and Howes (1954) and from the observations of Tolansky and Halperin (1954) of markings on octahedral faces of diamonds, conjectured to be pressure cracks, similar in origin to the ring cracks on glass. From there, it was decided that this experimental study of the artificial production of pressure figures on the octahedral face of diamond should be carried out.

A flat portrait stone was chosen - being a plane parallel plate form modification which arises from the over-development of a pair of oppositely placed octahedral faces. These faces being parallel, and the stone being completely transparent, this was an ideal specimen for the technique of simultaneous observation during application of the load.

The face selected for the experiments is seen in Fig.30. It is hexagonal in outline and the lower half is covered with growth sheets. The upper portion of the face is very smooth and unmarked except for a few trigon growth pits and several natural impact figures which can just be seen. Some of these are seen with higher magnification in Fig.31 and 32 and are of interest for the sake of comparison with those produced artificially. There were about 10 such natural features,

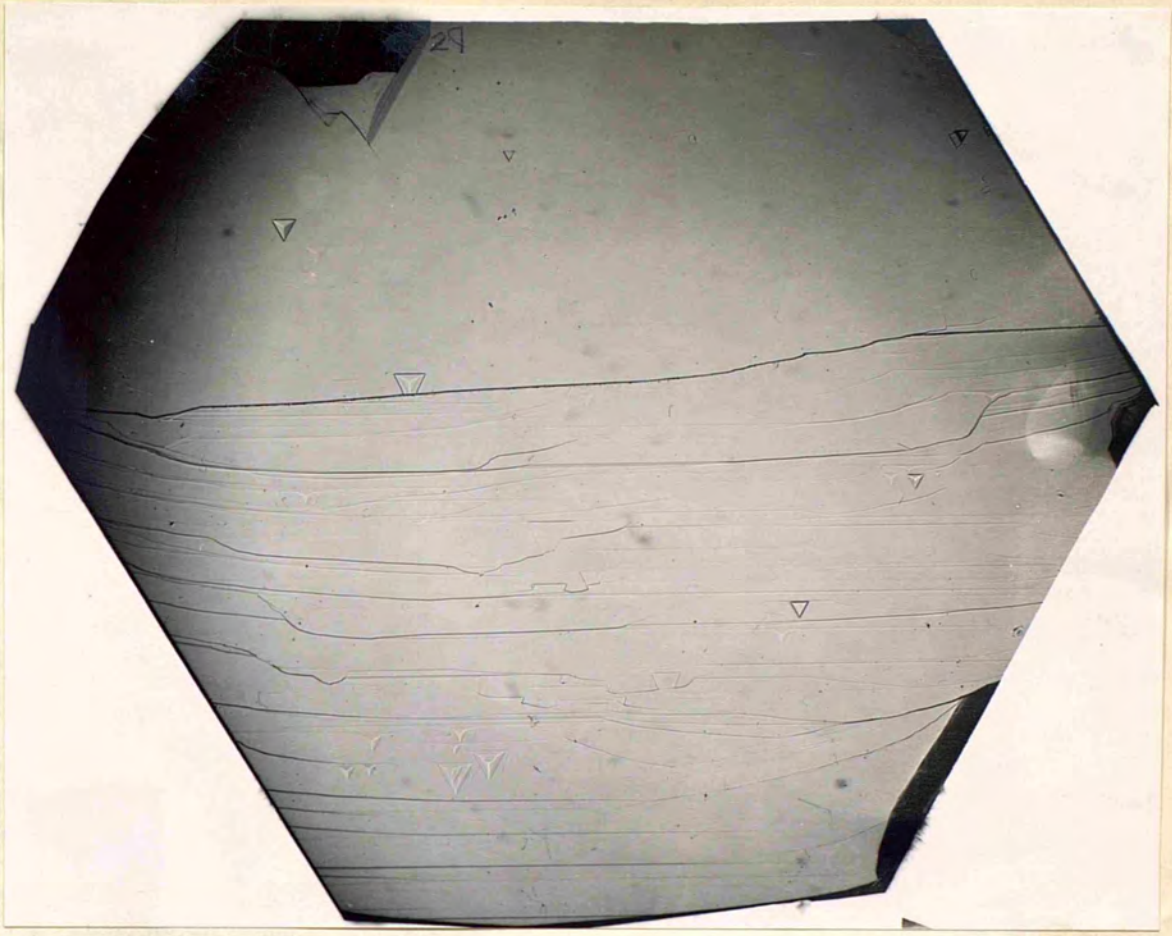

Fig 30
X30

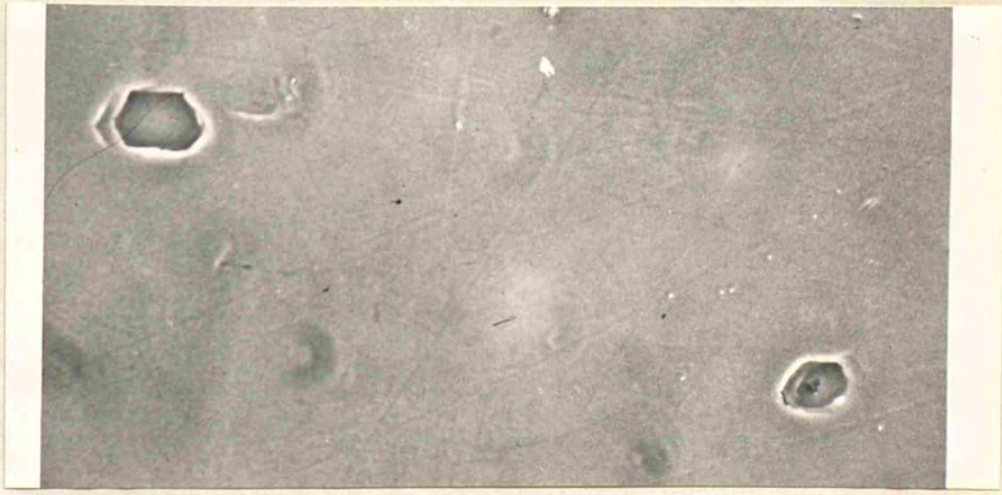

Fig 31 x 305

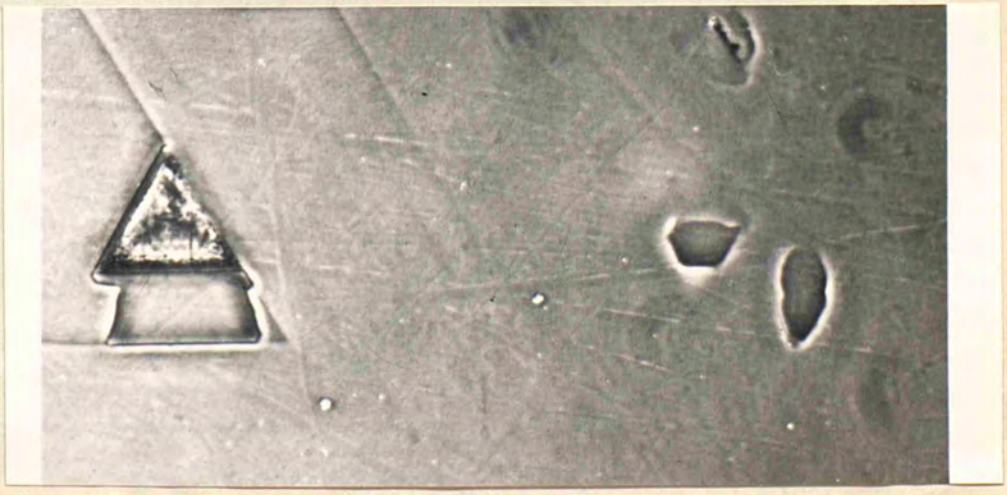

Fig 32 x 305

none as regular as those produced artificially and all much smaller in extent on the surface - which agrees with the conjecture that they were produced in the natural surroundings by impact on the surface (either static or percussive) of small neighbouring points or corners of other stones. However, it is to be noted that contrast-changes at the edge of both natural and artificial features are of the same order - see the phase contrast photograph of Fig.33, which would seem to indicate that the topographical distortion in each case is similar. This is in agreement with results found on glass for static and dynamic impact figures (Tolansky and Howes 1954) where height distortions were of the same order for primary ring cracks of completely different size and origin.

6.2 The Hexagonal Figures produced on the Octahedral surface

Application of a gradually increasing load leads to the formation of a regular hexagonal shaped pressure figure which is a completed crack with sides orientated parallel to the sides of the familiar growth trigons. The initiation of the crack is sudden.

Four of these pressure figures are seen in Figs.34,35 36 and 37. The first (Fig.34) appeared at a load of 6 kgm. following a slow increase from zero (the disturbance seen in the centre of the figure is due to the scratching off of the silver at this place). The second (Fig.35) appeared at 10 kgm. load. A further increase to 12 kgm. was applied before

Fig 33 x 190

Fig 34 x 525

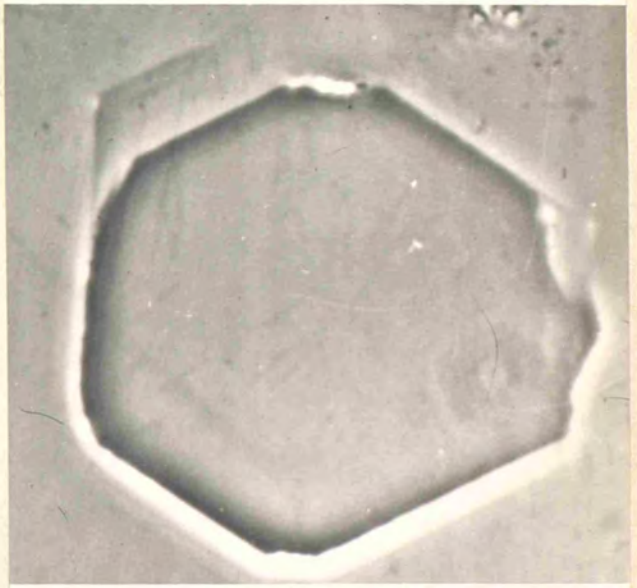

Fig 35 x 525

Fig 36 x 525

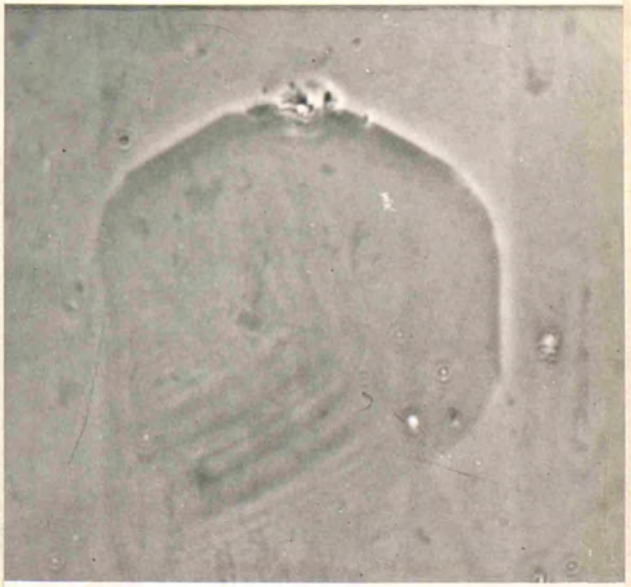

Fig 37 x 525.

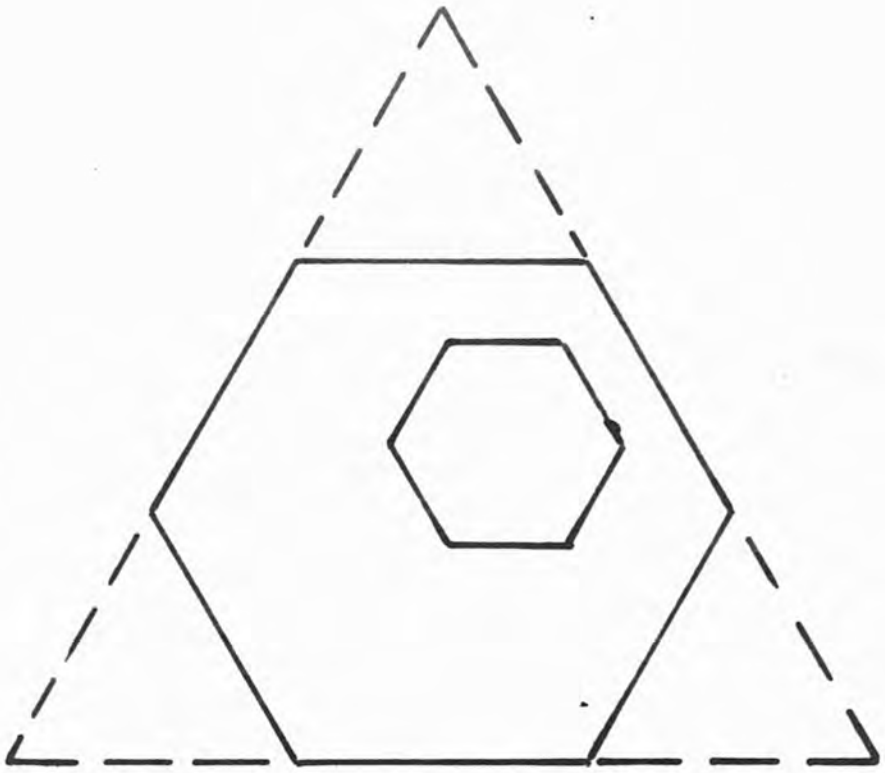

Fig 38.

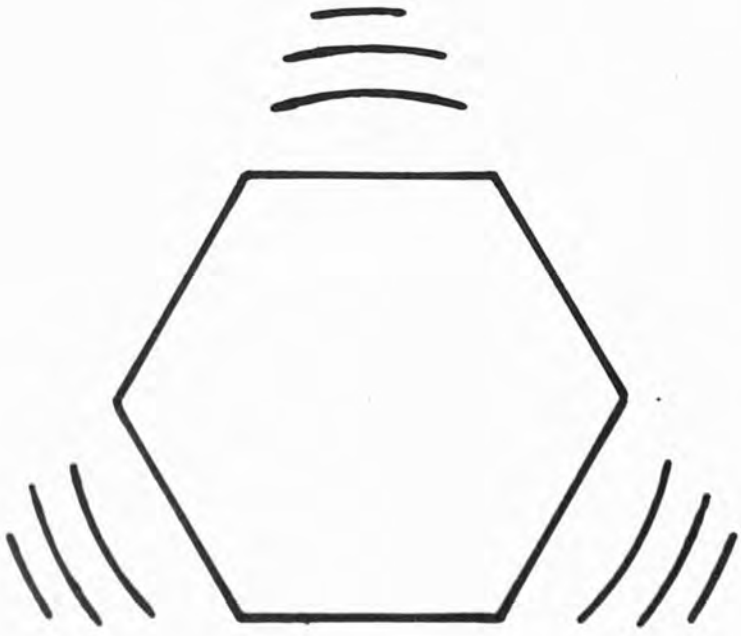

Fig 56

final release. The original hexagon became distorted a little and a multiple crack began to form. The third crack (Fig.36) appeared at 7 kgm., the load being increased very rapidly from zero in this case. For the fourth crack (Fig.37) the load was increased very slowly and was released rapidly the moment it was seen that cracking had begun (the critical load was not determined in this case) - thus the stress was released before the crack could complete the circuit. This establishes that crack does not automatically run to completion once initiated, but requires application of pressure for a specific period before completion occurs. It implies that there is some specific single point of initiation from which the crack develops travelling at a finite velocity - this must be some sort of highly localized surface weakness.

The orientation of all these pressure cracks relative to the edges of the octahedral face is the same and is shown schematically in Fig.38. (The broken outline represents the completed (111) octahedral face of which the face of the stone is part).

## 6.3 The Development of a Pressure Figure

The fifth and sixth crack features on the octahedral face were produced with a slowly increasing load - photographs being taken at different stages of development while the load was being applied. The black circular area seen in Fig.39 is the region of contact for a load of 0.5 kgm (i.e., the central black spot of Newton's Rings) and this is faintly

surrounded by a small number of interferenge fringes. As the load is increased the area of contact enlarges and Fig.40 shows the contact for 2.3 kgm. load. At 5 kgm. a crack appeared around the perimeter of the circle of contact and just outside it, as shown in Fig.41. The crack is a regular orientated hexagon and is seen now as white. Not only is the circular region of contact within the hexagon dark but there are three rounded dark regions opposite three of the sides of the hexagon. On removal of load the dark areas vanish leaving only the crack outline, which can be seen in Fig.42.

This phenomenon is typical. Thus Figs.43 and 44 show successive developments at loads 3.5 kgm. and 12 kgms for another crack (which began at 3.5 kgm) and once more the surrounding rounded triangular dark region is seen. The area of this region is effectively proportional to the load. As the portrait was less than 1 mm. thick it was considered unwise to increase the load still further in case complete fracture occurred, so it was reduced. At 1.5 kgm. the appearance was that shown in Fig.45 - the 3 dark regions rapidly shrinking inwards, and after complete removal it can be seen in Fig.46 that excessive loading has resulted in multiple or compound cracking which is characteristic of the phenomena. Of these multiple cracks, it is to be noted that the first inner one is the primary crack of Fig.43 and that the others have developed later as the load was increased

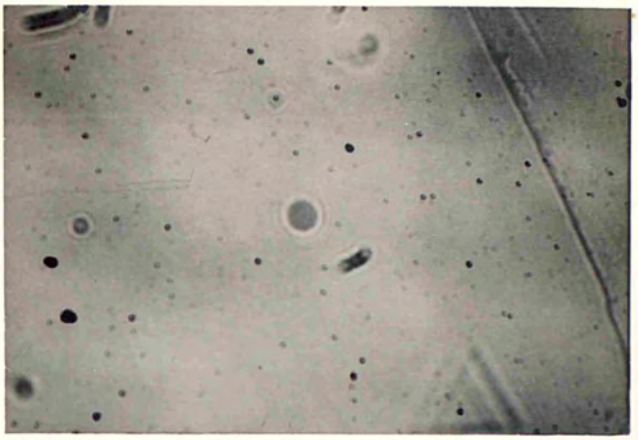

Fig 39 x 125

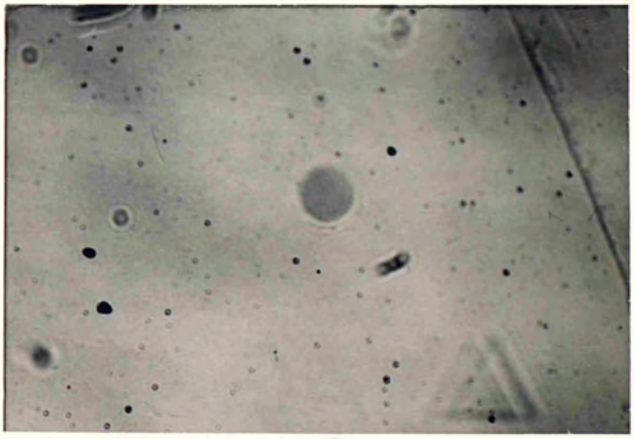

Fig 40 x 125

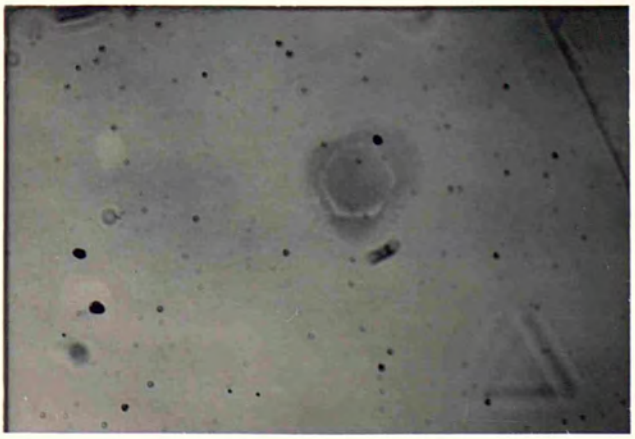

Fig 41 x 125

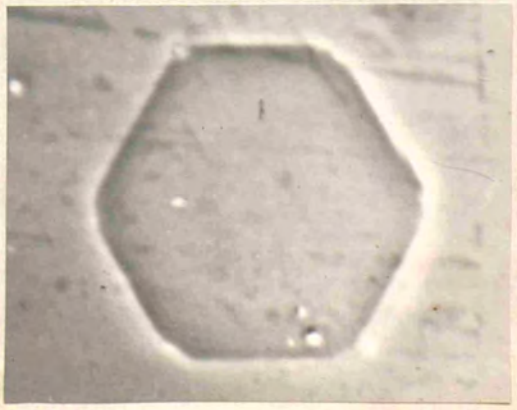

Fig 42 x 525

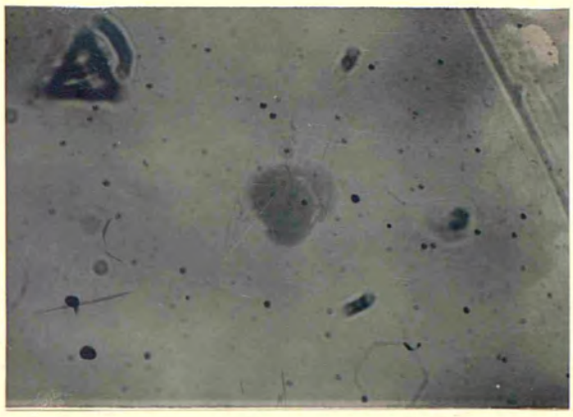

Fig 43 x 125

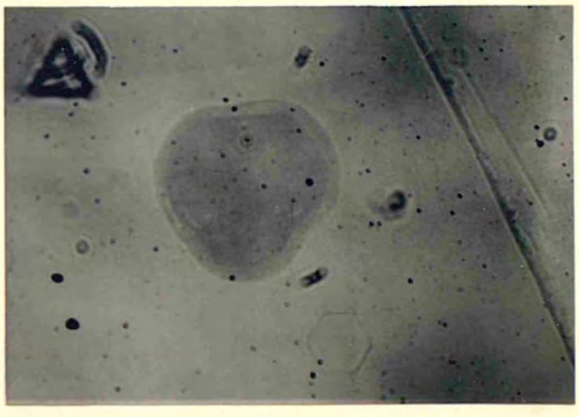

Fig 44 x 125

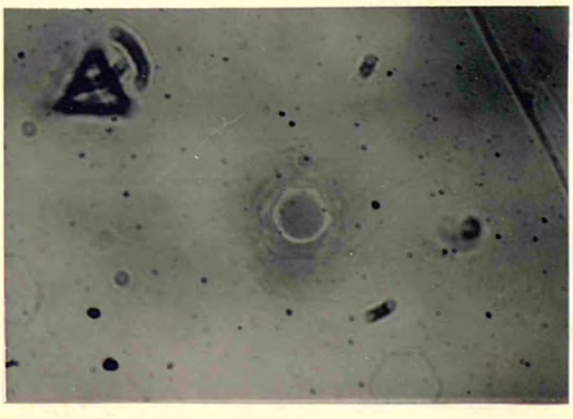

Fig 45 x 125

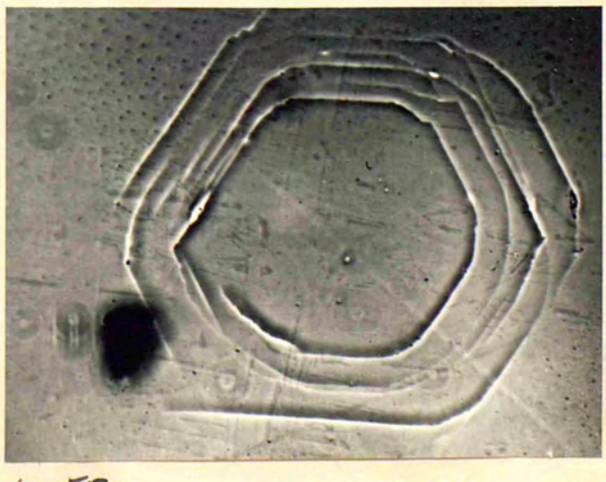

Fig 46 x 580

until the outer crack formed lastly at a load of 12 kgm or a little less. It is also seen that not all the cracks have completed themselves before the next one has been initiated - indeed on one side 4 cracks can be seen in Fig.46 whereas on another side as many as 8 cracks are seen. These multiple cracks are roughly concentric hexagons with straight sides but imperfect corners (the photographs of the final cracks are all taken by phase contrast microscopy).

In studying the development of crack figures by the two series of photographs given above (Figs. 39, 40 and 41, and Figs. 43, 44 and 45), it is very worthwhile also to study the series of the photographs given in Chapter 10 of the development of a pressure crack on the same octahedral face caused by a Tungsten Carbide ball impactor.

## 6.4 Interferometric Study

The permanent surface distortion effects left after release of load have been studied by multiple beam interferometry the diamond face being first silvered and then matched against a silvered flat. Monochromatic Fizeau fringe patterns across two primary cracks are shown in Fig.47 and across 3 primary and 1 compound crack in Fig.48. For reasons that have been given in the Chapter on Interferometry, a more convenient representation, effectively a true profile of a

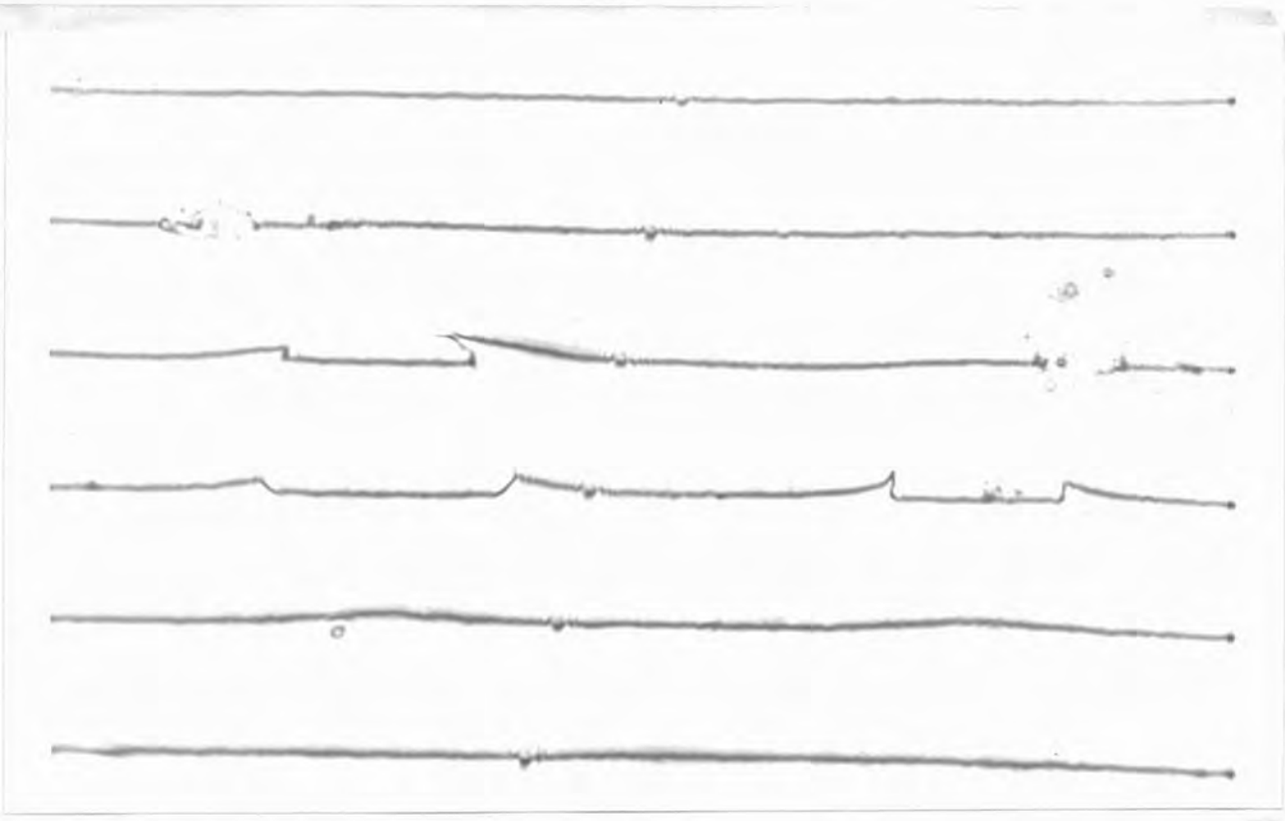

Fig 47 x 280

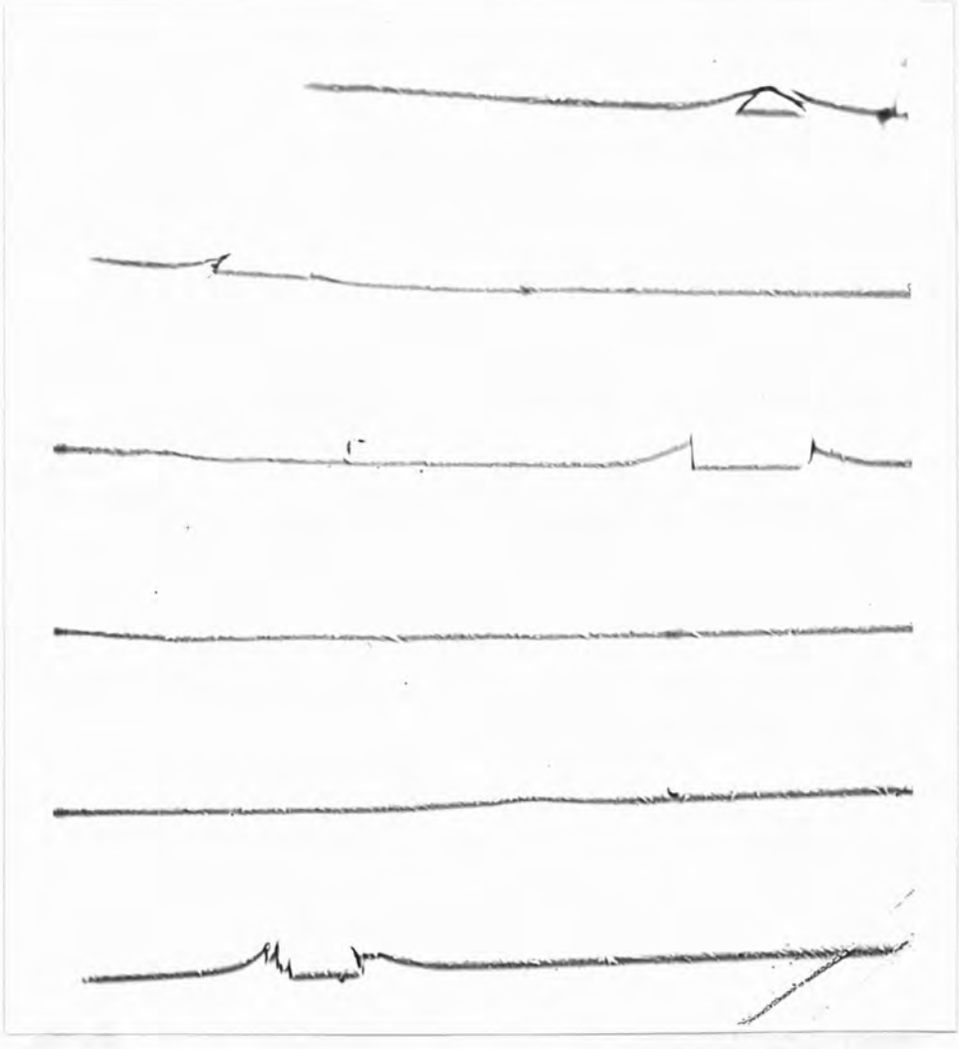

Fig 48 x 140

section, is given by the fringes of equal chromatic order. Thes have been used here with both high magnification and with high dispersion - in each case at least two orders are included to reveal the scale of the effects observed.

Fig.49 refers to the primary crack of Fig.42 and gives a section through the centre of the figure bisecting opposite sides. As a contrast Fig.50 is the section of the same crack but bisecting opposite angles. Figs. 51 and 52 refer to the compound crack of Fig.46, being sections bisecting opposite sides and angles respectively. Fig.53 is a profile of section parallel to one side in Fig.46 but outside the crack figure. The interpretations of these interferograms are shown to scale in Fig.54: the following conclusions may be drawn directly (A B C D and E refer respectively to the interferograms of Figs. 52, 53, 51, 50 and 49)

1) Material is piled up outside the crack, for the primary cracks the height of this is very small, not exceeding 300 A.

2) There is a sharp discontinuity at the actual crack, the level drops abruptly on the inside, while there is a smooth decline away from the crack towards the undisturbed level ( Any second order irregularities in the fringes are attributed to the combined defects in the reference flat used and the natural surface topography of the diamond). For the multiple crack, the mechanism of smooth rise and sharp drop,

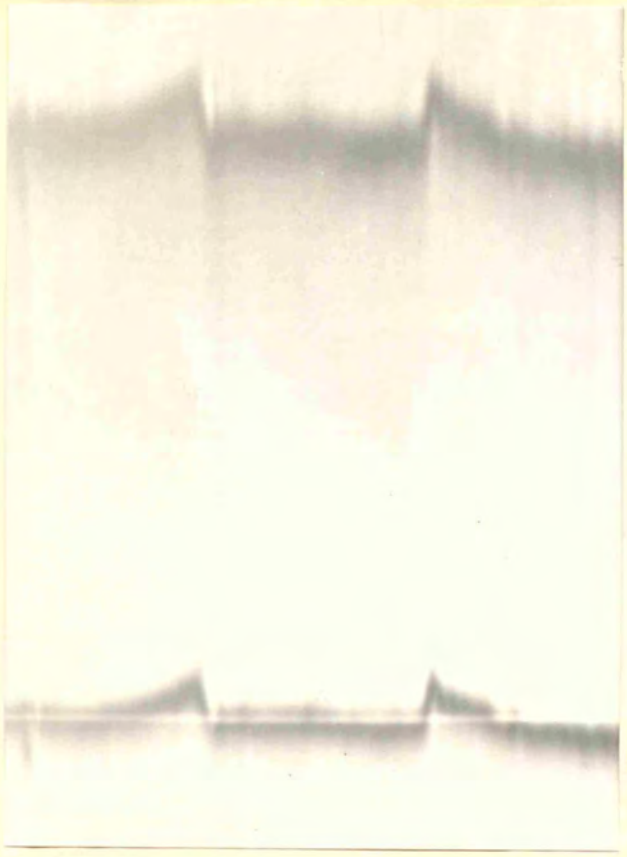

Fig 49 x 450

Fig 50 x 450

Fig 52 x 450

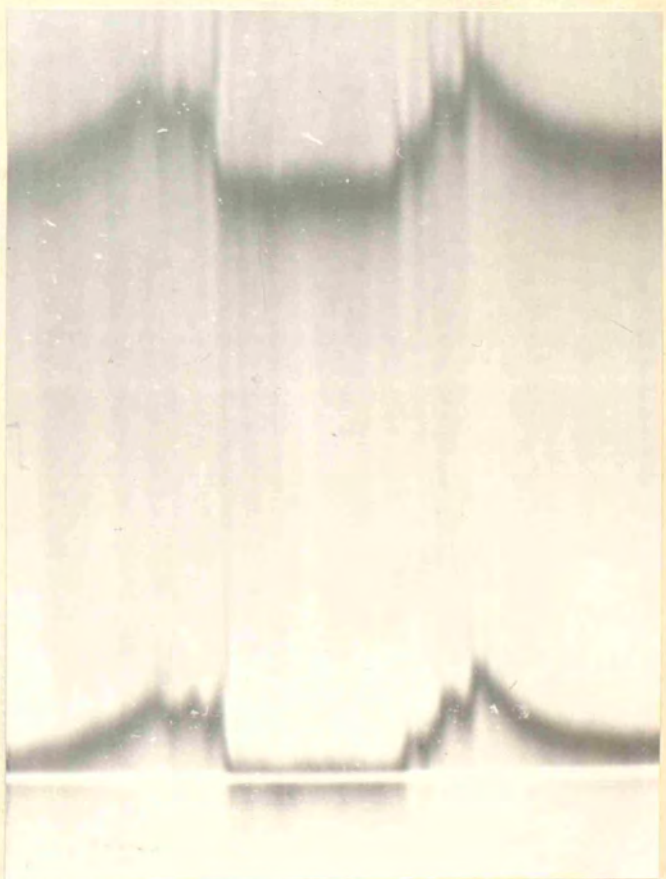

Fig 51 x 450

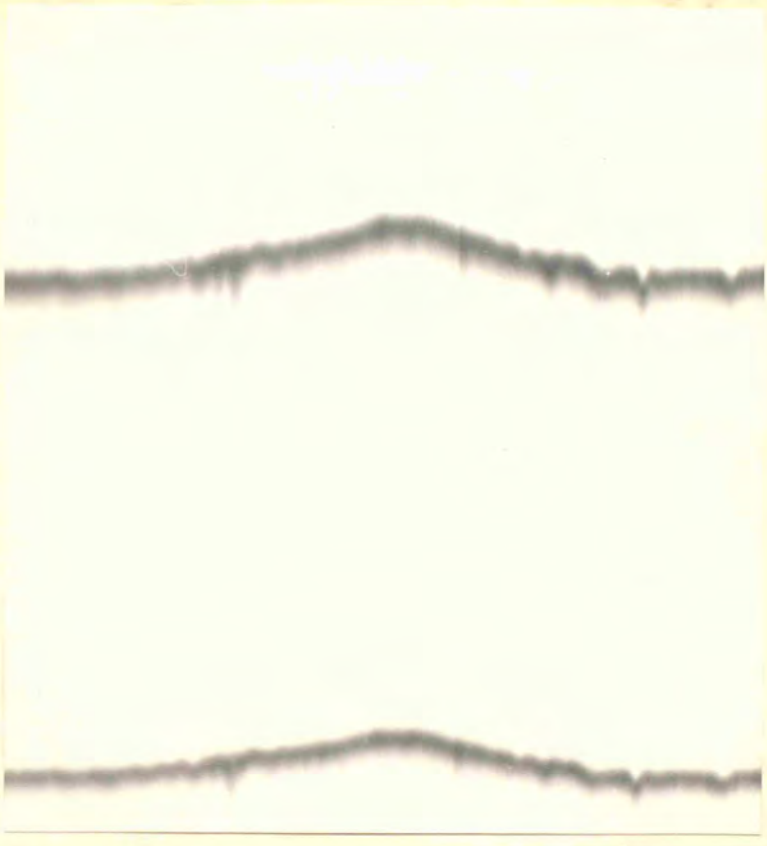

Fig 53 x 450

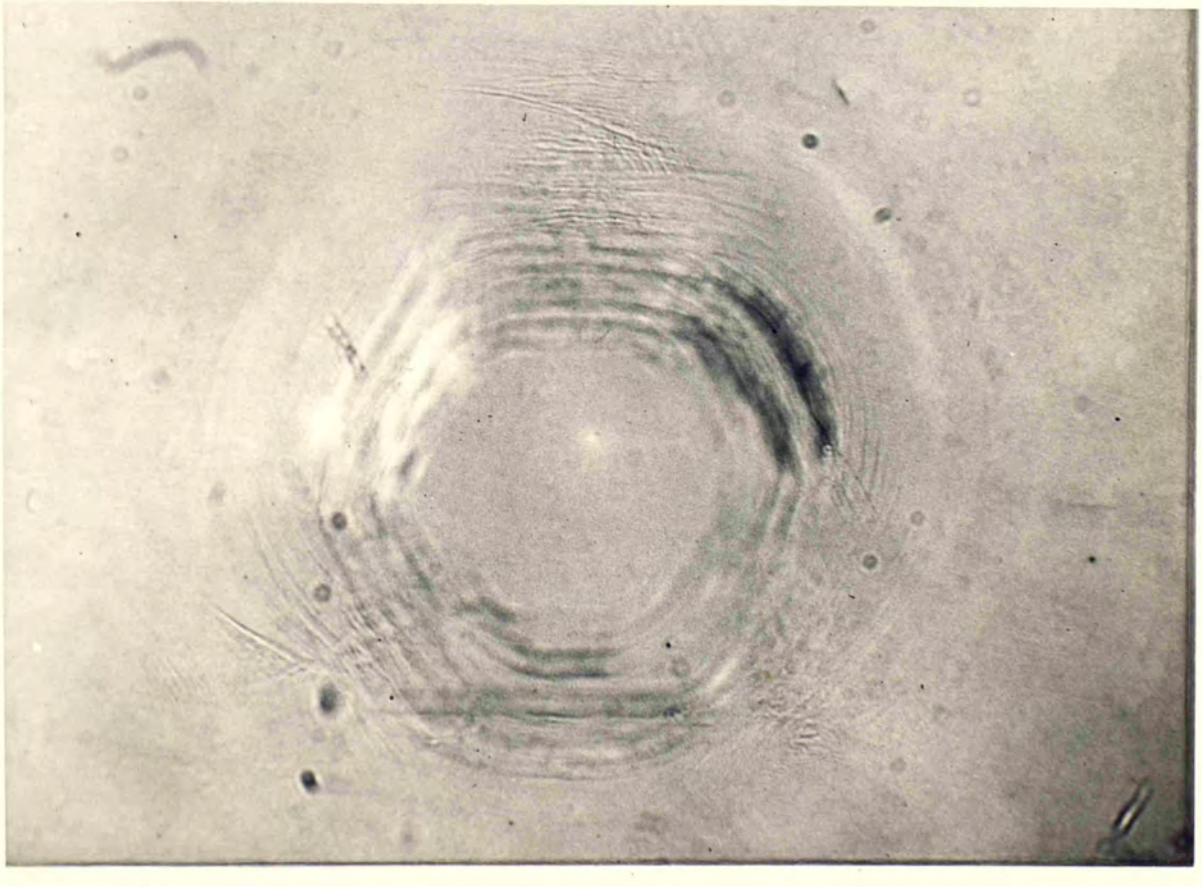

Fig 55 x 725

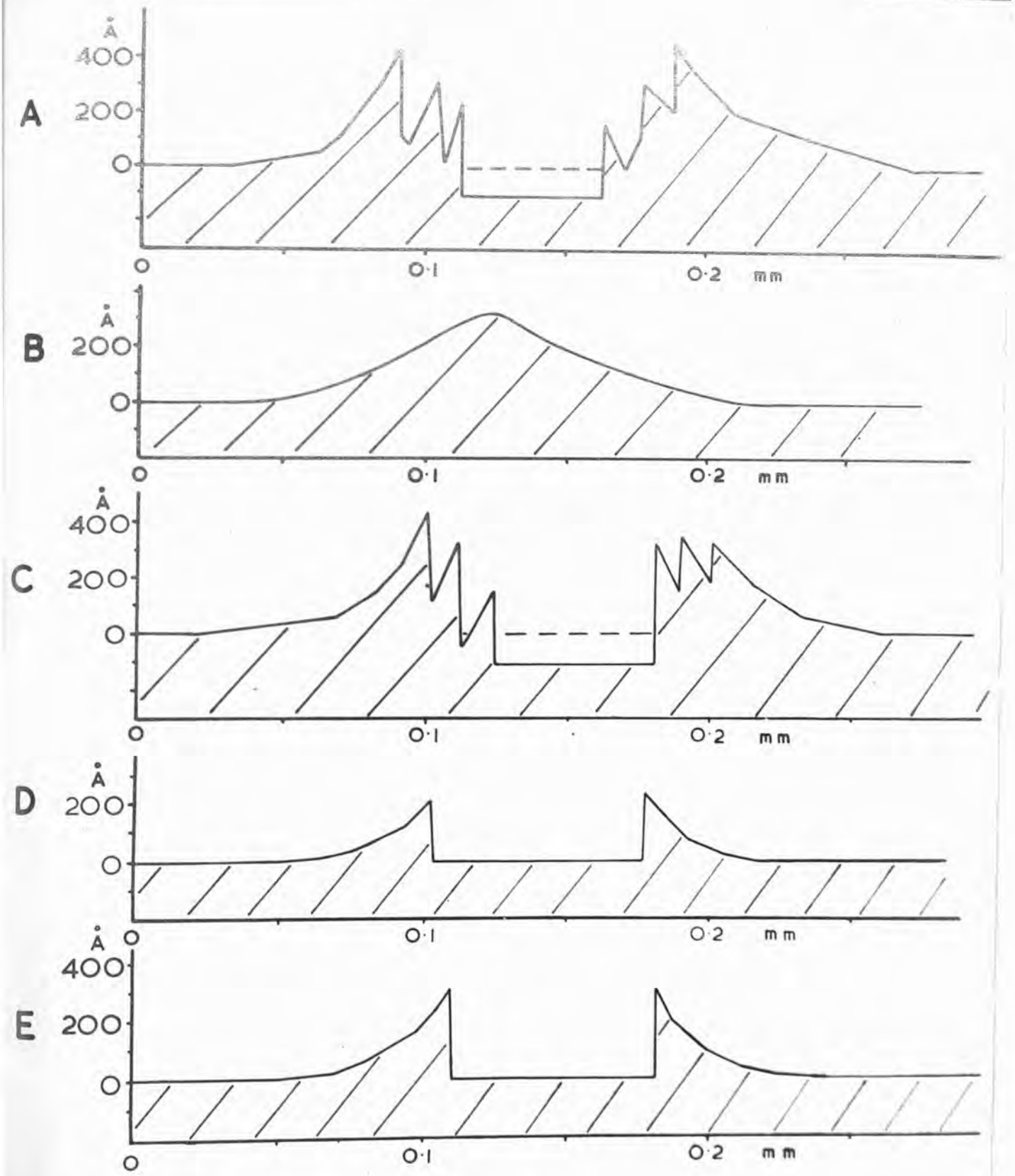
A
Å
400
200
0
0
0·1
0·2
mm
B
Å
200
0
0
0·1
0·2
mm
C
Å
400
200
0
0
0·1
0·2
mm
D
Å
200
0
0
0·1
0·2
mm
E
Å
400
200
0
0
0·1
0·2
mm

Fig 54.

repeats itself for each number crack.

3) The level within the crack is flat, not curved. For the primary cracks formed, this level is unchanged from the undisturbed region level - as far as is detectable. For the multiple crack the inner level is depressed by about 100 A below the undisturbed level.

4) The smoothness of the pile up surrounding the crack can be seen very clearly in Fig.53 showing a section across this pile up.

## 6.5 The Evidence of Internal disturbance

This investigation was undertaken only after further experiments on other diamond faces had produced very distinct signs of internal disturbance - this will be described in Chapter 8. For the octahedral face, the multiple crack already described, was observed using transmitted illumination and the polarized light technique previously described. Internal defects were found for this crack, being so deep in the crystal below the surface as to be quite outside the depth of focus of the microscope objectives used for studying the surface features - thus they are not visible on the surface photographs and when they themselves are brought into focus, the associated surface hexagon crack forms a blurred out of focus image.

The internal features, which can be seen in Fig.55, consist of groups of curved secondary internal cracks, opposite three alternate sides of the out of focus hexagon. They are represented schematically in Fig.56.

Again for the octahedral face, a better example of this type of disturbance is found later in Chapter 9 where a Tungsten Carbide ball is used on the Octahedron.

6.6 Discussion

It has been seen that the crack figures produced on the octahedral face are initiated suddenly, starting at one point, the crack spreading with finite velocity and requiring an applied stress for a finite time . The cracks take on a hexagonal shape with perfectly straight sides and usually sharp corners - although occasionally the corners are imperfect as is particularly noticeable in the case of the multiple cracks (second and sixth). This can be explained when the formation of a multiple crack is considered; the progressive flattening of the cracks, after each has been produced, by the extension of the area of contact with increasing load would cause additional strain and damage. That there are random points of surface weakness on the faces of diamonds, from which initiation of cracking occurs, is noteably similar in the case of glass where such weaknesses are accounted for by the Griffith Theory of seed cracks. Possibly for diamond, the weak points may be due to vacant sites in the surface crystal lattice, or again possibly due to the surface manifestation of sessile dislocations in the crystal.

For the six separate pressure cracks studied, the primary crack forms with a load of less than 10 kgms. A value

of the stress required to establish a complete crack is obtainable, for example from Fig.41 where the circular area of contact is 0.0035 sq.mm. for a load of 5 kgm. so that the required real average stress (i.e. load divided by circular area of contact at cracking point) is 1.4 x 10" dynes/Sq.cm. which is smaller than might have been anticipated considering the other strength properties of diamond. This is attributed to the fact that the crack figure establishes itself in easy cleavage directions since the six sides of the hexagons are strictly parallel to the lines of intersection of the (111) octahedral planes with the surface.

The dark regions outside three alternate edges of the hexagonal surface cracks throw light on the mechanism of cracking. Before cracking the area of contact is, as expected, circular (Fig.40). When the crack is established it occurs just outside the dark contact region, but from 3 of the hexagon sides the dark shadow areas spread so that the complete picture is as seen in Fig.41. The surface is bright between the two dark areas until the load is increased beyond the value for initiating the primary crack; then the contact area extends and merges with the three shadow areas to form a whole rounded triangular dark region as in Fig.44, within this region near the perimeter faint outlines of multiple cracks are visible, and these become easier to see when the load is reduced (Fig.45) but they are less visible on complete removal of load - due presumably to closing up of the cracks.

It may be thought that these external dark regions are extensions of the Newton's ring dark spot at the time of cracking but there are several reasons why this concept is invalid.

1. In Fig.45 where the load is being released, the true circular central dark spot is clearly seen and differs in intensity and character from the outside dark regions.

2. The surface distortions in Fig.54 do not favour the appearance of black spot outside the crack.

3. In particular hexagon cracks, three alternate sides are longer than the others (Fig.34 and 36) and the three outer dark regions project from these 3 sides.

4. If the triangular region after cracking was a dark spot due to anisotropy of the elastic properties of diamond, then it would be expected that the dark spot before cracking should be non-circular which is not the case.

It is proposed, considering the experimental evidence, that the visible pressure figure is the surface manifestation of deeper cracks penetrating into the body of the crystal in a manner analogous to the penetration long ago established in Hertzian cones in glass and illustrated in Chapter 4. The cracks, in diamond, will penetrate into the body in the cleavage direction, at angles to the surface conforming with the crystallographic configuration. These body cracks lead to the dark triangular regions seen, in plan view, outside the crack.

Diamond is brittle but not isotropic; thus it would

be expected to crack on static impact, rather than form an indentation by yielding, but not in exactly the same way as, for instance, glass. It is reasonable, however, to follow the classical treatment of Hertz for an isotropic substance, in so far as that under load, maximum shear stress will occur in the central region of the area of contact, and the maximum tensile stress just outside the perimeter of the area of contact. Thus cracking, which is due to tensile stress, will occur just outside the area of contact, but will be influenced by the crystallographic directions of easy cleavage of the diamond - this conforms exactly with experiment where it is found that the sides of the cracks on the surface are parallel to the directions in which the (111) planes intersect the surface.

There remains to be explained why the hexagon has three outer shadow regions and not six. The octahedron form of the diamond is such that three (111) planes intersect an octahedral face - not normally - but at an incidence of $70^{\circ}32'$ The internal cracking occurring at the critical load will tend to be in cleavage planes. Cracking will tend to take place, from the six sides of the hexagon surface figure, into the body of the crystal. Each pair of opposite sides of the hexagon represents lines of intersection of one of the three (111) planes mentioned above; and for any pair of these cracks, one will open along the (111) plane going away, out from the hexagonal surface figure (at $70^{\circ}32'$ to the surface) and in

this direction tensile stress is likely to be high. The other crack from the opposite side will tend to open along the (111) plane going down, but in towards the central region below the centre of the hexagon figure (again at $70^{\circ}32'$), where the tensile stress is likely to decrease rapidly. This will be true for each pair of opposite sides of the hexagonal crack, hence there is good reason for the observed asymmetry, the cracking developing more extensively into the crystal on the three sides of the hexagon parallel to the actual triangular edges of the octahedral (111) face. This is found to be the case experimentally on studying the orientation in the photographs. On release of the pressure, these cleavage cracks close up, becoming invisible but presumably they are still there. It is the development of these internal cleavage cracks which would lead to complete fracture of the crystal if the load were increased indefinitely.

This proposed asymmetrical cleavage-crack mechanism also serves to explain a noticeable asymmetry in the fringe displacements across some of the cracks observed. It can be seen in Fig.48 that where a fringe bisects two sides of a crack the exhibited pile up is greater on one side - four examples can be seen. Where ever this asymmetry occurs, the side of greater pile up is in fact the side which shows the extended cleavage crack. The two observations are therefore in agreement as also is the fact that in some cases (Fig.34 and 36) the hexagon cracks have 3 alternate sides longer than the other 3

and these longer sides are those showing the extended cleavage crack dark regions.

The internal disturbance, already described (see section 6.5), is different in origin to the cleavage cracking above. It is inside the body of the crystal and is quite visible, when focussed, after the load has been completely removed, whereas the cleavage cracking disappears as load is removed. Also, it consists of groups of curved secondary line-cracks occurring in the alternate hexagon regions to those of the dark cleavage-cracking areas. These curved markings in the crystal closely resemble the familiar hackle marks on fractured glass - which have also been found on the conchoidal surfaces of a ring crack - see Chapter 4. It is reasonable to conclude that the dark areas represent the regions of easier cracking along a cleavage plane, whilst the alternate three 'hackle' regions are the more resistant regions to cracking.

A most important feature revealed by the interferometric studies described, is that they appear to establish the fact that there can be micro plastic flow in diamond at room temperatures. The smooth gradual pile up of the material surrounding the hexagonal figures, and the depression of the central area in the case of the multiple crack, strongly suggest a plastic flow. No evidence can be found for micro slip in the pile-up regions, within the limits of the observational technique; and in any case this would not explain the central depression found for the multiple crack -

which is much more marked for pressure figures formed on the other diamond faces.

Finally, it has been noted that, for the primary cracks formed, there is no central depression - it may then be wondered where the material in the pile up comes from. It is conjectured that, as the crack extends into the body of the crystal at an angle, it opened up, and consequently the material above it rises. Hence the surface must rise correspondingly, which gives the pile up. For the multiple cracks, the inside level is depressed and the pile up is correspondingly more; here the pile up is a combined effect of the cracks and the depression over the central area.

# CHAPTER VII

## STUDY OF PHENOMENA ON DODECAHEDRAL FACE OF DIAMOND

### 7.1 Introduction

The only dodecahedral face available for experimentation was an artificial face of a diamond of octahedral habit. This was obtained by sawing an octahedral stone in half - through the so called two point face of the diamond industry. The resulting (110) face can be seen in Fig.57; it has not been polished and the saw marks can clearly be seen - as can also some of the pressure figures produced (other markings seen are due to the silver having been scratched off the face at these places). The other side of this stone consists of two octahedral faces meeting at a girdle edge of the octahedron - thus the stone, although a transparent diamond, cannot be seen through or observed with transmitted light. This has meant that no observation could be made during tests and that no information was obtained regarding internal disturbances.

The cracks were produced using the Penetrascope instrument alone, applying different loads, and then observing the effects if any under a microscope - thus the control on the testing was less than in previously described experiments on the octahedral face

### 7.2 The Pressure Crack figures produced on the Dodecahedral surface

Since the critical load to be applied to initiate a

crack could not be determined directly, a range of loads was applied in a series of tests ranging from 0 up to 24 kgm. In all, ten pressure figures were produced, the smallest load required for production being 7 kgm. and the other loads ranging up to 24 kgm: in these tests the rate of application of load was sometimes varied deliberately, in order to see whether any detectable variation occurred. In some instances the production of the pressure figure could be heard and was often indicated by a sudden small load reduction.

A number of the figures are shown in the phase contrast photographs of Figs. 58, 59, 60, 61 and 62 having increasing degrees of complexity. The maximum loads applied (i.e., the approximate critical load for initiation of the crack, or the largest of the multiple cracks) were respectively 7, 10, 13, 24, 24 kgms. corresponding to nominal stresses (i.e., the maximum load applied divided by that area circumscribed by the largest crack figure in each case) of 1.5 x 10", 1.9 x 10", 1.8 x 10" and 2.1 x 10" dynes/sq.cm. These values compare with 1.2 x 10" dynes/Sq.cm. for pressure figures formed on the octahedral face (this value is lower than the real average stress 1.4 x 10" dynes/sq.cm. evaluated using the circular area of contact at the moment of fracture - as would be expected). Attention is drawn to Fig.61 and 62 both of which were formed with 24 kgm loads but the former is by somewhat rapid application, whilst the latter was slowly applied.

These pressure figures are hexagonal in shape, but

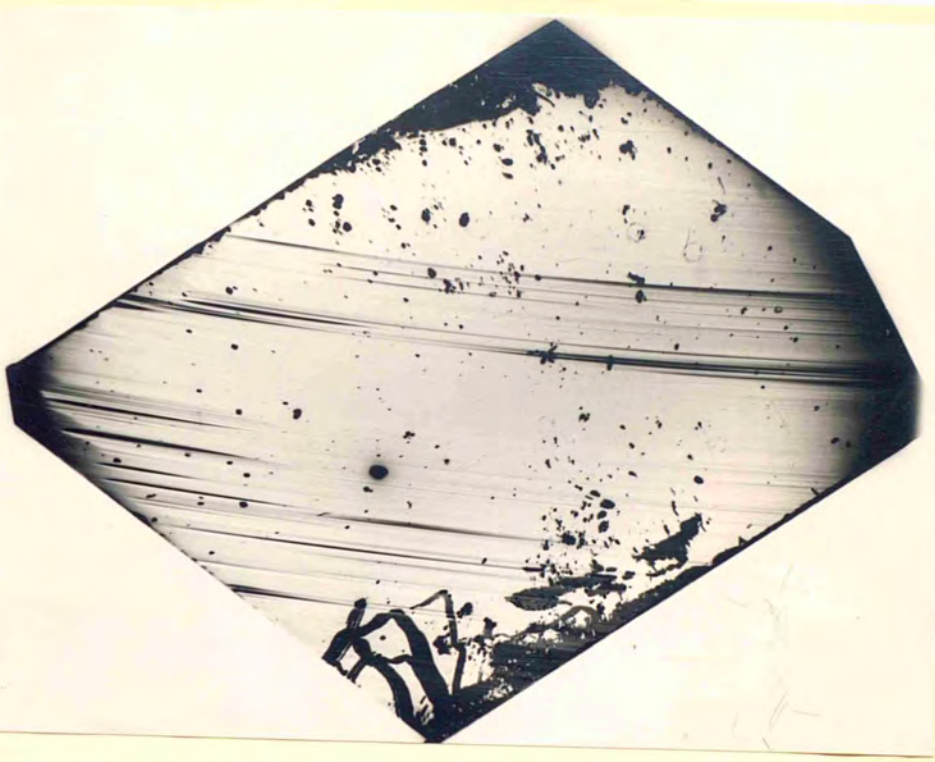

Fig 57 x 20

Fig 58 x 545

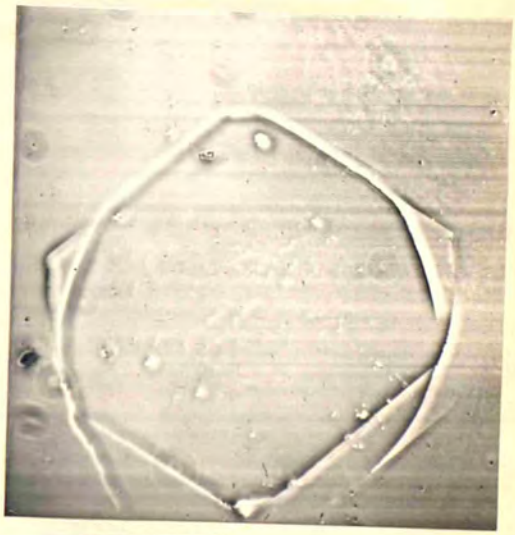

Fig 59 x 545

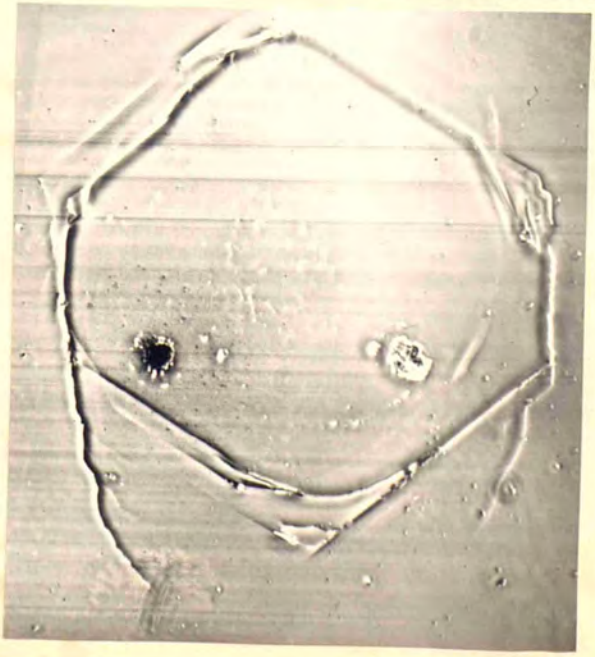

Fig 60 x 545

Fig 61 x 545

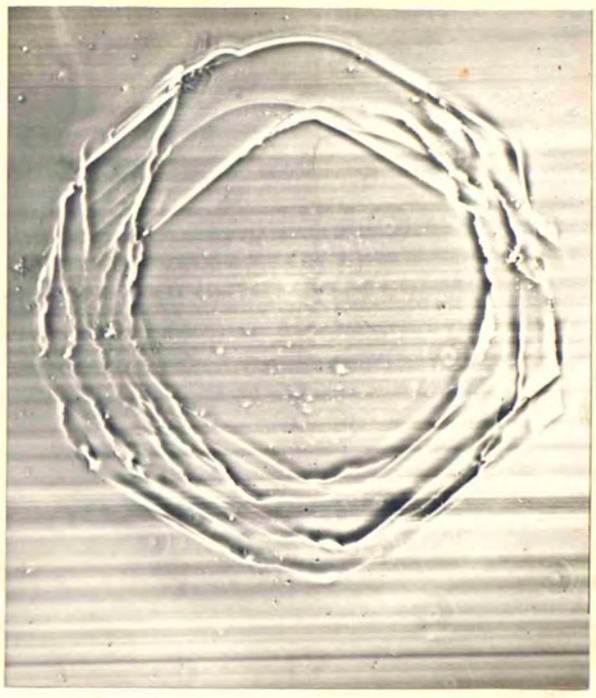

Fig 62 x 545

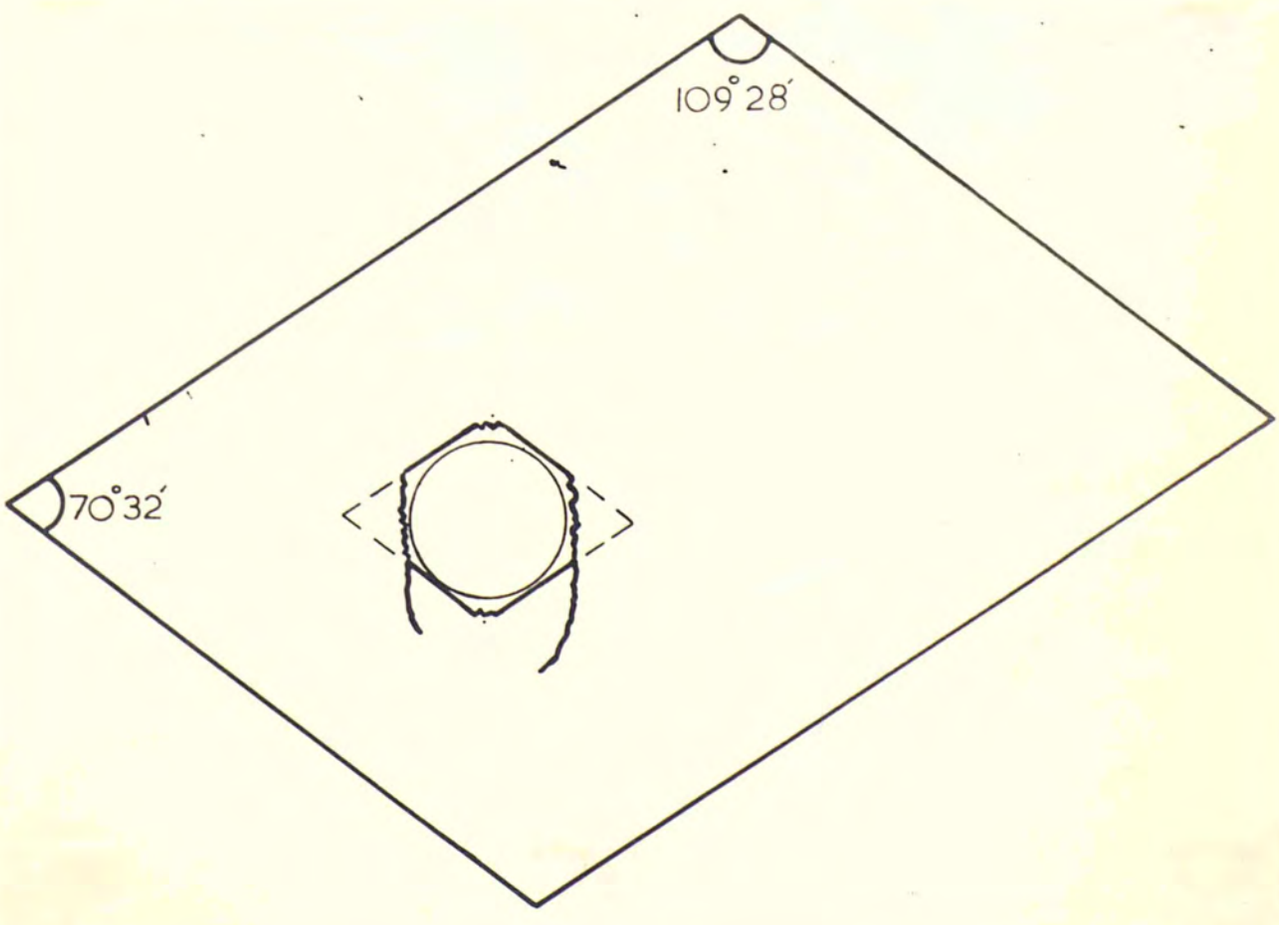


Fig 63

differ distinctly from the hexagons formed on the octahedral face. In all the photographs of these cracks it is clearly seen that there are two types of sides to the hexagon: four sides are straight and near-perfect while one pair of opposite sides are always irregular, at times serrated and furthermore, even in the case of primary cracks, tend to develop projection beyond the hexagon pattern. The orientation of all the figures with respect to the edges of the stone is the same and also the irregular pair of sides is the same pair in each case. This orientation is shown diagrammatically in Fig.63 - here the observed crack is shown in heavy outline. The inner circle represents the region of applied load, and the broken line extensions show the completed crystallographic directions parallel to the crystal edges.

## 7.3 Interferometric Study

The irregular curvature of the sawn dodecahedral surface made application of multiple beam interferometry rather difficult. However, fringe patterns were obtained for one crack by using the micro-flat technique in conjunction with the special jig described by Tolansky and Omar (1953). Fig.64 shows Fizeau fringes forming a typical pattern for the pressure figure of Fig.62 while in Fig.65 is illustrated typical fringes of equal chromatic order corresponding to the same crack figure. Because of the curvature on the surface the undisturbed region of the surface gives rise to curving fringes upon which the fringe distortions due to cracking are

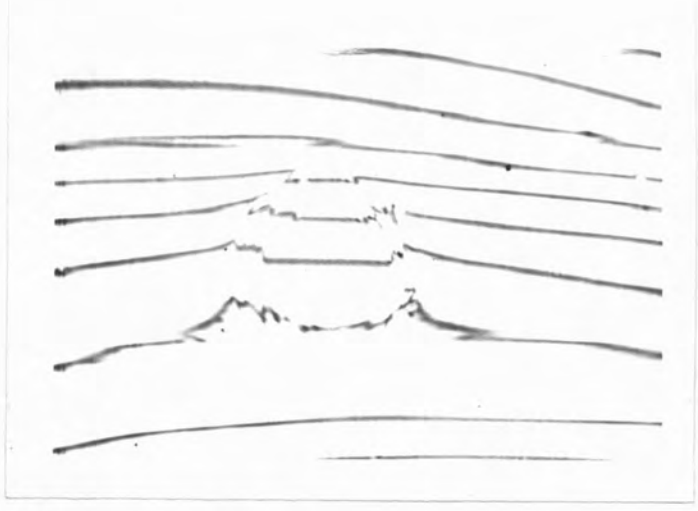

Fig 64 x 190

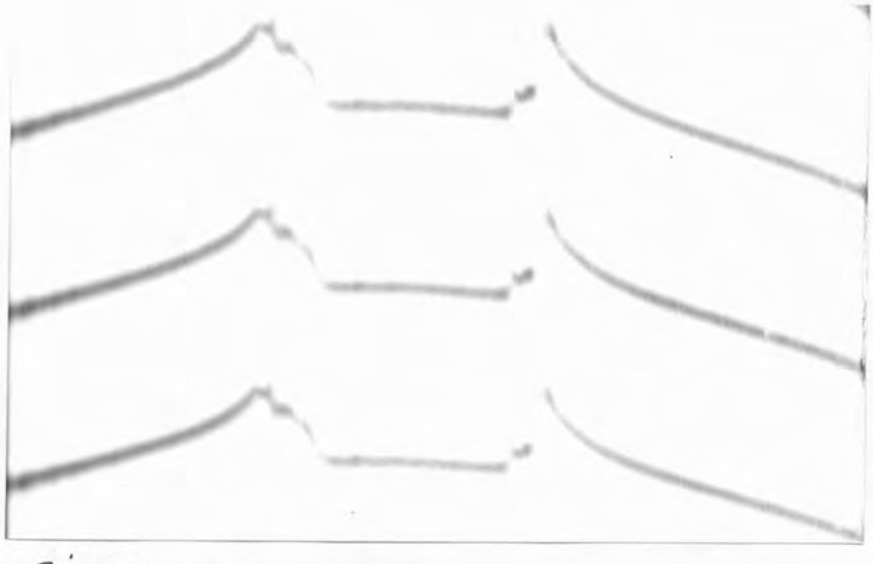

Fig 65 x 320

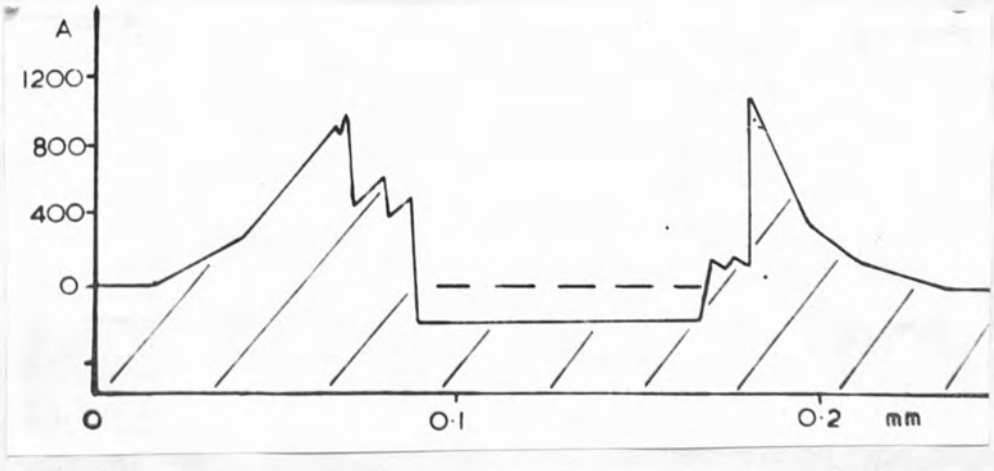


Fig 66

superimposed, in the region of the pressure figure. This background curvature has to be taken into account in calculations made from the fringes. Fig.66 shows to scale the measured calibration of the white light fringes of Fig.65. The profile closely resembles those for the cracks on the octahedral face, having features corresponding to what can be considered now as general topographical characteristics of pressure figure phenomena. The section illustrated by the calibration of the fringes is one bisecting two opposite irregular sides of the crack.

## 7.4 Discussion

The dodecahedral face appears to be more resistant to pressure cracking than the octahedral face, the normal average stresses for initiation of cracking being 1.8 x 10" and 1.2 x 10" dynes/sq.cm. respectively.

The directions in which the cracks spread from the surface into the body of the crystal could not be ascertained since observation during actual loading was impossible for this stone. However, from the crystal symmetry, the orientation of the surface figures can be explained.

Fig.3 shows an octahedron with a dodecahedral plane shaded (the 2 point surface being the vertical shaded plane). Experimentally it has been seen that the pressure figures are orientated on the 2-point face so that four sides of the hexagon are parallel to the four edges of the 2-point face of

the stone. It can be seen that along all six sides of the hexagonal crack figure, octahedral plane (i.e. cleavage planes) intersect the dodecahedral face; four of these are perpendicular intersections, while the other two (for the irregular pair of sides) are intersections at $35^{\circ}$ 16'.

Thus the four straight clear crack sides coincide with the perpendicular intersections of cleavage planes with the surface, while the two irregular sides coincide with $35^{\circ}16'$ slant intersections of cleavage planes with the surface. This gives good evidence for believing that cracking has occurred under the influence of two contingencies. First, the maximum tensile stress around the perimeter of the region of contact according to the Hertz Theory and second, the orientation of the easy cleavage (111) planes with respect to the dodecahedral face. The irregular cracks, forming the odd pair of opposite sides, are due to the secondary (111) cleavage that has taken place there. This secondary cleavage would be less under control than the perfect primary cleavage occurring at the other four crack sides, and this may account for its irregularity and for the extension cracks which run away from the pressure figures from these two edges.

It might be considered, as an alternative explanation, that the irregular serrated sides and corresponding projections are a zig-zag of short cleavages following each other alternately in the two principal cleavage directions. This at first sight appears to be an unlikely mechanism; yet etching

experiments have revealed that diamonds grow by thin laminated sheets (Pandya and Tolansky 1954), and the separation of these sheets is such that the zig-zag cleavage might possibly arise by stepped cleavage from sheet to sheet.

The interferometric study made for a typical multiple pressure crack, shows that the surface distortions occurring on the dodecahedral face are of the same nature as those apertaining to crack figures formed on the octahedral face, but that the extent of the distortion is greater in the former case as can be seen in Fig.66. The greater stress, built up in order to initiate a crack figure on the dodecahedral face, produces a greater disturbance upon its sudden release, than that found in the octahedral face experiments.

# CHAPTER VIII

## STUDY OF PHENOMENA ON DIAMOND CUBIC FACES

### 8.1 Introduction

Two types of cubic faces were available. The first was on a naturally occurring cubic diamond stone (i.e., of cubic habit). Such stones are very rare, usually being so full of impurities and inclusions that they are opaque, and always having surfaces too rough to permit of precision optical techniques being used. The stone used in the experiments was as described being completely opaque, but had one of the cubic faces polished. The finish on the surface was very poor, and there were cracks running right across the surface; so that care had to be taken in making the impacts in clear regions on the surface. As in the case of the dodecahedral face, impacts were made just with the Penetrascope alone, the pressure figures being studied under a microscope after the tests were completed and load had been removed.

The second face available was a close approximation to a (100) face obtained by sawing a transparent octahedron across the (100) girdle plane. The stone was actually the remains of truncating a diamond of octahedral habit by sawing through two parallel cubic planes, one being a girdle plane and the other a cubic plane parallel to it. It thus formed a small thick plate with two cubic plane faces - one large and the other smaller. These faces were polished quite well so

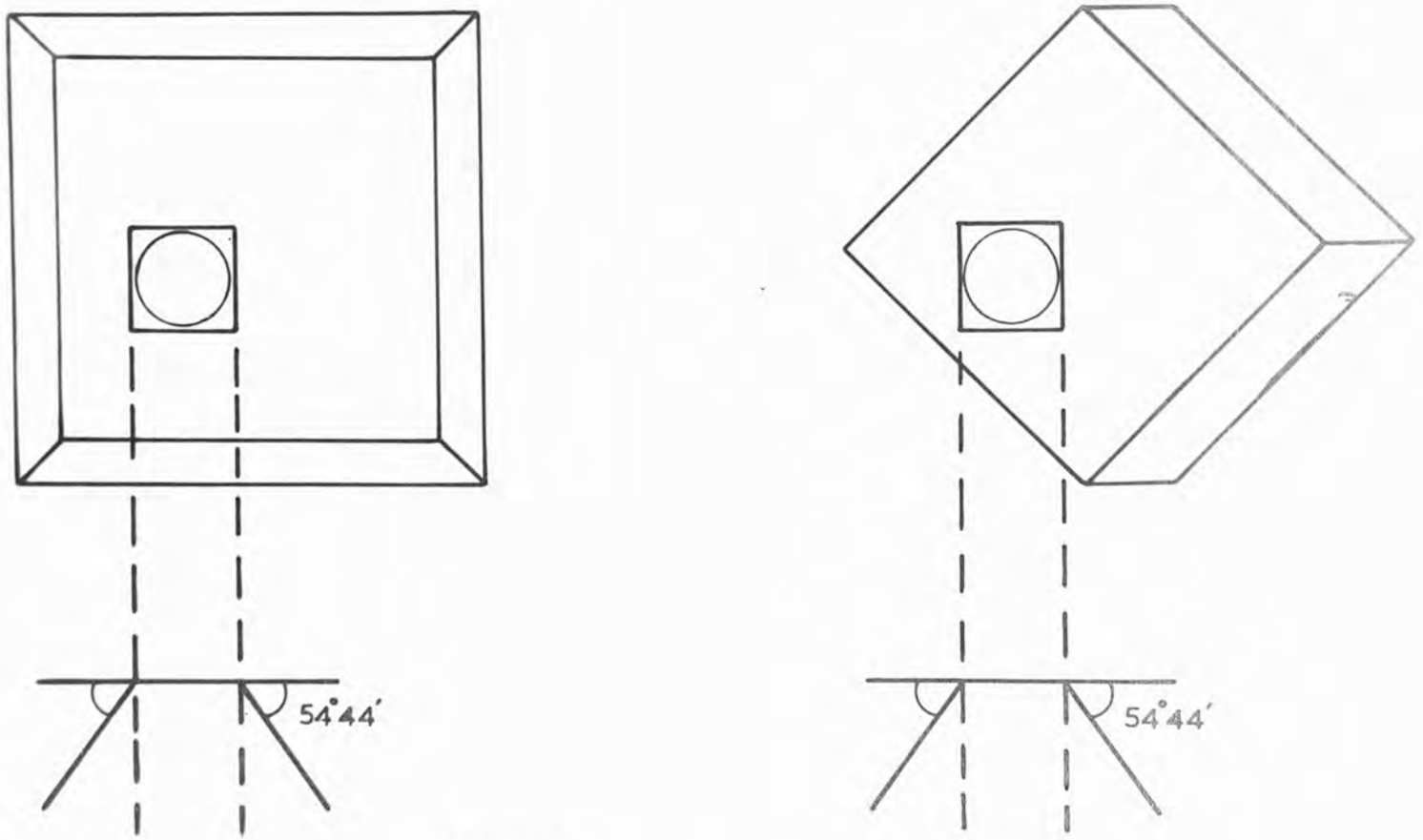


Fig 67

that the stone, in this form, was suitable for observations to be carried out during testing with increasing load. Unfortunately the smaller face severely limited the field of view of the girdle cubic face upon which tests were to be made; this limitation combined with the fact that the crack, when it did occur, caused extensive disruption, meant that only one test experiment could be done on this face.

8.2 The pressure figures produced on the natural cubic face

The figures produced are basically squares, but generally have rounded broken corners. They are all orientated so that their sides are at $45^{\circ}$ with the edges of the cubic face (i.e., the diagonals of the pressure figures are parallel to the edges of the face) as seen diagrammatically in Fig.67 where the inner circle again represents the region of applied load.

Four examples are shown in Fig.68, which were produced by applying maximum loads of 20 - 26 - 30 - 30 kgm. respectively from top to bottom of the photograph. These loads, again, represent only an approximation to the critical load required to initiate the largest of the multiple cracks for each pressure figure. The corresponding nominal average stresses (i.e., maximum load applied divided by that area circumscribed by the largest crack figure) for these loads are 1.8 x 10", 2.1 x 10", 2.1 x 10" and 1.8 x 10" dynes/sq.cm. respectively, the areas involved being larger than the corresponding

areas for cracks on the dodecahedral and octahedral faces.

For a load of 30 kgm., it is seen that, from one of the pressure figures, very extensive uncontrolled cracking occurred extending away from the figure and reaching to the edge of the nearest face on one side. This extended crack, although apparently similar to the 'tail' cracks projecting from the dodecahedral face pressure figures, is more likely to be directly connected with weaknesses in the boart stone already prevailing; thus the localized stress in the test area initiates fracture cracks similar to those already described, which were on the surface of the stone when it was first obtained.

8.3 Development of pressure figure on the Truncated cubic face

Observations were made from below through the small parallel cubic face of the development for an impact from above on the girdle cubic face. Fig.69 shows the Newtons rings and dark spot for a load of 0.2 kgm. At 4 kgm. the area of contact has increased as seen in Fig.70; the discontinuity that can be detected in the circular fringes is due, it is believed, to damage of the tip of the diamond ball impactor, this will be dealt with in Chapter 9. The load was increased still further until at a load of 29 kgm. a pressure crack occurred on the cubic surface, dark shadow areas instantly appearing opposite the four sides of the crack. It was noted that, immediately after the cracking, the load applied by the Penetrascope was

not stable, but crept down slowly to an approximately stable value of 22 kgm; the appearance, at this load, can be seen in Fig.71. As soon as the photograph had been taken, the load was reduced to zero; the final appearance of the produced crack on the surface is shown by phase contrast in Fig.72, but it is evident from Fig.71 that considerable internal disturbance is associated with this superficial cracking phenomena.

The multiple crack produced is again basically square, but the corners are very rounded. Its orientation with respect to the edges of the crystal face is shown schematically in Fig.67 where it is seen that the sides of the square crack are, here, parallel to the edges of the diamond cubic face, as opposed to the orientation on the natural cubic face with respect to its edges.

It is important to note that in this test, although the load was <u>not</u> increased beyond the initial cracking point but was released almost at once, a distinctly multiple crack was formed with extensive associated shadow areas, i.e., no initial primary cracking occurred before multiplicity set in, which is quite different to the mechanism found for impact on the octahedral face of diamond where primary or multiple figures could be produced under perfect control. The critical value of the nominal average stress at cracking in this experiment was 1.4 x 10" dynes/sq.cm. which is lower than the corresponding stress for the natural cube face although still greater than that stress for the natural octahedral face. Also, from Fig.71 the area of the circle of contact at cracking

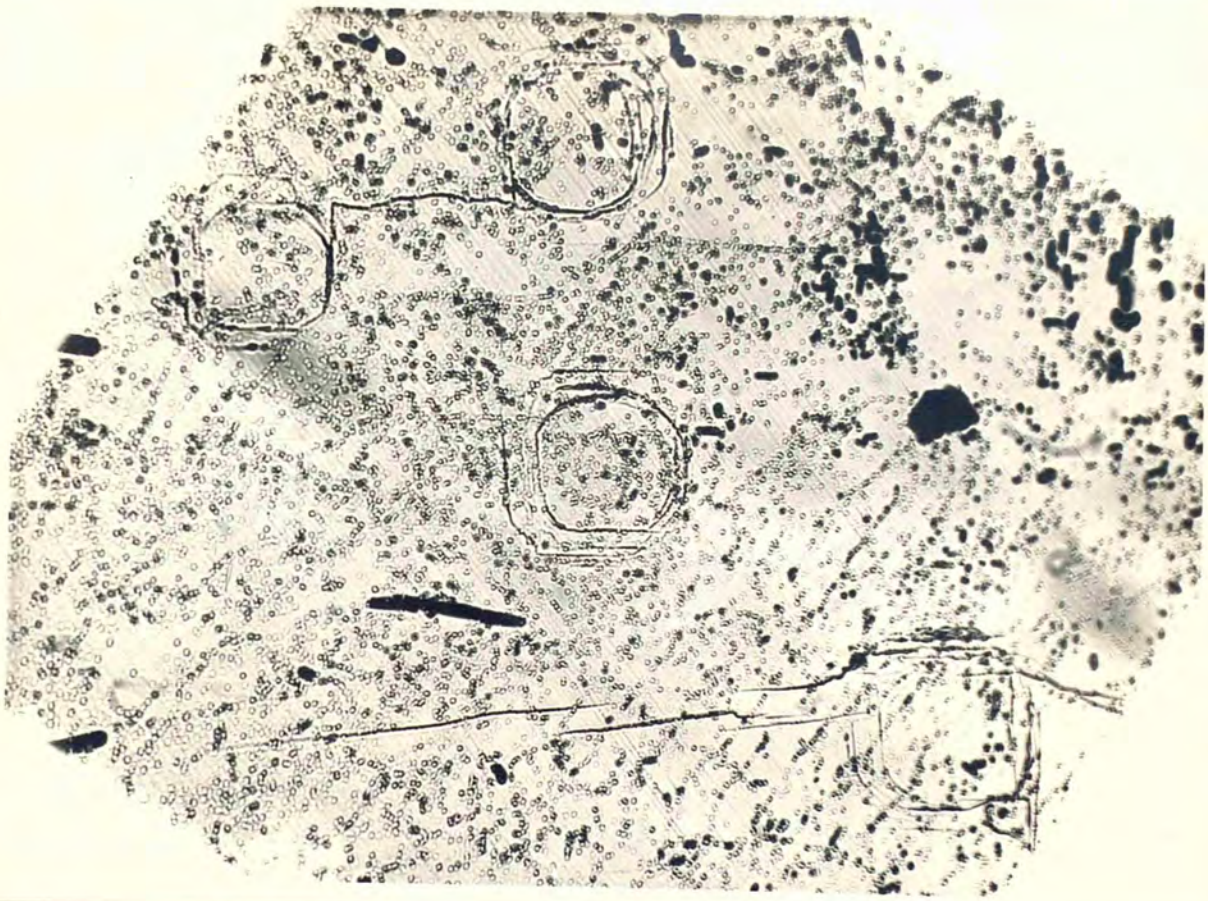

Fig 68 x 170

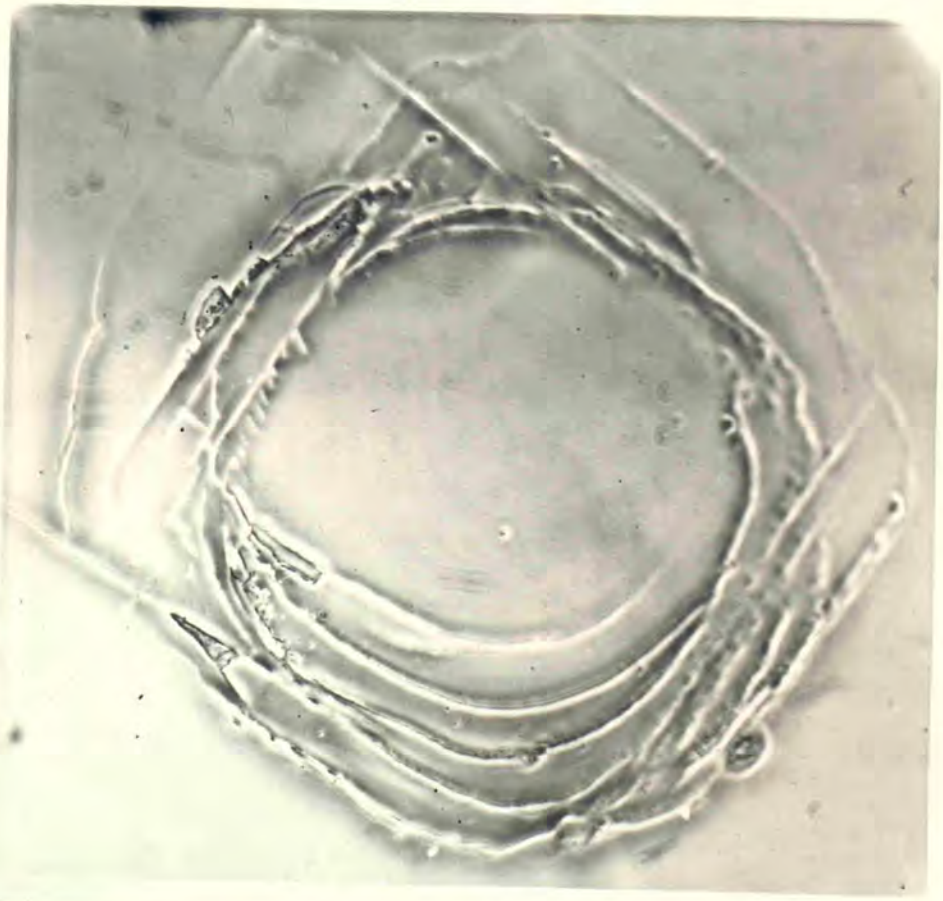

Fig 72 x 625

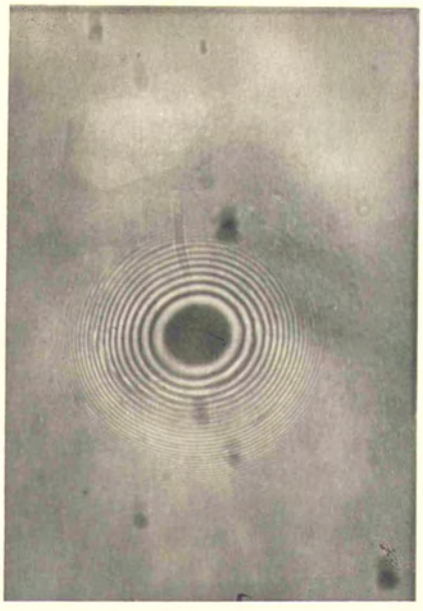

Fig 69 x 250

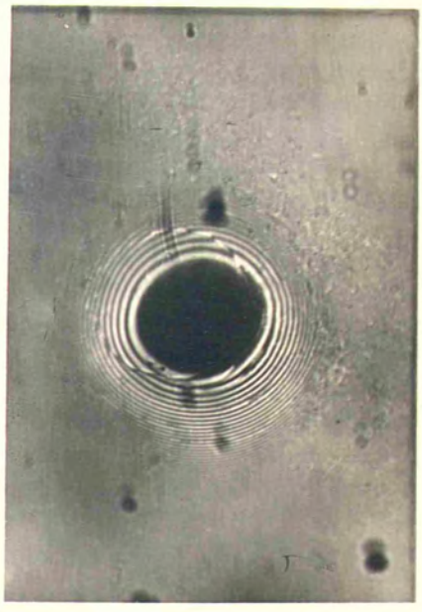

Fig 70 x 250

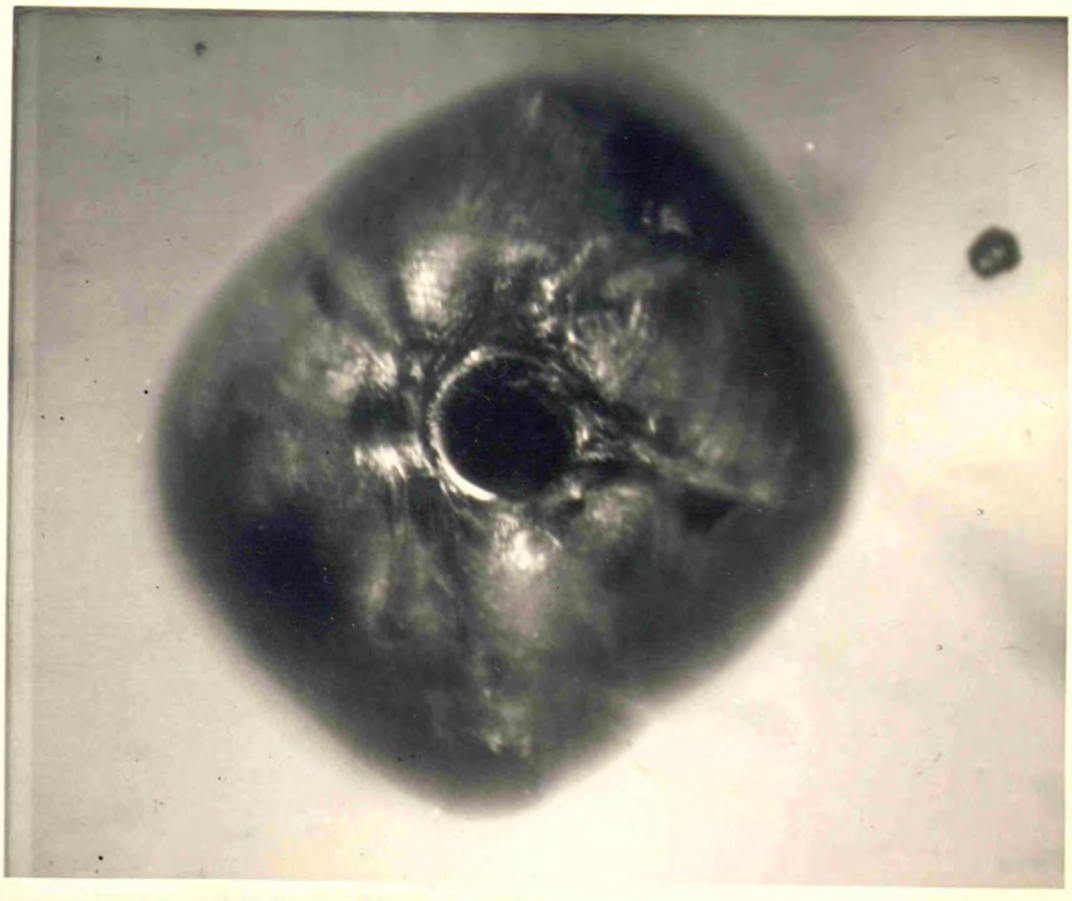

Fig 71 x 250

can be measured as 86 x $10^{-4}$ sq.mm, so that, the critical load being 29 kgm, this gives the critical value of the real average stress as 3.3 x 10" dynes/sq.cm: which is considerably higher than the value of 1.4 x 10" dynes/sq.cm. found for cracking on the octahedral face.

8.4 Interferometric Study of cracks on the two Cunic faces

For the natural cube face, Fig.73 shows the Fizeau fringe pattern for the four pressure figures seen in Fig.68. Despite the poor state of the surface polish, which is shown up by the fringes, these do show that the surface distortion follows the general characteristics found previously for all pressure figures - but on a slightly bigger scale. Particularly, the spread of the distortion over the surface surrounding any one figure is relatively large, and extends over a much greater region than in the case of the octahedral or dodecahedral faces.

The typical fringes of equal chromatic order shown in Fig.74 for a section bisecting opposite sides of a square pressure figure on this face, confirm this greater distortion. While the calibrated profile of these fringes drawn to scale in Fig.75 show also that the height of the surrounding pile up and the depression of the central region both considerably exceed that found on the natural octahedral face. Indeed it is seen here that the amount of depression occurring in the central region exceeds the amount of material displaced

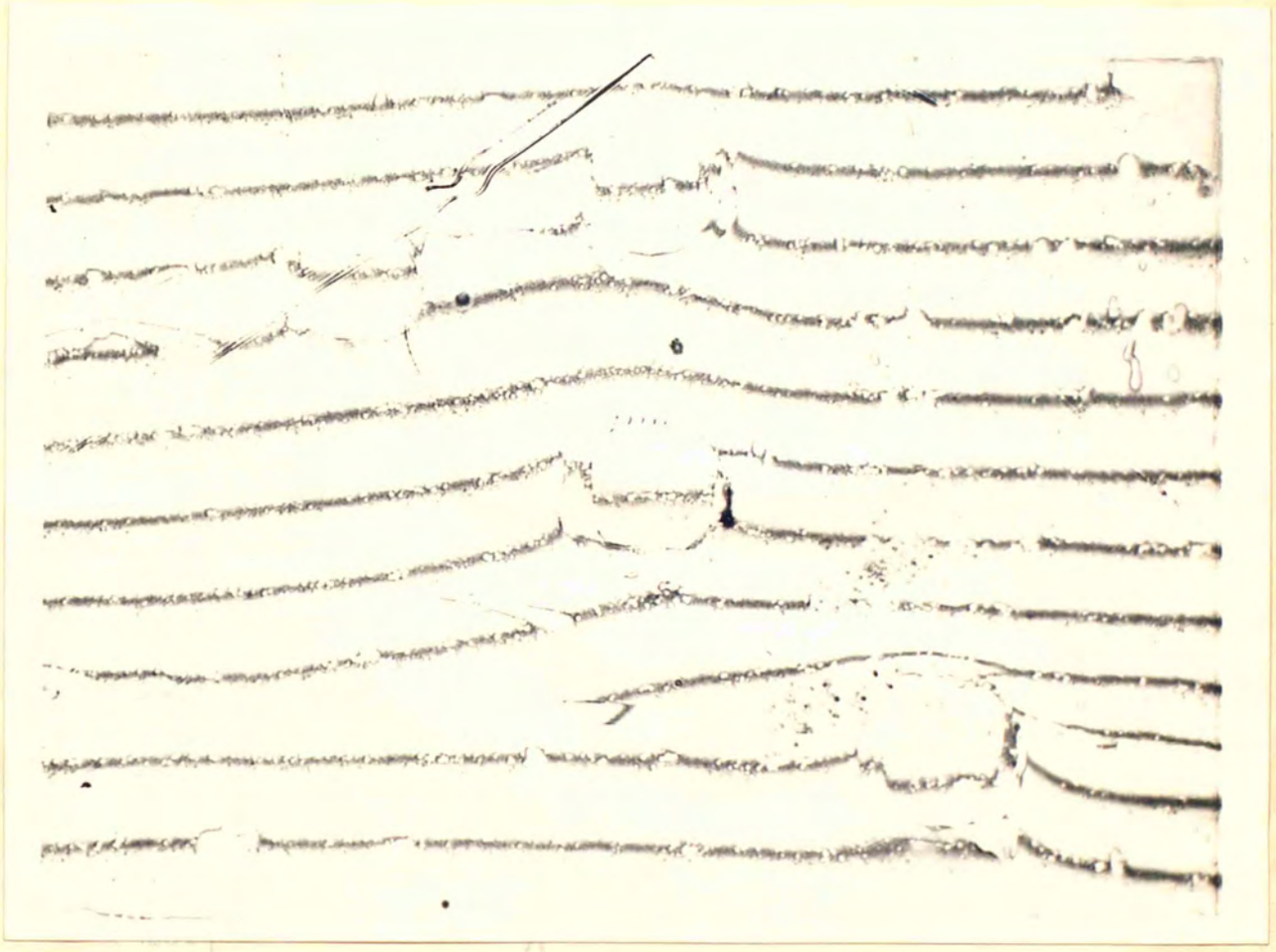

Fig 73 x 175

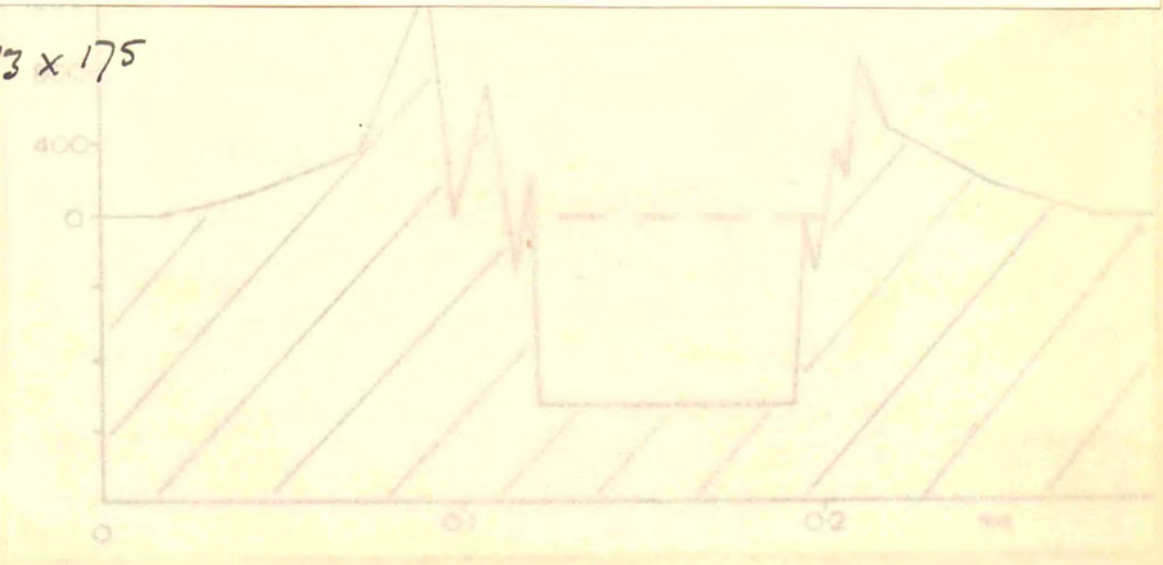


Fig 75.

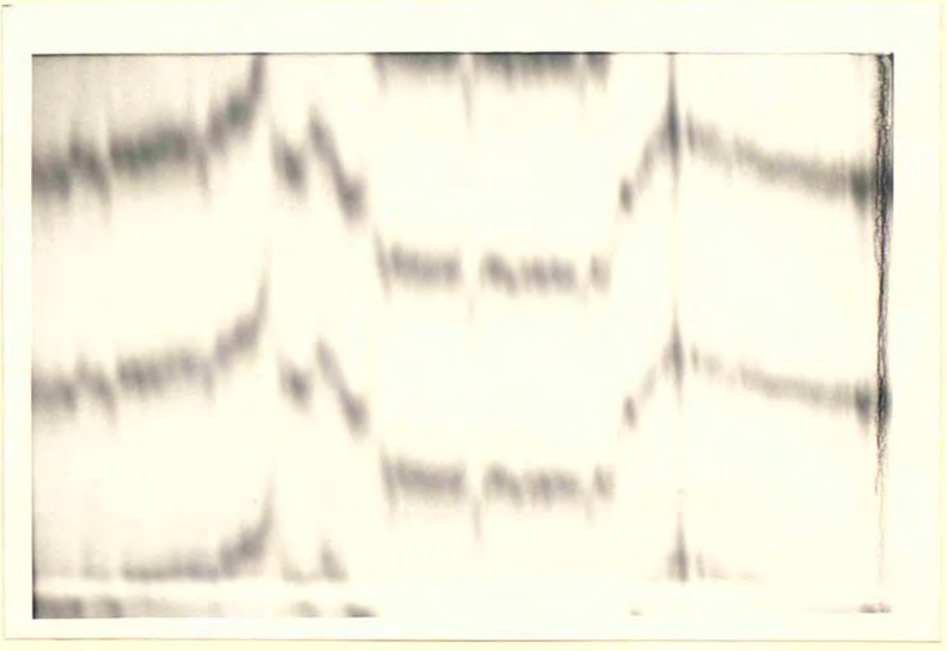

Fig 74 x 450

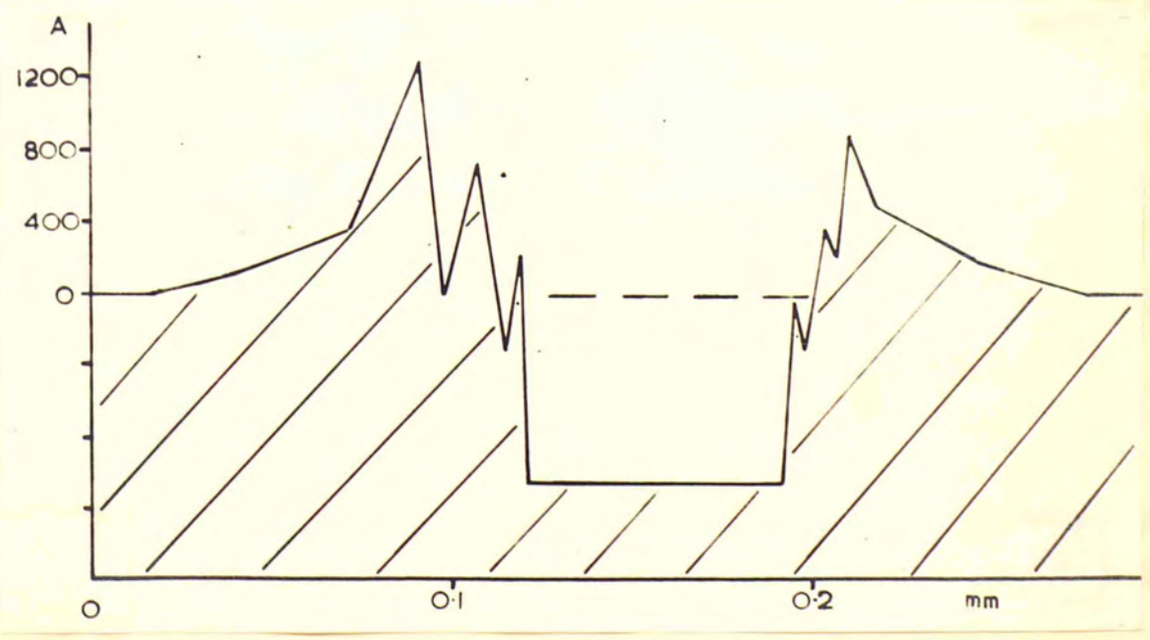


Fig 75.

into the 'pile up' on either side: this characteristic was found only on the natural cube face. The ragged nature of the fringes in Fig.74 is entirely attributable to the poor surface finish of the natural cube face.

For the truncated (100) cubic face of the octahedral stone, two Fizeau fringe patterns are shown in Figs.76 and 77 for the multiple crack formed, with dispersions arranged so that the fringes in the two pictures are respectively at right angles. The familiar features of a multiple crack figure are seen surrounding the region where the load was applied; but again, as with the natural cube face, the distortions are much more extensive then on the other two faces. The surrounding surface disturbance, due to the formation of the pressure crack, extends over an area of perhaps some nine times that of the area of the pressure figure itself, also the flat level within the crack is strikingly below the undisturbed surface level. This is much more vividly shown by the fringes of equal chromatic order in Figs.78 and 79, which are for two different sections across the multiple pressure figure, the first being a section bisecting opposite sides, the second bisecting opposite angles, i.e., along a diagonal of the square. The other two photographs of these type of fringes complete the picture of the surface distortions; Fig.80 shows a section parallel to a side but just outside the crack figure, i.e., running through the tangle of cracks, while Fig.81 is for a section outside the figure, through a corner of the square

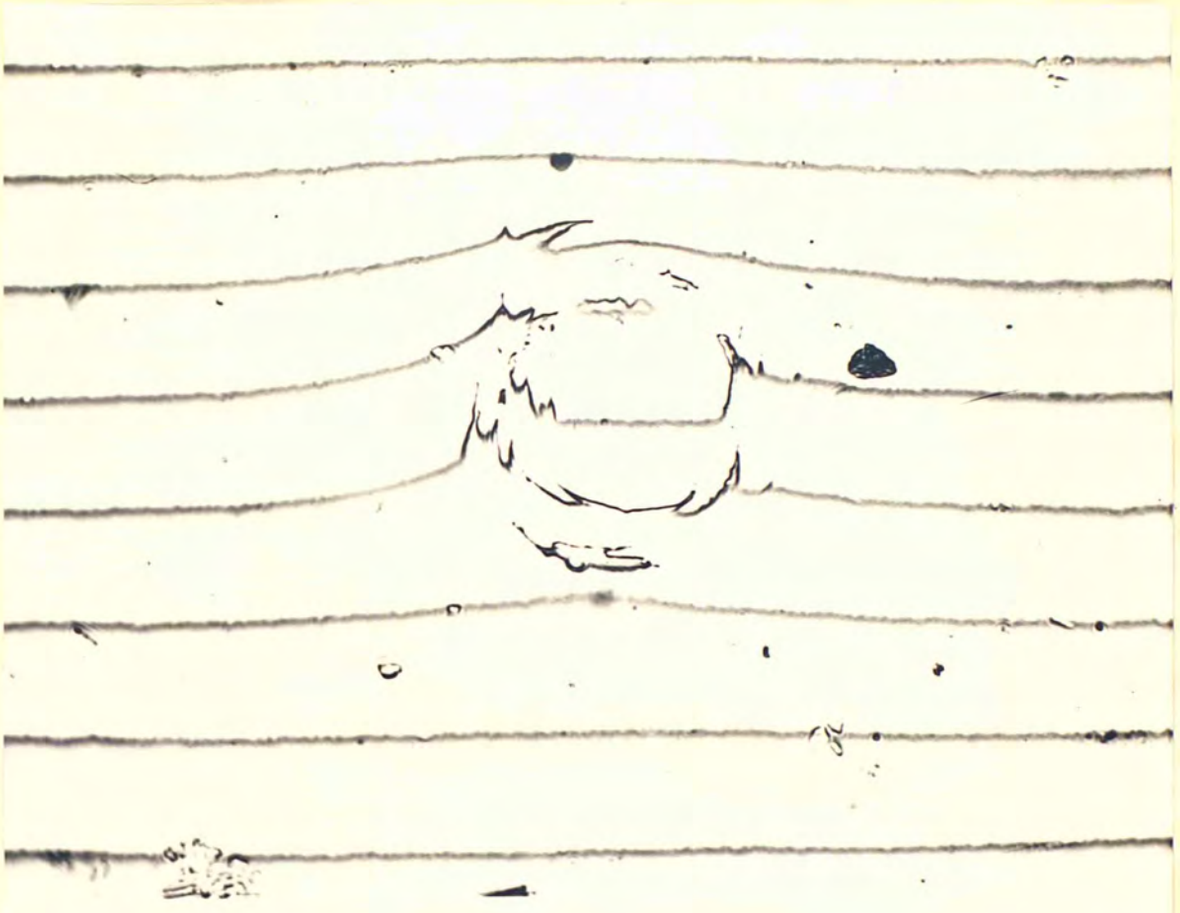

Fig 76
X275

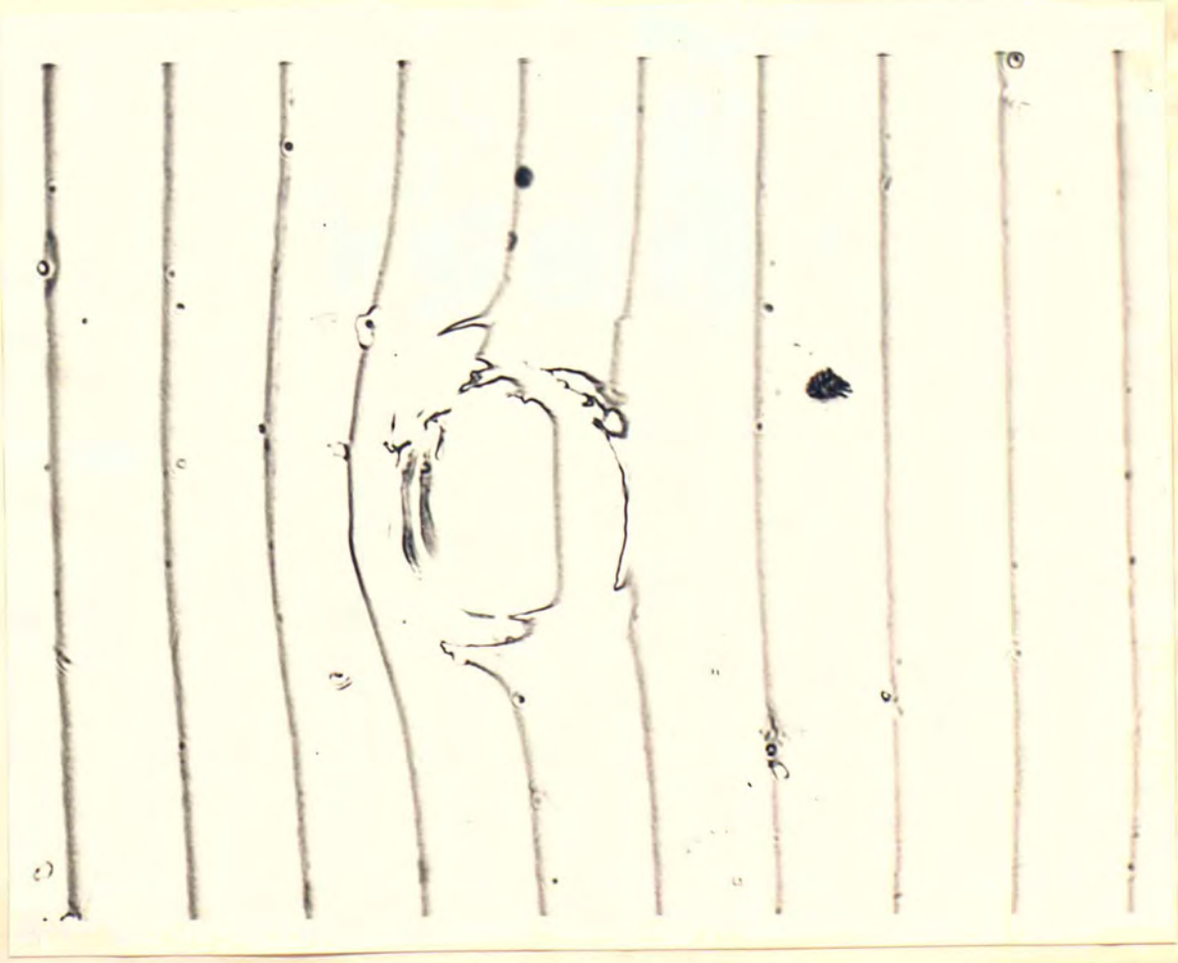

Fig 77
X275.

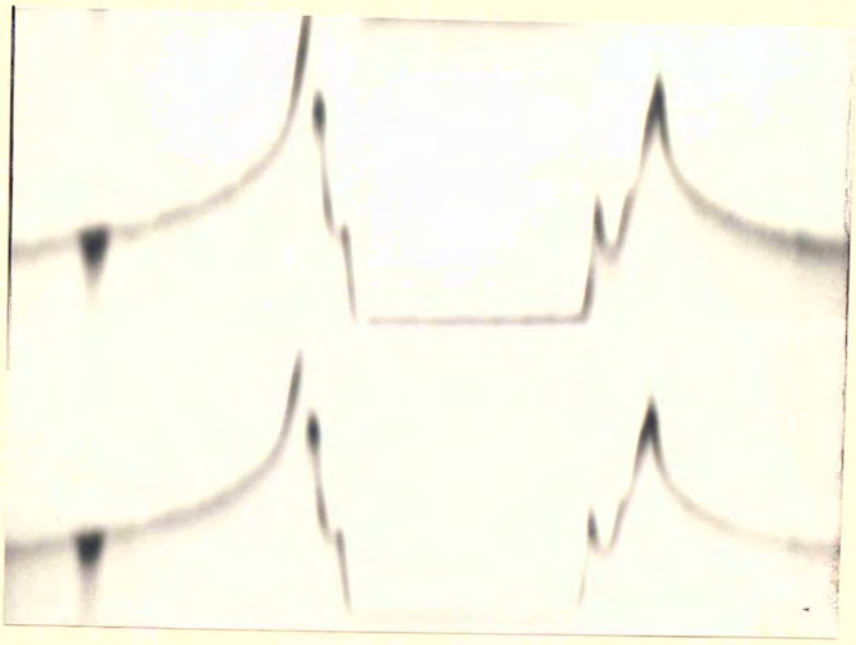

Fig 78 x 320

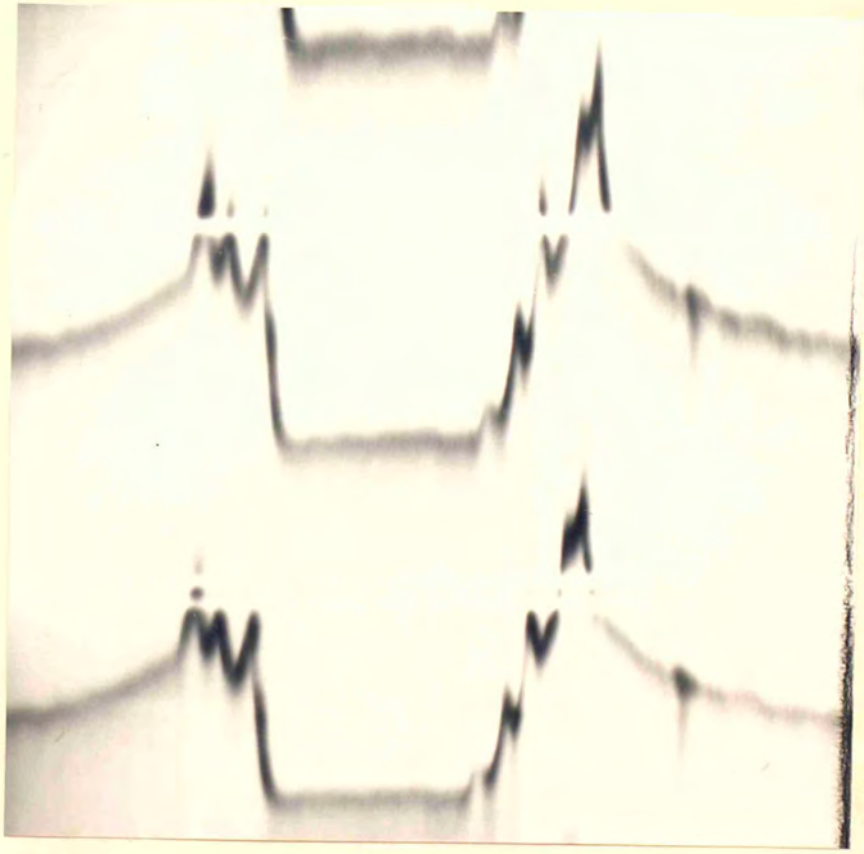

Fig 79 x 320

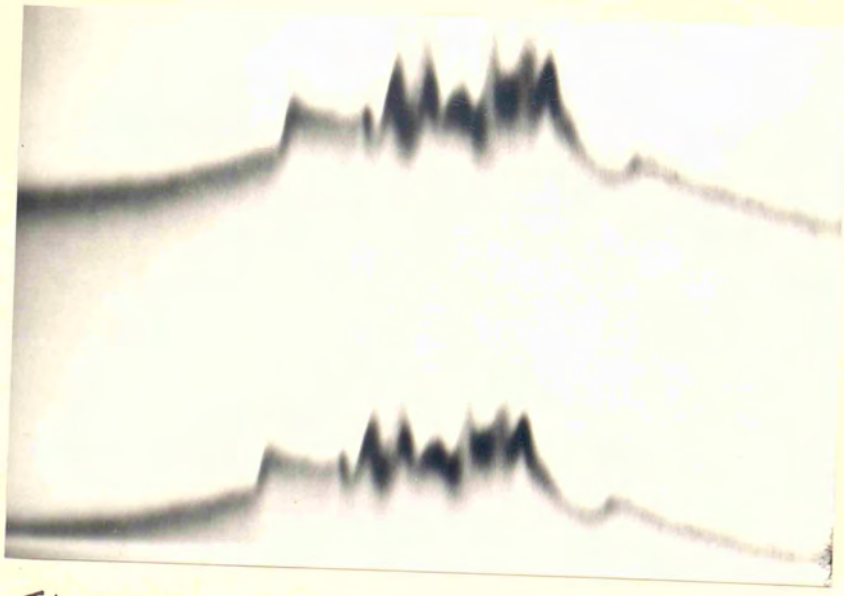

Fig 80 x 320

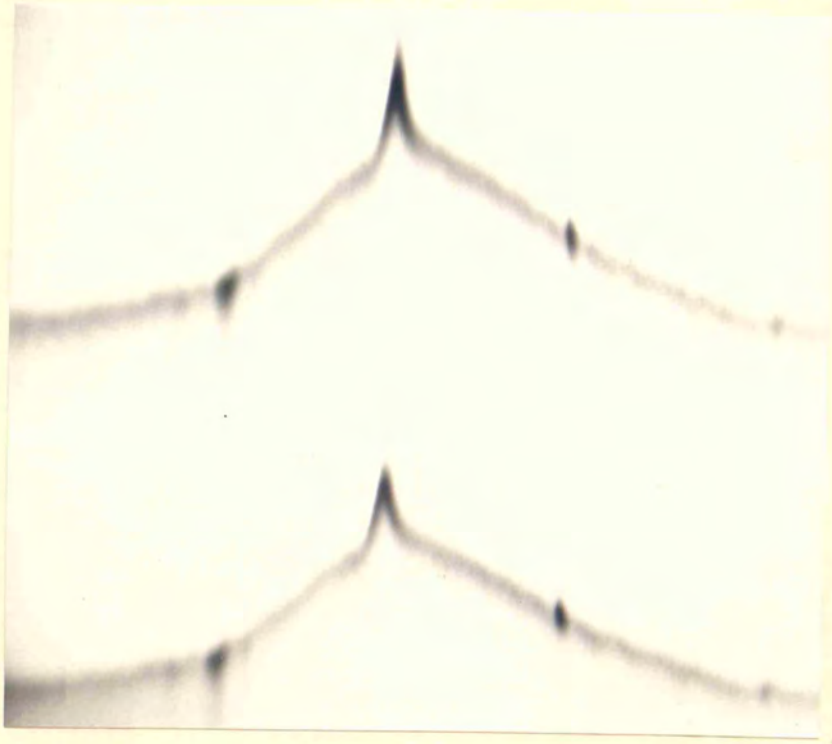

Fig 81 x 320

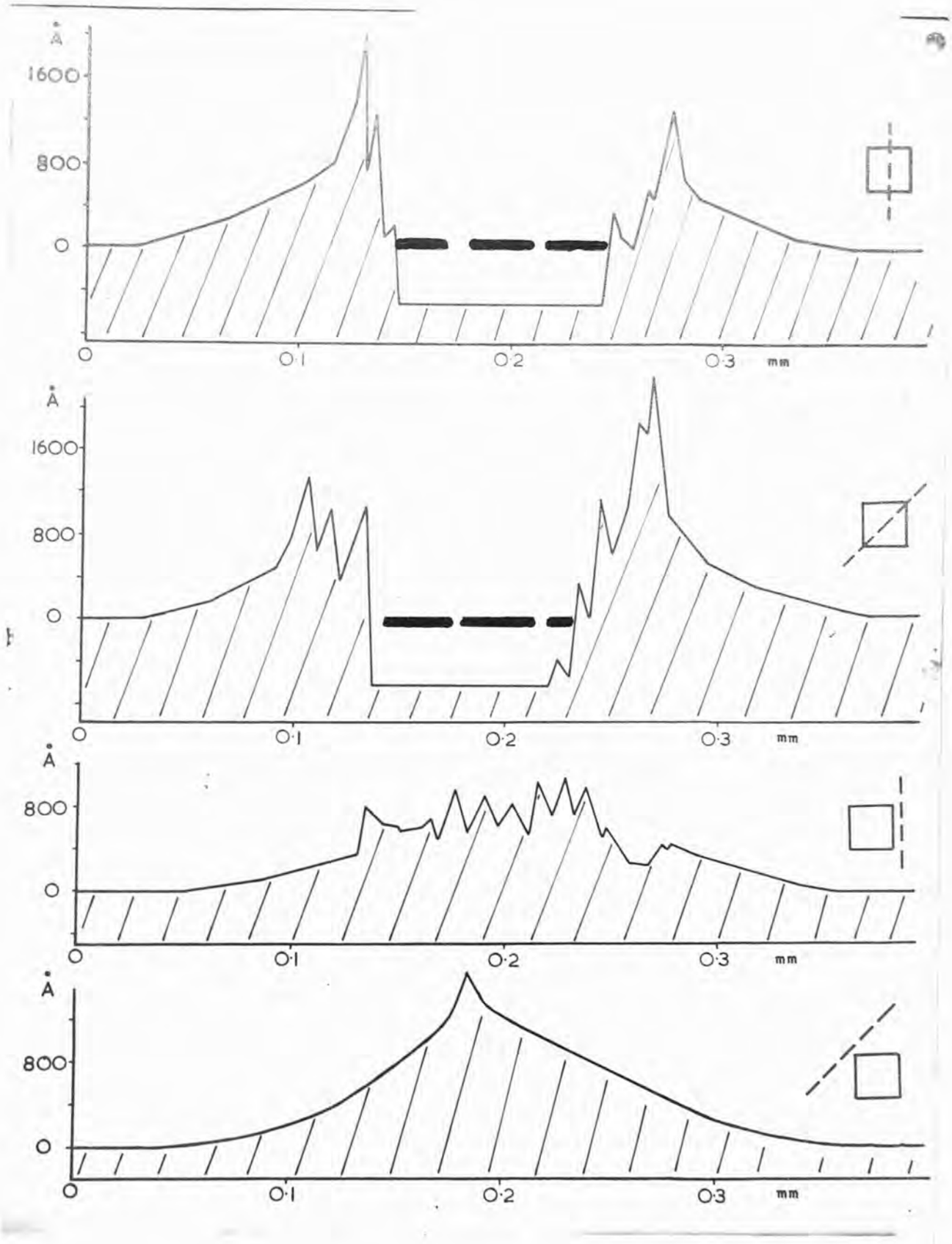
Å
1600
800
0
0·1
0·2
0·3
mm
Å
1600
800
0
0·1
0·2
0·3
mm
Å
800
0
0·1
0·2
0·3
mm
Å
800
0
0·1
0·2
0·3
mm

Fig 82

and parallel to a diagonal. The calibrations of these profiles are shown to scale in Fig.82 where, by the side of each, is illustrated the orientation of the section with respect to the square outline of the crack.

8.5 The Associated Internal Disturbance

The natural cube boart stone was completely opaque, so that it was impossible to find out anything about the disruptions in the body of the stone - although it is certain that they were extensive judging by the extent of the superficial distortions.

For the truncated cubic face of the diamond of octahedral habit, the internal disturbances are of two types. The square dark shadow area of Fig.71 is equivalent to the shadow areas found for the impact on the octahedral face and may be taken as similar cleavage cracking into the crystal.

A second type of internal cracking was observed for this pressure figure, which consists of non-crystallographic circularly curving lines which are inside the crystal. This phenomena can only be detected in transmission, but the violence of this secondary internal disruption accompanying the surface crack of Fig.72 is shown in Fig.83 in which the contrast has been greatly improved by using the technique of crossed polariods. It is seen here that this complex pattern lies just below the surface of the crystal face impacted, the square crack on the surface, although being out of focus, is not excessively de-focussed.

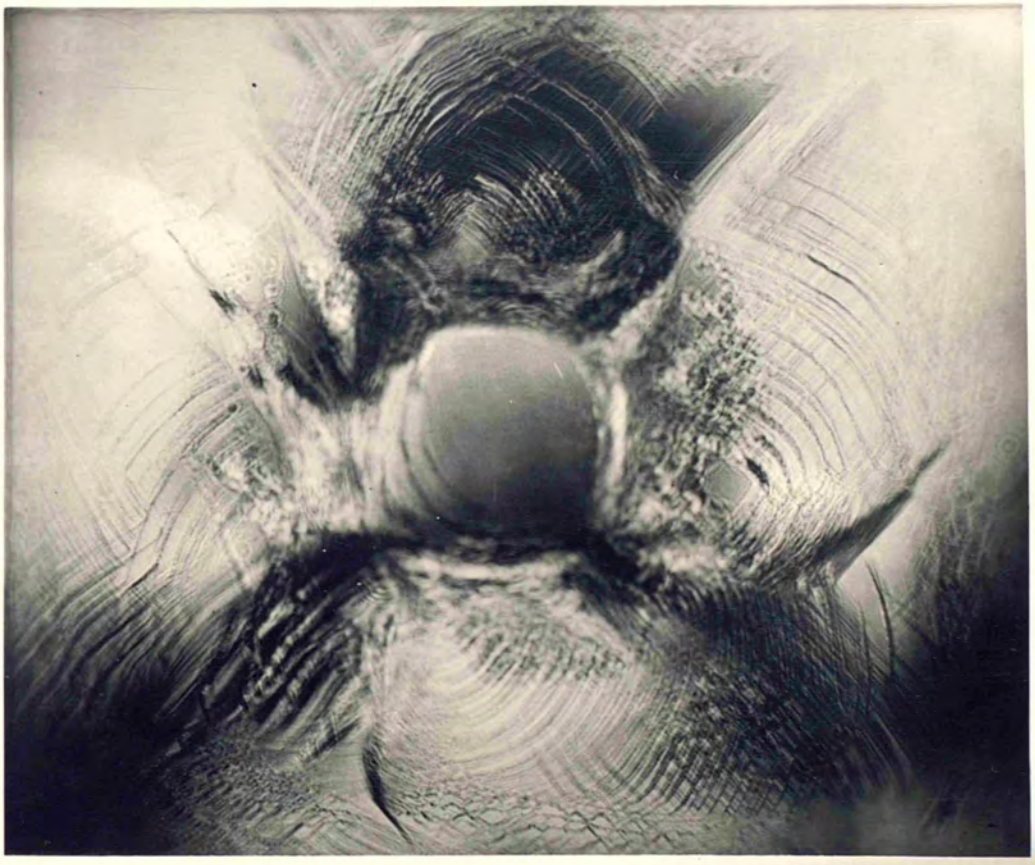

Fig 83 x 260

The main characteristic of this internal distortion is the complex of conchoidal shaped curving crack lines which cross into each other. These are effectively four groups of interlacing circular arcs, each centred on one of the four corners of the square surface crack pattern; they are similar in appearance to the fine crack lines already described, opposite three of the sides of the hexagon cracks on the octahedral face.

8.6 Discussion

The natural cube face of diamond appears to be the most resistant to pressure cracking of the four faces examined. The critical stress on this face is on average 2.0 x 10" dynes/sq.cm. as compared with 1.2 x 10" and 1.8 x 10" dynes/sq.cm. for the octahedral and dodecahedral faces respectively. On these three faces it has been found that there is a certain amount of scatter in the value of the critical stress, so that not too much weight must be given to the value of 1.4 x 10" dynes/sq.cm. found for the single test on the truncated cubic face investigated, particularly when it is noted that the diamond ball impactor used was damaged itself during this test, which may have influenced the critical stress for crack initiation.

It is notable that more damage is done where the applied load is very high before cracking occurs, the stress release being more violent. Thus, for the more resistant faces, when cracking does occur, it does more damage to the crystal than on

faces where only a small load is required to produce a crack. This increased violence explains the much greater internal disturbance occurring at initial cracking for the truncated cubic face than was detected for the impacts on the octahedral face; it also explains, coupled with intrinsic weaknesses of the boart stone, the breaking cracks found right across the natural cube face after a pressure figure had been produced at 30 kgm. load.

The orientations of the cracks on both cubic faces investigated conform with the intersections of crystallographic (111) planes with the two faces. Thus, for a face of a natural cube (111) planes intersect it along lines that are parallel to the diagonals of the square face; while for a truncated cubic face of an octahedron, the lines of intersection of (111) planes with it run parallel to the sides of the square face. Since the cubic faces considered are both portions of (100) planes, the angle between the intersecting (111) planes with these faces are all the same being $54^{\circ}\ 44'$. The configurations for the two faces are shown in Fig.67 (in plan and elevation), where the circles re present the areas of applied critical stress for producing pressure cracks.

The dark shadow area for the crack figure produced on the truncated cubic face, seen in Fig.71, is square in shape and has exactly similar orientation to the square pressure crack itself, with which it is also concentric. It is interpreted as being the sum of four shadow areas, each adjoining one side

of the square crack figure; these appear suddenly as the crack is formed, and simultaneously to give the composite shadow area. Following the arguments given in Chapter 5 for the octahedral case, where there were three shadow areas, these are taken to be cleavage cracks developing into the crystal, from the square surface crack, along the corresponding four (111) cleavage planes which intersect the surface as shown in Fig.67. These cracks close up and become invisible when load is released.

For the natural cubic face no such associated shadow areas could be observed because of the crystal's opacity. However, the orientation of the square surface crack is exactly the same, crystallographically, as that of the cracks on the truncated cubic face; also the general characteristics of the surface distortions of these pressure figures are so similar to those of all the other figures produced on all faces, that it can be safely assumed that the mechanism in this case is no different from that described above for the truncated cubic face pressure figures.

Since all four (111) planes meet a (100) plane at equal angles to it, then it is to be expected that the surface distortion around a pressure figure on a (100) face should be 'squarely' symmetrical. This is found to be the case for the truncated cubic face of the octahedral diamond (see Figs.76 and 77). The fringes over the crack figures on the natural cubic face do not give such a good indication of symmetry; but it is thought that here any asymmetry is, almost certainly, due to

the irregularities in the surface and weaknesses in the body of the crystal, which once cracking is initiated, gave rise to the extensive fracture cracks that were seen on the surface after the experimental tests.

The corners of the pressure cracks on both cubic faces are more rounded and imperfect than on the other two faces impacted. This upholds to some extent the assumption, derived from the Hertzian stress field for a sphere pressed in contact with a plane, that the greatest tensile stress is around the circular perimeter of contact. Thus, for a brittle crystallographic material, breaking under tensile stress along cleavage directions due to impact of a sphere, a hexagon pattern would be more perfect than a square pattern - since the corners of a hexagon are nearer to the inscribed circle of maximum tensile stress than are the corners of a square, so that perfect cleavage would be expected to be sustained to the full extent of the pattern in the one case rather than in the other.

The surface disturbances on the two cubic faces, indicate, even more strongly than before, the occurrence of micro plastic flow. The smoothness of decline of the 'piled up' regions from heights of about 2000 A shown in the photographs of fringes of equal chromatic order are strong evidence, particularly the profile shown in Fig.81 (scale drawing in Fig.82) of a section just outside the pressure figure on the truncated cubic face. Also the depression of the central area within the figures, which is very marked for both cubic faces,

cannot be explained at the moment except by assuming micro plastic flow. The experimental fact already mentioned, that for the natural cubic boart stone the amount of depression occurring in the central region exceeds the amount of material displaced into the pile up, is probably due to the greater compressibility of this particular stone due to the many pockets of impurities and inclusions - so that with the initiation of a crack the material immediately underneath the applied force is dynamically compressed by the stress release, and becomes more compact.

For the internal cracking of both types, previously described, it is interesting to note that the extent of the spreading of each into the body of the crystal, as seen in Figs.71 and 83, is approximately the same; and this amount is practically the same as the extent of the surface micro-distortion as shown by the fringe patterns of Figs.76 and 77. For the secondary cracking, associated with the pressure figure on the truncated cubic face, it can be seen that although the corners of the figure are the centres of the groups of interlacing circular arcs comprising the secondary cracking, the total effect of these on the surface distortion is not very marked. For a section taken across a diagonal with fringes of equal chromatic order (Fig.79) does not seriously differ from one taken bisecting the sides of the pressure figure (Fig.78). These secondary internal cracks are <u>non-crystallographic</u>, and may be due to some form of dynamic shattering at the release of

the stress upon initiation of the pressure crack. These markings, associated with the truncated cubic face, seem similar to those found on the fractured surface of glass where an impact ring crack has developed right to fracture (see photographs in Chapter 4).

# CHAPTER IX

## THE DIAMOND AND SAPPHIRE BALL IMPACTORS

### 9.1 Description of Diamond Ball Impactor

The impactor used throughout the whole of the experiments on diamond so far described, and also on some of the experiments on glass, was a specially prepared cylinder of diamond with a hemispherical ball end of diameter 0.78 mm. The diamond used to make this impactor was an octahedral stone; this was first ground into a cylinder, and then the end of the cylinder was ground and polished until a smooth spherical surface was produced such that the tangent plane to the hemispherical end, which was normal to the axis of the cylinder, was a cubic (100) plane of the original diamond octahedron. The cylinder was then mounted so that it could be fitted vertically into the Penetrascope impacting instrument; hence the contact plane between surface impacted and impactor was a cubic plane of the diamond impactor.

The radius of curvature of this tip was found to be 0.39 mm. by using a microscope coverslip in conjunction with a corrected 4 mm. objective to produce Newtons Rings fringes between the diamond and the glass. The polish on the ball tip, as revealed by the fringes, was quite good.

### 9.2 The Cracking of the Diamond ball impactor

During the observations made while the load was increased in the last series of experiments on the truncated cubic face,

it was noted that at an applied load of 4 kgm. a discontinuity occurred in the Newtons rings fringes surrounding the dark spot of contact. It was suspected that this was due to a crack forming on the impactor itself. After the test was completed, the tip of the impactor was investigated microscopically under high power when it was found that considerable cracking had occurred around the tip, in what appears to be very rounded squares, approximately concentric. This phenomena can be seen in Fig.84 and is presumed to be a multiple pressure figure on the tip of the diamond ball similar in origin to the figures produced on the plane diamond surfaces. Three of the sides, at least, show straight portions and these are all at right angles to the adjacent straight portion, so that the figure can be taken as a much rounded approximation to a square. This is as would be expected for a pressure figure on the tip of the ball, since the tangent plane at this tip is a (100) plane similar in fact to the plane of the truncated cubic face upon which the impact was made.

Since this tangent plane is cubic, it is understandable why the diamond ball was undamaged during the experiments carried out on the octahedral and dodecahedral faces: for it has been found by the experiments that the cubic plane is more resistant to cracking than the other two planes. However, tests were done, using the diamond ball, on the natural cubic face before the experiments on the truncated cubic face, and it may well be that the tip of the diamond ball impactor was first weakened (to the

extent, possibly, of primary cracking) during these tests before the multiple cracking occurred during impact on the truncated cubic face.

9.3 The Accompanying Distortion

When this pressure figure was found on the diamond impactor the radius of curvature of the tip was remeasured in a similar way as described earlier. It was found to be now 0.50 mm. It would thus appear that on cracking, the spherical tip had also flattened as the multiple pressure figure was produced. This may be taken as another indication of micro plastic flow in diamond, analogous to the evidence of the central depression within the multiple pressure figures formed on the different diamond faces - particularly the two cubic faces.

9.4 The Experiment on the Diamond Octahedral face using a Sapphire ball Impactor

The diamond ball, could no longer be considered for controlled experiments since the amount of non-elastic deformation during tests of the ball itself was now an unknown quantity, and it might fracture completely; thus it was returned to the makers for repolishing or copying. It was replaced by a Synthetic sapphire sphere of 1 mm. diameter which was mounted suitably for use with the Penetrascope instrument.

Since the following test was the first to be done on diamond using an impactor, of material known to be considerably

softer than diamond itself, the experiment was made on the octahedral face of diamond as this was known to be least resistant to cracking. The load was applied by the slow motor drive and a series of photographs were taken at different stages.

Fig.85 shows the Newtons Rings fringes between sapphire ball and octahedral face for zero load - it can be seen that there is a fairly good polish on the ball. At 2.9 kgm. the dark-spot had developed to the extent shown in Fig.86, the localized area of disturbance of the fringes on the left hand side of these two photographs is due merely to a persistant grease spot on the sapphire ball. At 8.9 kgm. load, distortion of the fringes occurred as shown in Fig.87. The discontinuities in the fringes occur at lines which are seen to run across the field of view. The maximum load applied was 9.6 kgm. - complete shattering of the tip of the sapphire ball having occurred by then (Fig.88). At this shattering, the fringe pattern has become very complex and there is evidence of many straight crack lines running across the face of the ball tip which is obviously shattered. To the left side of the remnance of the Newtons dark-spot can be seen a continuous dark line forming three sides of a hexagon; it is shown later that this is the only distortion on the diamond surface, being a partly formed pressure figure. The load was then reduced, the appearance of the contact area for 1 kgm. being seen in Fig.89 which shows up more clearly the crack

Fig 84
X710

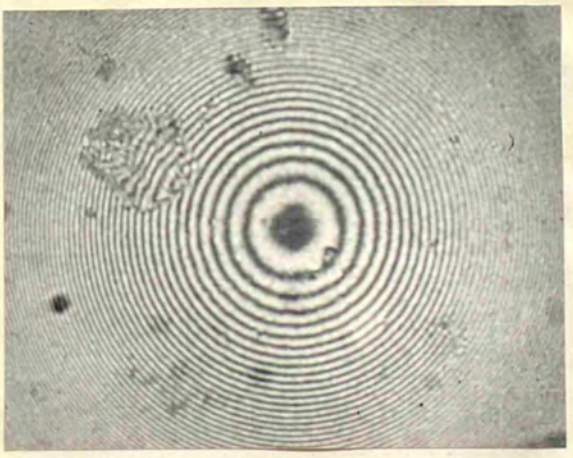

Fig 85 x 380

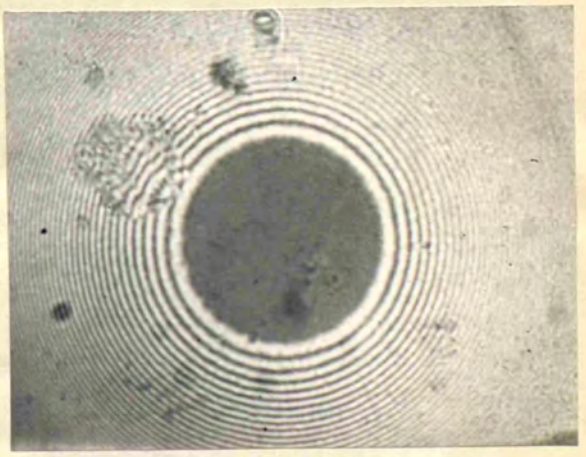

Fig 86 x 380

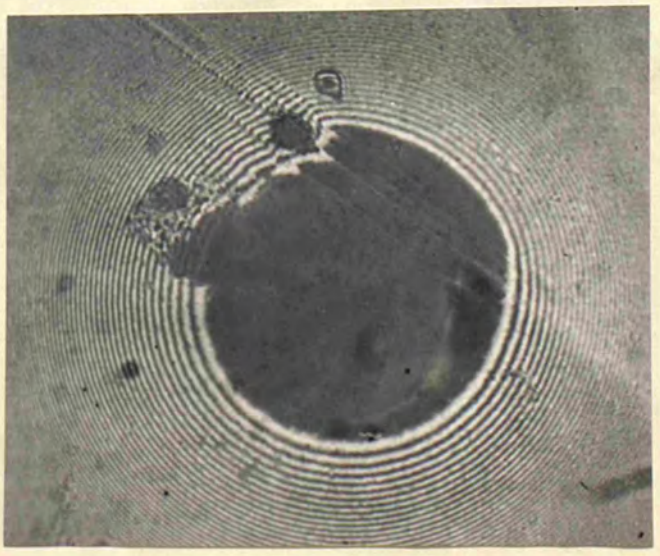

Fig 87 x 380

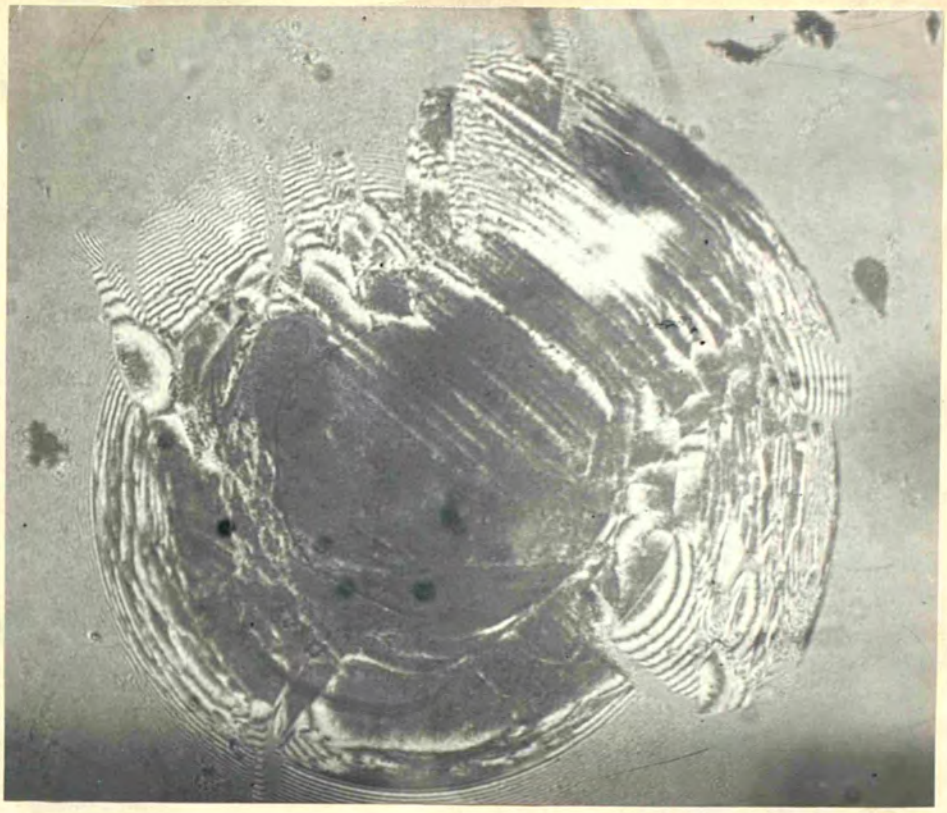

Fig 88 x 380

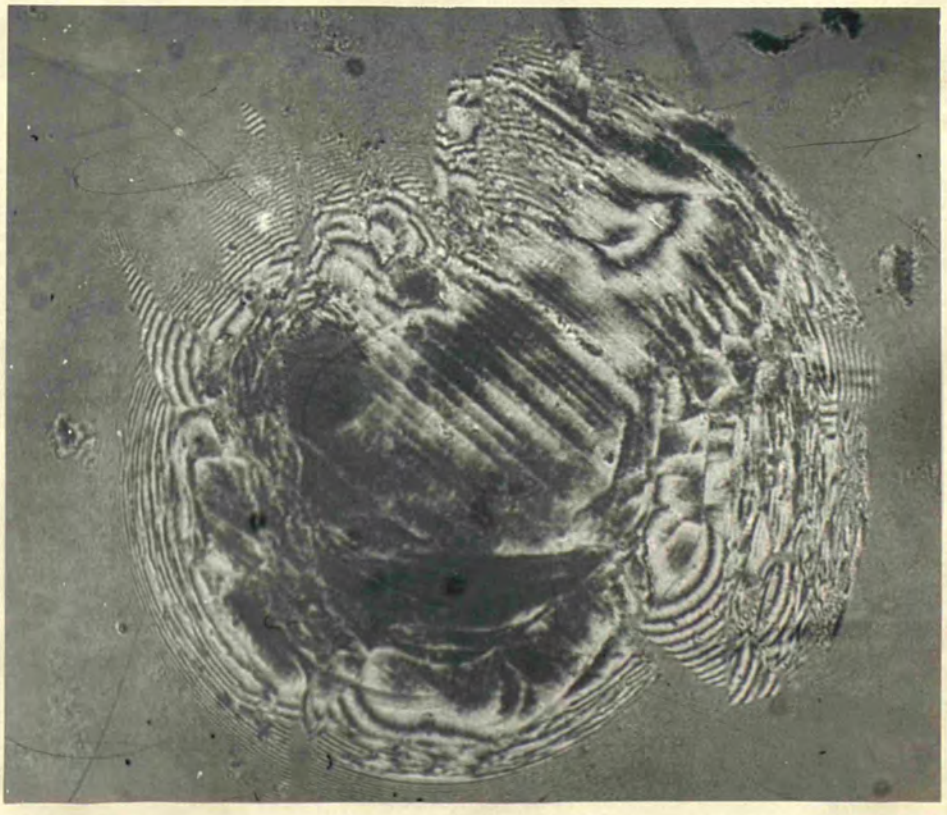

Fig 89 x 380

lines on the ball surface. The load was then completely removed and the effects on the diamond and sapphire surfaces studied independently.

9.5 The Resulting Distortions on the two surfaces.

When the impactor had been removed right away from the surface of the octahedral diamond, it was seen that the half hexagon already referred to was indeed a partly formed pressure figure. This can be seen in the reflexion phase contrast photomicrograph, Fig.90. It is much less clearly defined than other pressure figures formed on this surface in previous experiments, having corners much more rounded. The size of the figure is bigger than that of the primary cracks formed with the diamond ball impactor on this face ($55 \times 10^{-6}$ sq.cm. as compared with $44 \times 10^{-6}$ sq.cm), this is due partly to the large size of the ball impactor ( diameter 1 mm compared with 0.78 mm.) and partly to the greater compressibility of sapphire, so that the area of contact was greater at cracking point. This larger size may possibly account for the roundedness of the figure, but it is more likely due to the crystallographic deformation of the sapphire as it shatters, altering the stress concentration within the diamond. That the surface distortion for this crack figure is of the general pattern, is shown by the fringes of equal chromatic order in Fig.91. Here the dispersion and the magnification are seen to be extremely high, the maximum height displacement of the pile up around the crack being no more than 100 A

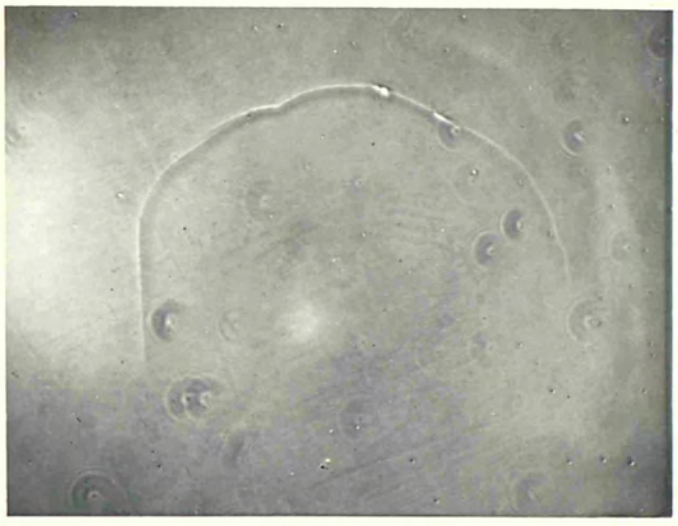

Fig 90 x 555

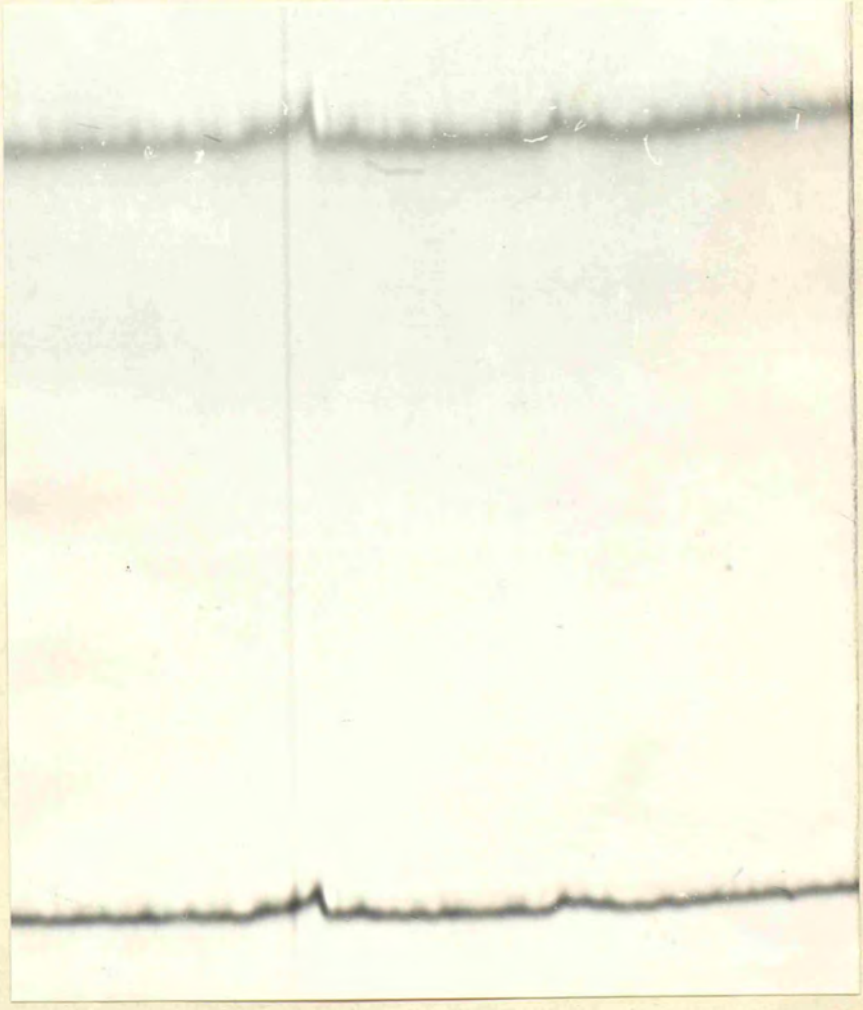

Fig 91 x 320

Fig 92 x 400

(the section is that bisecting the two half formed sides of Fig.90).

The final appearance of the tip of the sapphire ball is seen in Fig.92 with high magnification. It is obvious that complete shattering has occurred - small interference patterns being seen in the air gap of micro cracks. The many parallel straight lines occurring right across the flattened surface of the ball tip are almost certainly slip lines it being deduced that multiple slip occurred when the deformation extended beyond the elastic limit, this then being followed by conchoidal fracture around the perimeter of the contact area.

The occurrence of extensive slip on the distorted sapphire ball is in strong contrast with the formation of a pressure figure found when the diamond ball was permanently distorted, with the accompanying probability of micro plastic deformation in this latter case.

# CHAPTER X

## THE TUNGSTEN CARBIDE BALL IMPACTOR USED ON THE DIAMOND FACES

### 10.1 Introduction

The use of the sapphire ball impactor having set the precedent for using materials softer than the impacted diamond; it was thought worthwhile trying another hard material, less brittle than synthetic sapphire, which would be more likely to plastically deform than to slip when the static impact was made. Since the material would inevitably be less hard than the diamond surface impacted it was necessary to obtain balls of as small a diameter as possible so that for the maximum loads applied by the Penetrascope the average stress over the area of contact would be the maximum obtainable.

Sintered Tungsten Carbide balls were obtained of minimum diameter 1 mm. (graded). The hardness of Tungsten Carbide is in the order of 2000 V.D.H., which is approximately the same as that of synthetic sapphire. Three of these balls were mounted suitably for use with the Penetrascope, and each was used for a test on a diamond surface, observations of the region of contact being made during the tests.

The three surfaces used were the natural octahedral face of the diamond previously impacted with the diamond and the sapphire ball impactors, a dodecahedral face of a diamond of octahedral habit, and a cubic face of another diamond of octahedral habit. These last two stones were both in the

form of transparent parallel faced plates obtained by sawing and polishing across pairs of parallel planes on either side of the 2-point plane and the girdle plane respectively (see Fig.3). Impact loads were applied up to the maximum of 30 kgm. in each case; for the octahedral face a primary pressure formed at 16 kgm. and developed multiplicity by 30 kgm., on the other two faces no pressure cracking could be obtained with the tungsten carbide balls used.

The cracking on the octahedral faces was far more disruptive than had been previously obtained on this face, the internal disturbances being of a similar order to those pertaining to the crack figures produced by the diamond ball on the truncated cubic face. In all three tests, the tungsten carbide balls were permanently flattened over the regions which had been in contact with the diamond surfaces, considerable plastic deformation having taken place.

10.2 The full development of a Pressure figure on the Octahedral face

The complete series of photographs taken during the impact test on this surface are shown in Figs.93 to 103 where the corresponding load (W) in kgms. is shown beside each photograph. It is seen that cracking is initiated at a load of 16 kgm., when the figure formed is almost exactly the circumscribing hexagon to the circle of contact; shadow areas spread from three of the six sides, there being signs of internal disruption opposite the other alternate sides.

As the load was still further increased, both internal effects developed - but not symmetrically. In Fig.97 the shadow area at the top is seen to have extended before the other two, and in Figs.98 and 99 it is clear that two areas have developed while the third has been inhibited. This last photograph was for the maximum load of 30 kgm., and presumably if it had been possible to increase the load further, the third shadow area would eventually have spread out similar to the other two areas. In the hope that this might still happen the 30 kgm. load was left on for an hour, by which time the load had crept down to 28.8 kgm (probably due to relaxation of the apparatus under the extreme stress conditions). The load was again increased up to the maximum value but no further development occurred.

The load was then slowly reduced mechanically: almost immediately, with a faint crack sound, the third shadow area suddenly extended, to give the completely symmetrical pattern of internal disturbances seen in Fig.100, the load having been reduced only to 29.2 kgm. The load was reduced to zero after this, and it can be seen in Figs.101 and 102 that, whereas the shadow areas disappeared progressively as the load decreased, the disturbances opposite the other three sides remained unchanged. Also, it is to be noted that the shadow areas retreat asymmetrically, the first to disappear being the same one that last developed fully, only after a long delay. As the ball came away from the surface it moved very slightly over to one side (again, this is probably due to relaxation of the apparatus

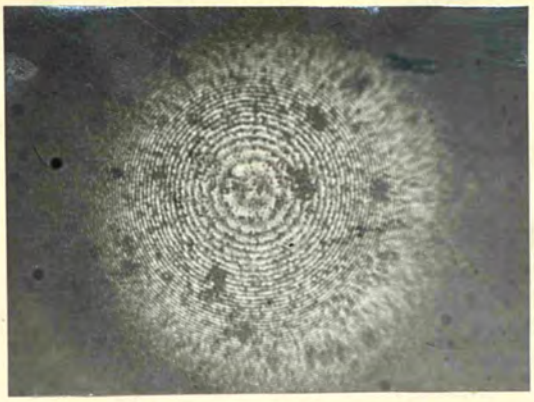

Fig 93 x 235 W=0

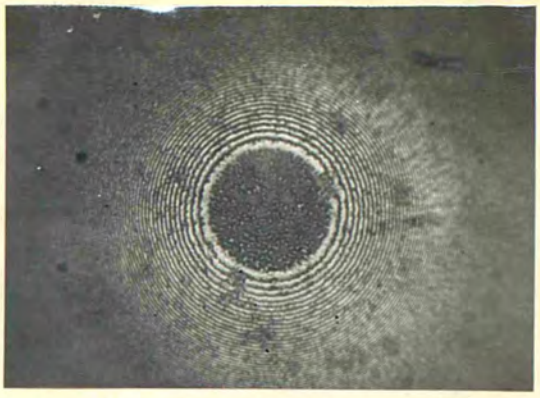

Fig 94 x 235 W=3

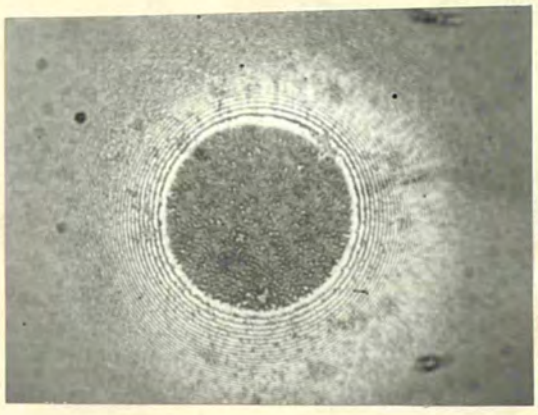

Fig 95 x 235 W=9

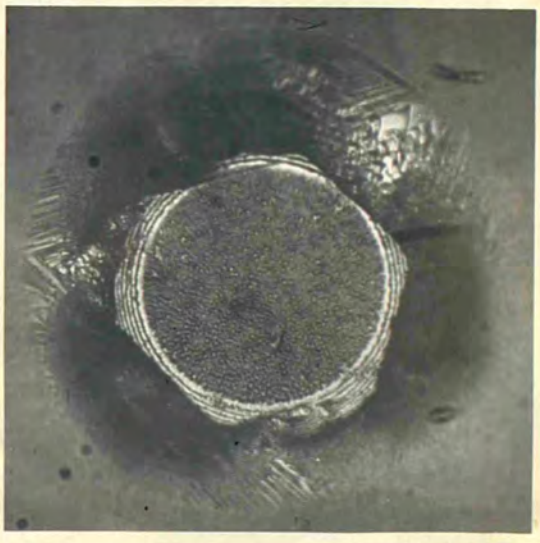

Fig 96 x 235 W=16

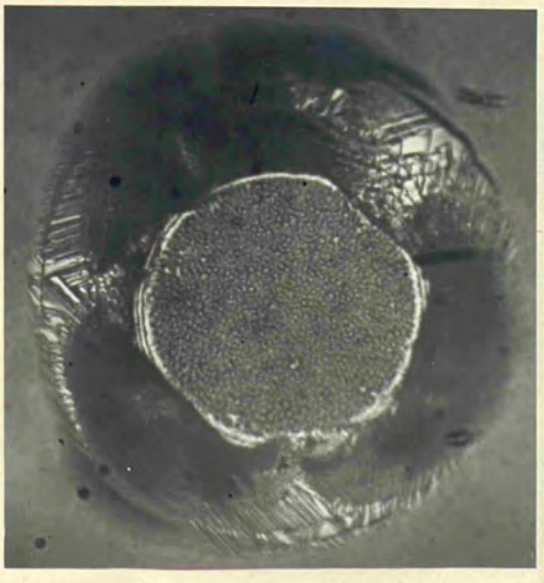

Fig 97 x 235 W=20

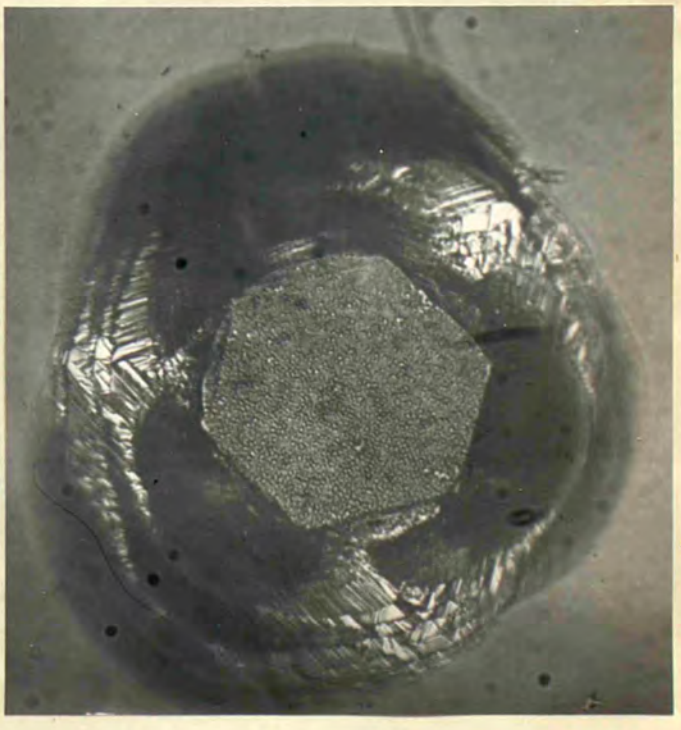

Fig 98 x 235 W=26

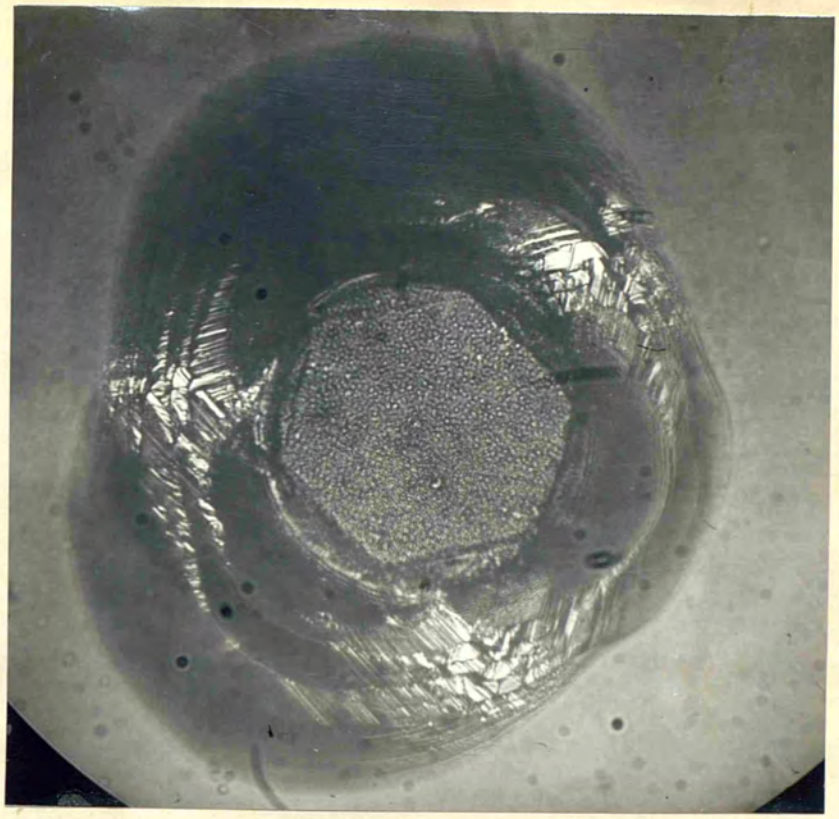

Fig 99 x 235 W = 30

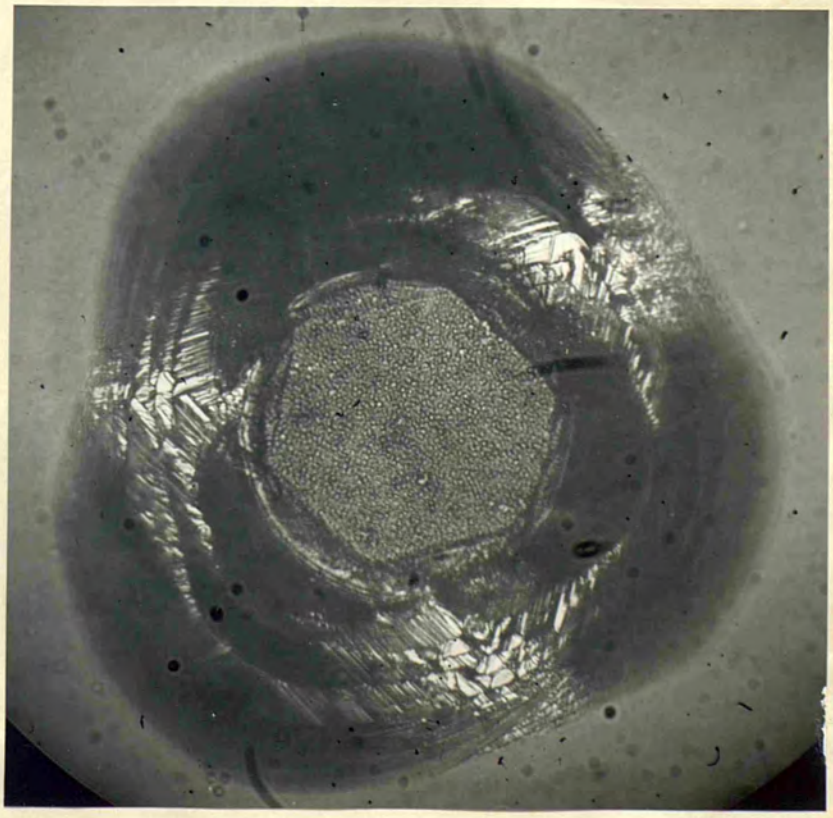

Fig 100 x 235 W = 29.2

Fig 101 x 235 W=6

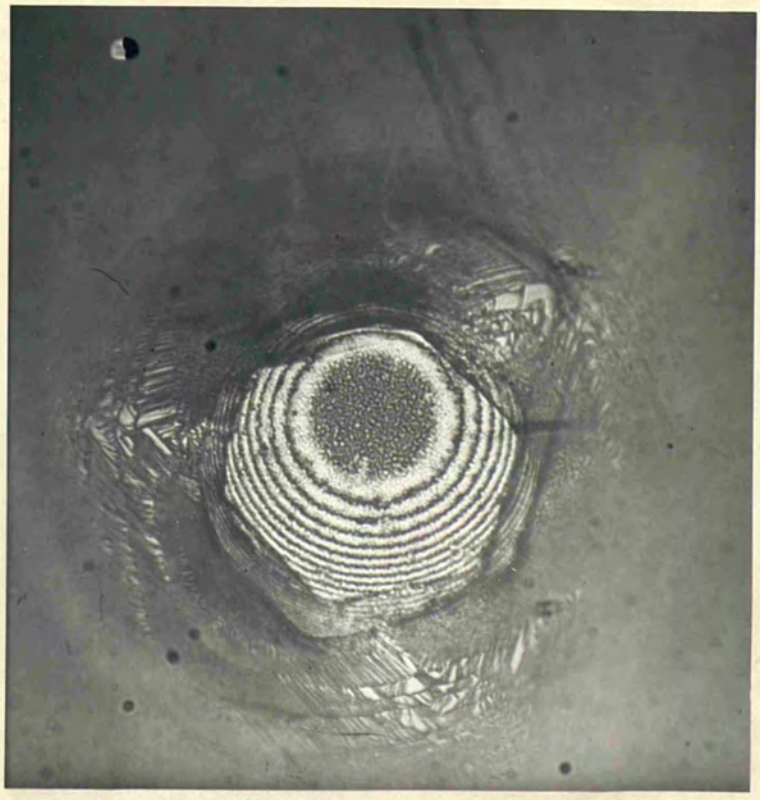

Fig 102 x 235 W=0.5

Fig 103 x 235 W=0

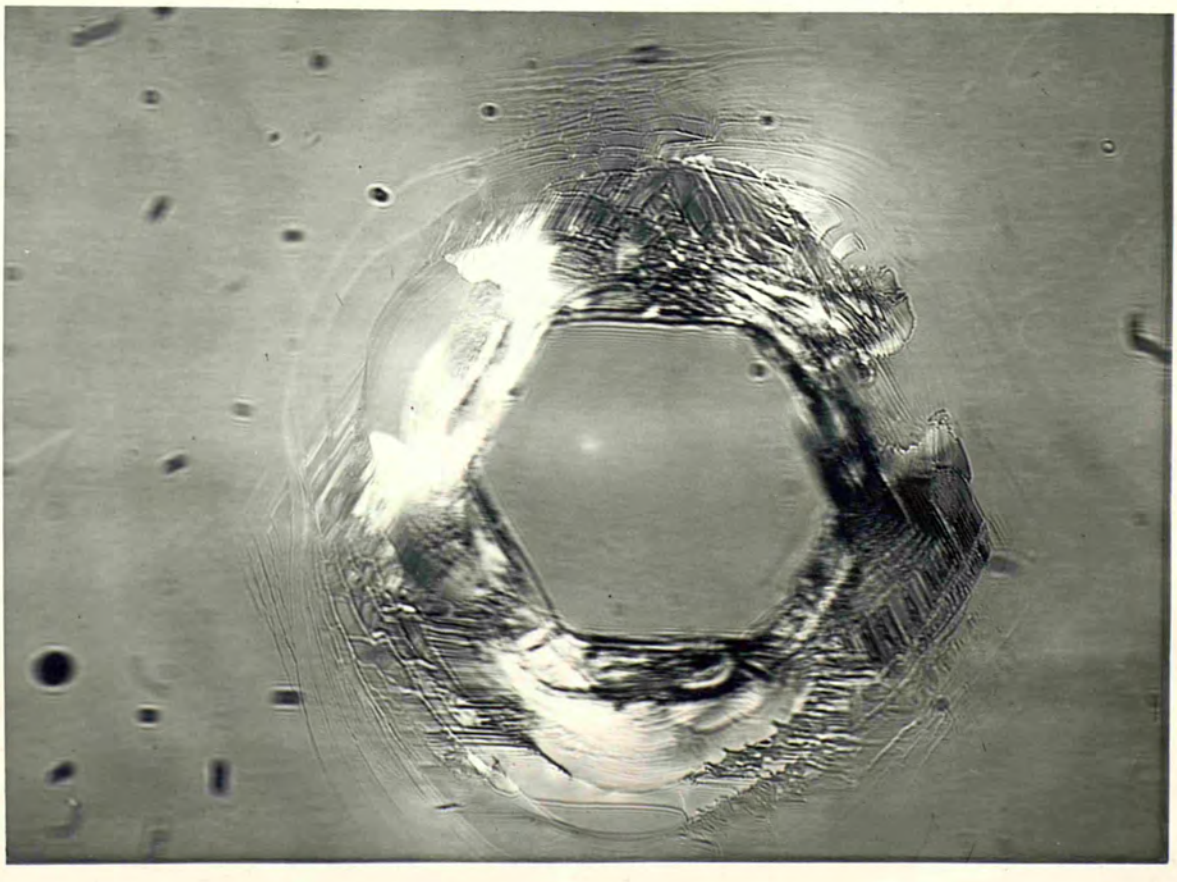

Fig 104 x 300

on stress release).

In Fig.103 the final pressure figure can be seen, the ball having been raised clear of the diamond surface and removed completely. Note that all these photographs have been taken from below, through the underface and the body of the stone; thus all the pictures are mirror images of what would be seen by looking at the impacted surface directly (i.e. Fig.103 is a lateral inversion of Fig.106).

10.3 Optical Study of the Crack produced on this face

The first investigation was to observe the internal secondary crack lines by looking at the stone (impacted surface direct) in transmission with polarized light the analyser and polarizer being crossed. These cracks are clearly seen in Fig.104, where it is evident that they occur below the surface - since the outline of the surface hexagon figure is out of focus. It was found that the further these secondary cracks were away from the pressure figure the deeper they were below the surface - which indicated that they occurred roughly on planes acute to the surface going away from the pressure figure.

This photograph gave a first indication that there are two types of this secondary cracking. The first is seen to be sets of multiple straight lines, there being two sets for each of the three alternate sides of the hexagon as shown schematically in Fig.105. These lines are not perfectly in focus in the photograph, where attention is concentrated elsewhere, but can be seen very clearly in many of the photographs of the

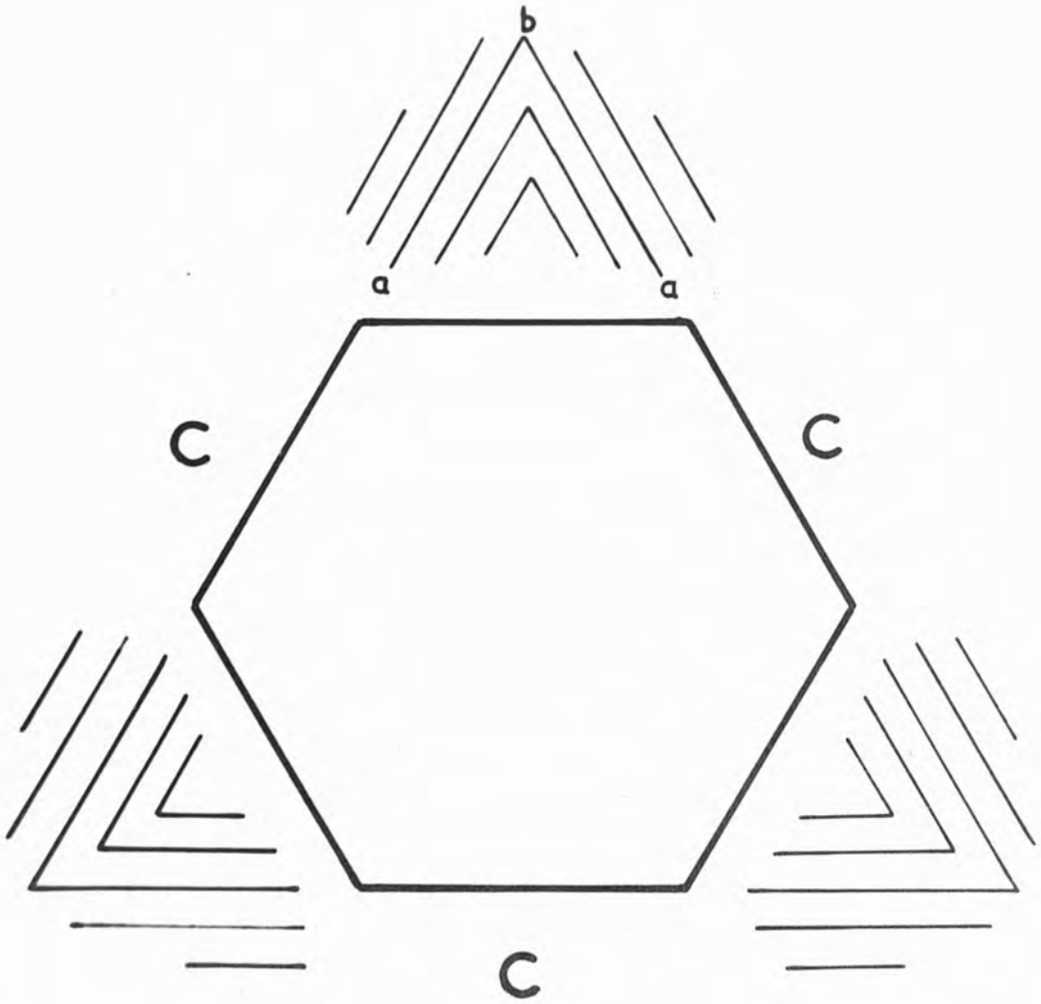


Fig 105

series taken while under load (e.g. Figs.96 to 102); there are three principal directions for these lines which are parallel to the other three alternate sides of the hexagon (the sides where the shadow areas occur while under load). This means that the three directions are identical with the directions of the lines of intersection of crystallographic (111) planes with the octahedral face. This type of secondary phenomena, consisting of straight lines and being crystallographically orientated, is dissimilar to any other internal disturbance detected in previous experiments.

The second type of secondary internal disturbance is clearly seen in focus in Fig.104, and lies beyond the first type - also being deeper in the crystal. This occurs opposite the same three alternate sides of the hexagon as above, and consists of three sets of slightly curving irregular cracks running approximately parallel to the sides. This phenomena is exactly similar to that found for the pressure figure formed on this same face by a diamond ball impactor (see Fig.55). It is slightly more extensive but the characteristics are identical (see the schematic diagram of Fig.56). This phenomena also corresponds with the secondary internal cracks found associated with the pressure figure formed on the truncated cubic face, in that the lines are curving and non-crystallographic.

The surface pressure figure is seen in the reflection phase contrast photograph of Fig.106, the face having first

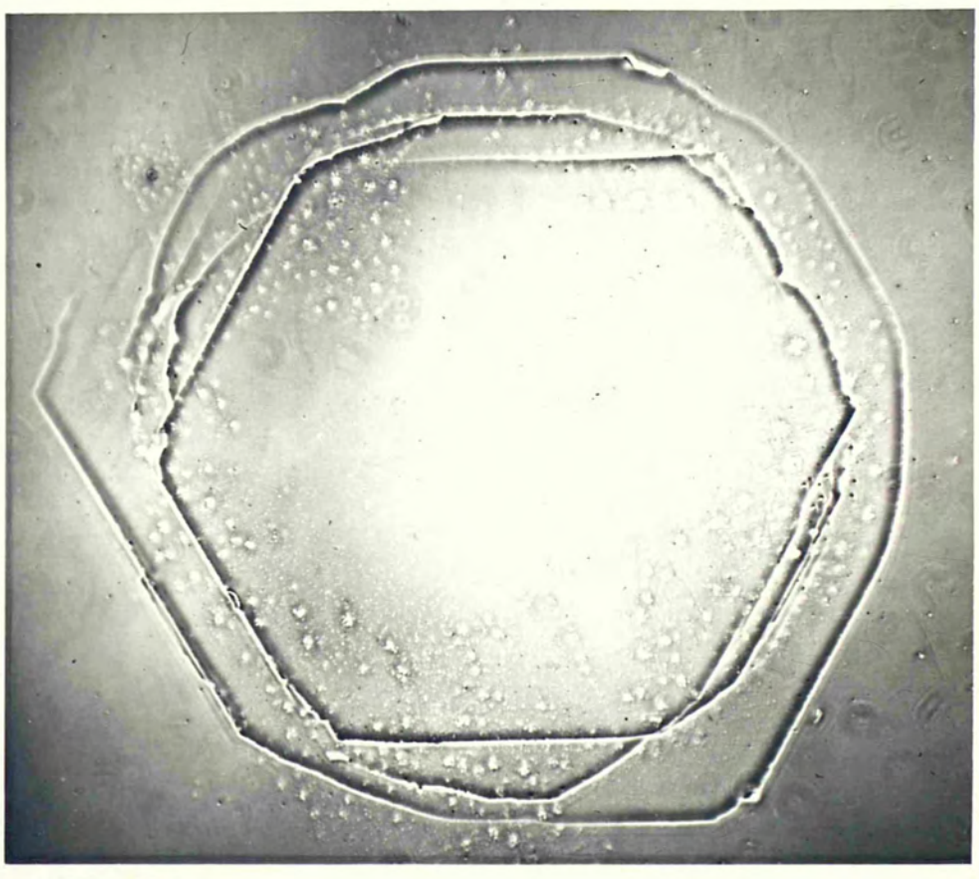

Fig 106 x 555

been silvered. It is to be noted that the primary crack is an almost perfect hexagon while the outer crack of the multiple figure is very imperfect in its hexagonal shape, although it is still orientated truly.

Lastly, the silvered surface of the diamond was matched against a silvered glass flat in order to obtain multiple beam interference fringes for the detection of the surface distortion accompanying the formation of the pressure figure. Figs.107 and 108 show the Fizeau fringe patterns crossing the figure; the first photograph showing a fringe bisecting opposite sides, the second showing a fringe bisecting opposite angles, of the hexagonal crack. The corresponding fringe patterns, using fringes of equal chromatic order, are shown in Figs.109 and 110. The calibrated sectional profiles given by these last two photographs are drawn to scale in Fig.111. These profiles indicate that there would seem to be greater symmetry across opposite sides than was found in previous cases of pressure cracks on this face; also, the height displacements are shown to be twice as much as those for the previous pressure figures, which were all formed at critical loads considerably smaller than the 16 kgm. necessary for the production of the primary crack in this later test, using an impactor of larger diameter.

10.4 The Effect on the Impactor

It has already been stated that in these tests on diamond surfaces using tungsten carbide balls, the balls were permanently

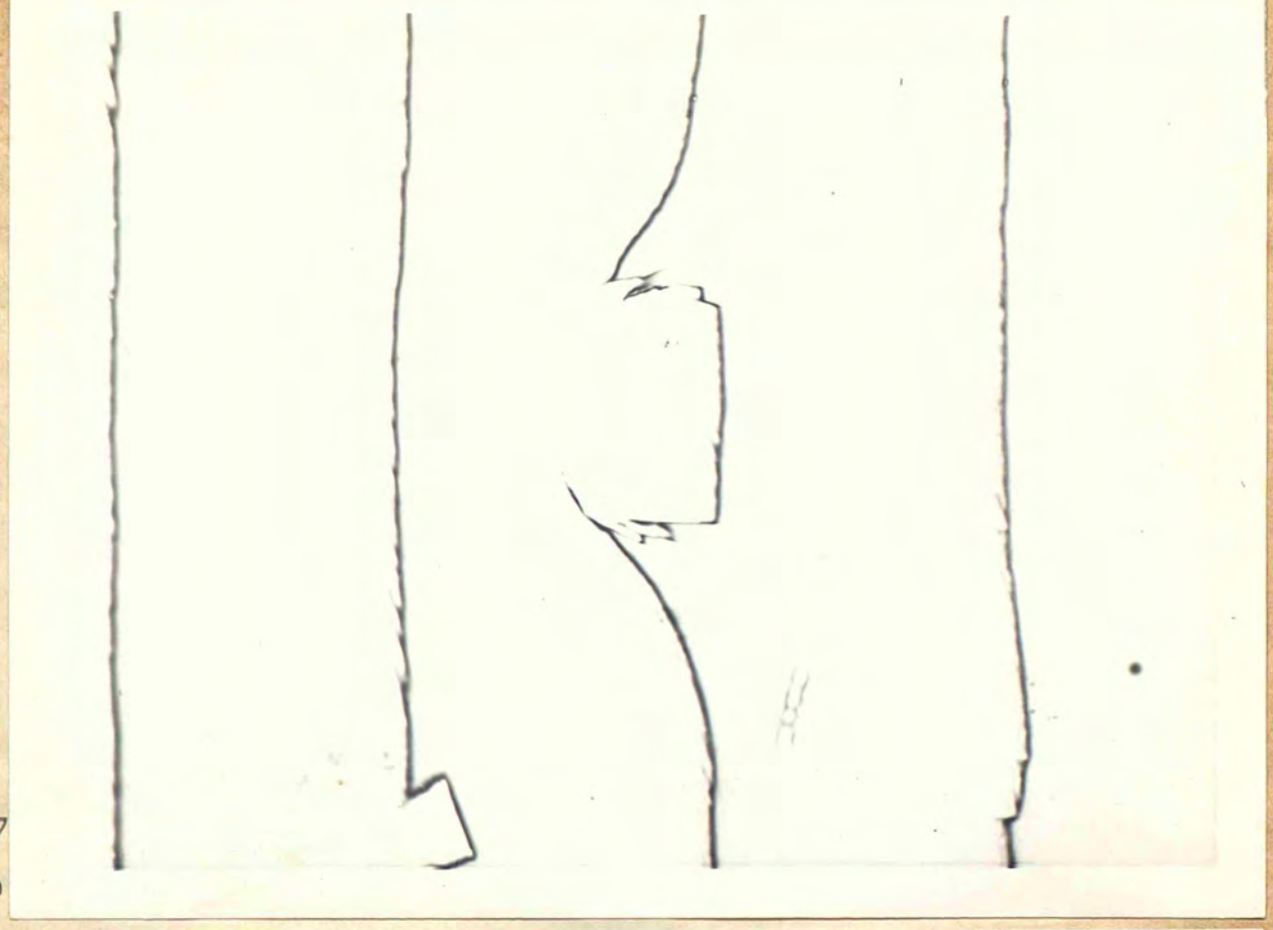

Fig 107
×220

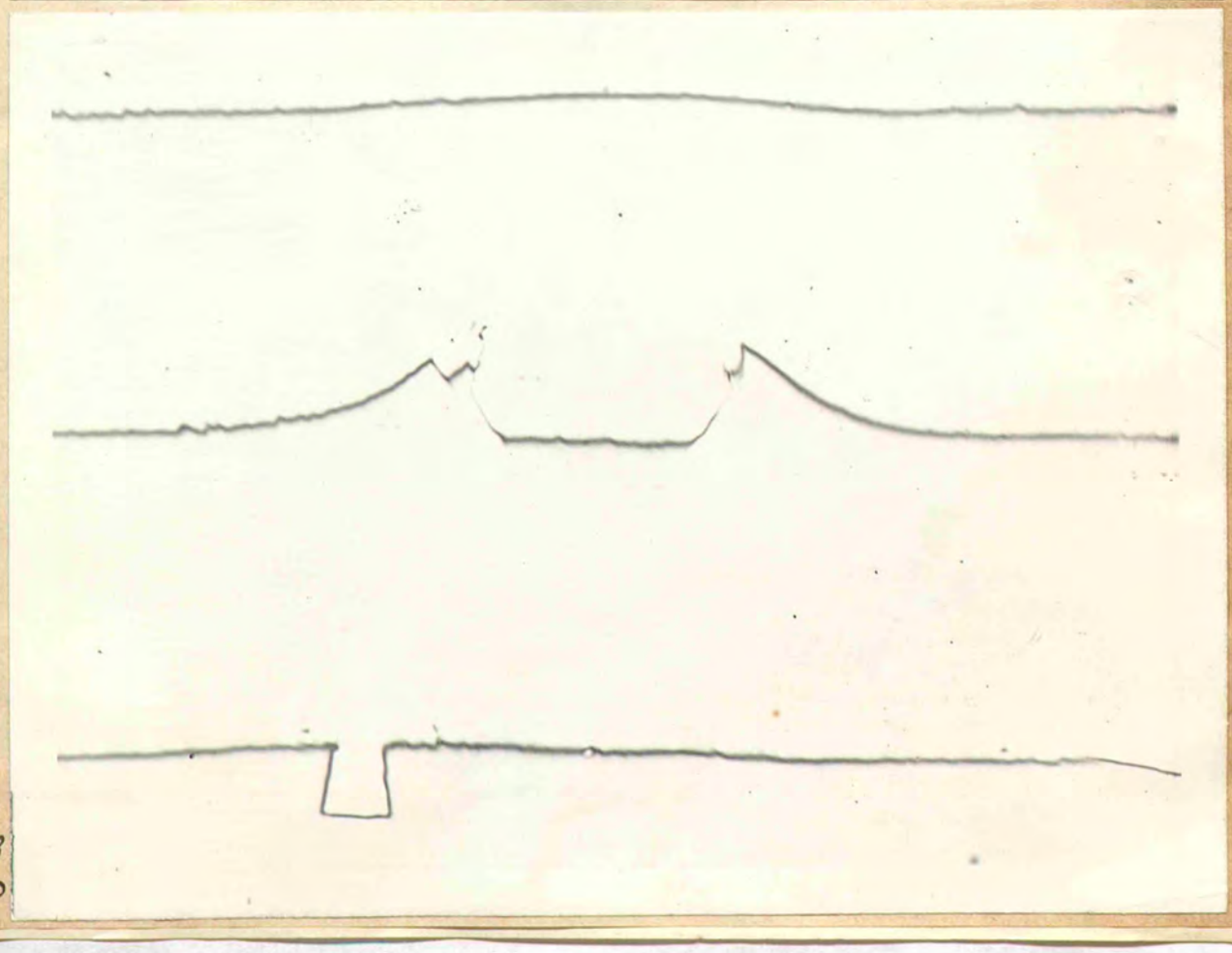

Fig 108
×220

Fig 109 x 320

Fig 110 x 320

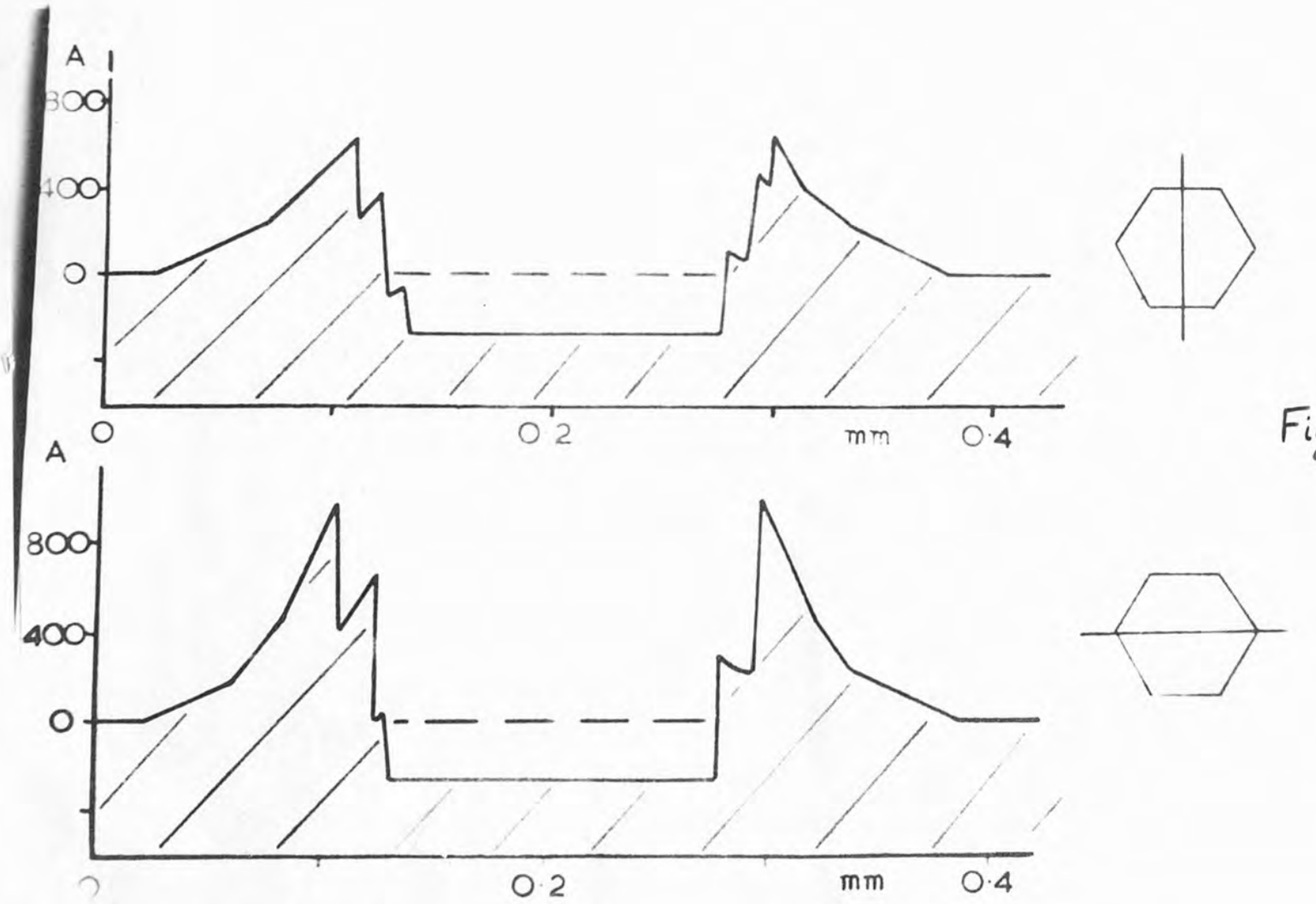


Fig 111

flattened during the testing. The radii of curvature of the balls were measured by the Newtons Rings interference fringes method mentioned elsewhere (see Chapter 9). The concentric fringe patterns, obtained by this method, are shown in Figs.112 and 113 for the tungsten carbide ball (graded 1 mm.diameter) used for the experiment on the octahedral face just described. These two photographs show respectively, the patterns obtained before and after testing. The usual method was followed, of plotting n, the fringe order, against $d^2$ , the square of the diameter of the respective fringe, in order to obtain the radius of curvature from the slope of the graph. The resulting graph lines are seen in Fig.114 (A being for the ball before use, B after testing). The sphericity of the ball before use was good, and its measured diameter was 1.07 mm., from the straight line A. After the test was done it can be seen from line B that away from the tip of the ball the sphericity is undisturbed, the line being straight and of the same slope as line A; but for the region of the tip of the ball the graph curves, with consequent change of slope. For the tip itself, over an area of about 0.13 mm. diameter, the line is again straight but has a completely different slope, showing here the ball is approximately spherical, the radius of curvature being 1.56 mm. instead of the original 0.535 mm. Thus considerable localized flattening has occurred in the region where contact was made, although the bulk of the ball impactor has remained undisturbed - beyond a distance of approximately

Fig 112 x 450

Fig 113 x450

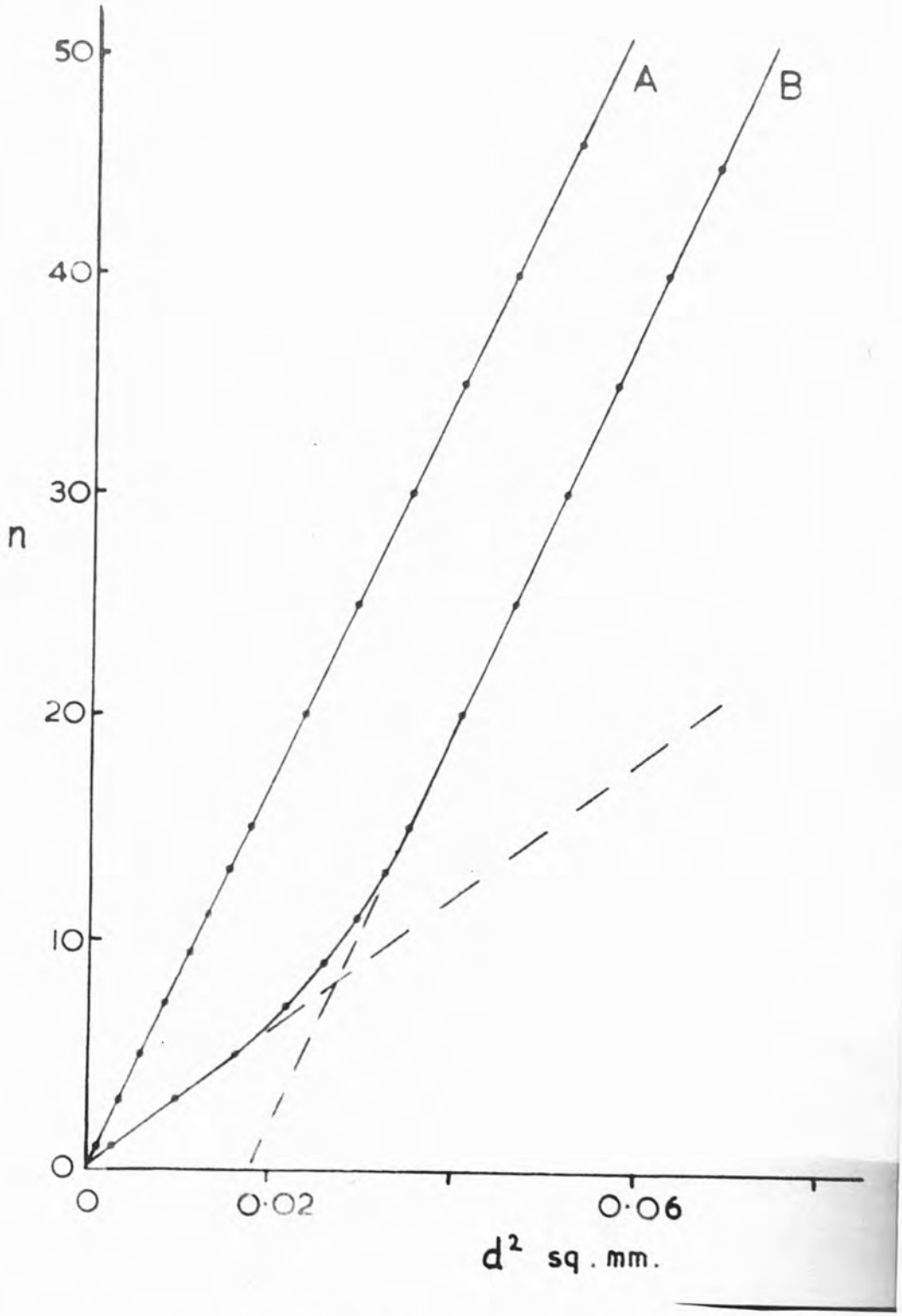


Fig 114

0.1 mm. from the tip.

The flattened tip of the tungsten carbide ball was observed under a microscope using a high power objective and can be seen in Fig.115 where some straight lines can be detected on the surface. Since tungsten carbide is a sintered product and definitely not crystallographic, these lines are of interest. Their orientation with respect to each other is shown diagrammatically in Fig.116 where it is seen that they comprise four short lines which form approximately four sides of a hexagon, and within these are two longer lines which are almost at right angles to each other and quite clear in the photograph.

10.5 The tests on the other two faces of Diamond

With similar Tungsten carbide balls of approximately 1 mm. diameter tests were made on the Dodecahedral and cubic faces, already described, up to the full maximum load of 30 kgm. without any cracking being obtained. After both these tests, the surfaces were examined at the region where contact had been made, but no change in the surfaces could be detected at all. The balls, in both tests, were considerably flattened at their tips - approximately to the same extent as the flattening occurring for the previous test on the octahedral face (no lines could be seen on the surfaces of these two balls after testing).

With the deformation of the balls, the applied stress is reduced, for the same load, since the area of contact

Fig 115 x 400

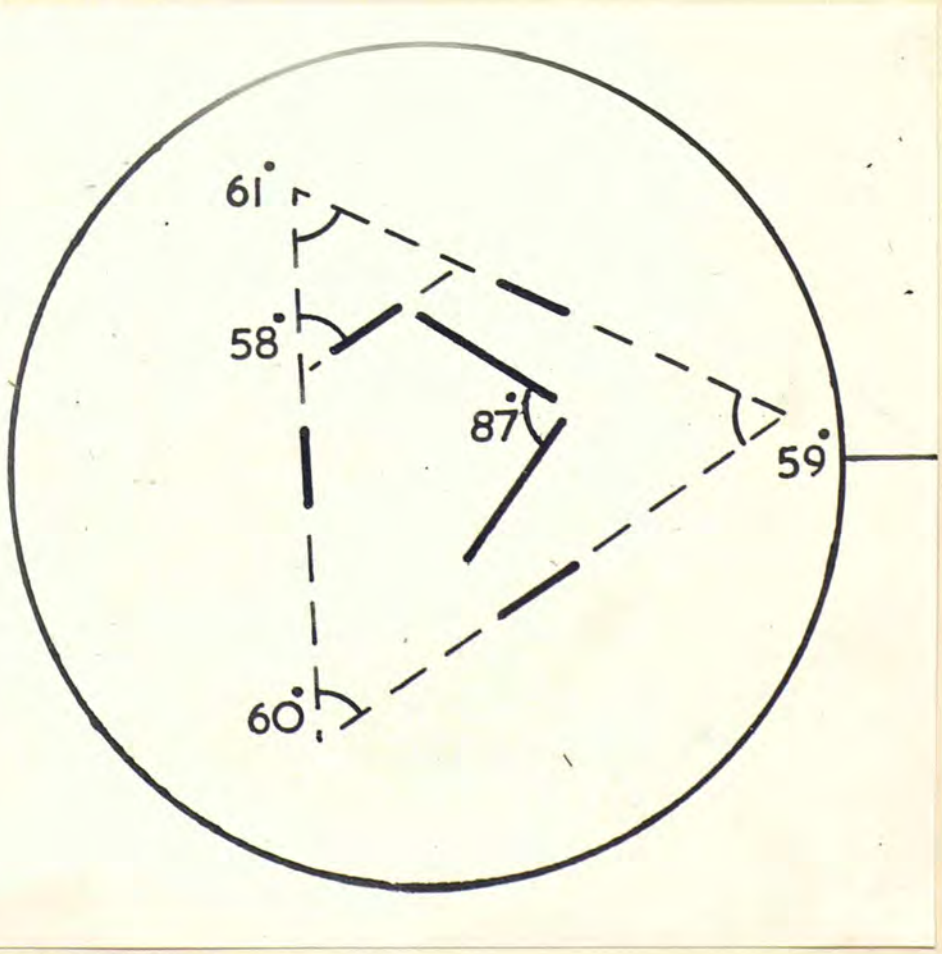


Fig 116

increases. The maximum load in both tests was 30 kgm., and by observing through the crystal the corresponding area of contact was seen to be the same in both cases, .0245 mm. whence for both surfaces, the maximum applied real average stress was 1.2 x 10" dynes/sq.cm. This compares with a real average stress of 1.1 x 10" dynes/sq.cm. necessary for initiation of cracking on the octahedral face by the tungsten carbide 1 mm. ball. Thus, it is clearly seen that the octahedral face is less resistant to pressure cracking than the other two faces: it is also to be noted that in spite of an increase in load of from 16 kgm. up to 30 kgm., the resulting stress has increased relatively little owing to the deformation of the ball.

10.6 Discussion

It has been seen that, contrary to what was previously expected, diamond can be cracked by static impact of a sphere, the material of which is considerably weaker than diamond itself: it is also shown that the octahedral face is more vulnerable to this cracking than the dodecahedral or the cubic faces. The pressure figure produced on the octahedral face at a load of 16 kgm. by the 1 mm. diameter Tungsten Carbide ball, required a minimum average stress of 1.1 x 10" dynes/$cm^2$ - the critical area of contact being 0.0142 sq.mm. For the same Octahedral face, the diamond ball impactor of 0.78 mm. diameter produced cracking at a real

average stress of 1.4 x $10^{11}$ dynes/sq.cm. for both the primary pressure figure and the primary crack of the multiple figure, the critical areas of contact being 0.0036 and 0.0025 sq.mm. and the loads 5 kgm. and 3.5 kgm. respectively (see Chapter 5). It would appear from a comparison of the above data that, as the scale of the experiment was increased, the strength of the surface decreased; remembering that this is based upon only three pressure crack tests; it may be hazarded that it is due to a strength-area relationship similar to that found for glass in analogous experiments.

Although the actual stress necessary to initiate the cracking in this experiment was less than in the previous tests, the consequent disruption, both inside and on the surface of the crystal was considerably more: it is obvious from an examination of the photographs (Figs.55 and 104) that the internal disturbance has increased, and it can be seen from the calibrations (Fig.111) of the white light fringe patterns that the height displacements on the surface are twice as much as obtained previously. This is explainable by taking into account for the last test a greater energy release once cracking is initiated, due to the release of the potential energy stored in the elastically deformed tungsten carbide ball. It is because the diamond ball is much more resistant to elastic deformation, that cracking in the former tests occurred at considerably lower loads - the stress being already high due to the small areas of contact through lack

of deformation.

In the series of photographs taken for this last test, four circular areas of contact can be seen for four progressively increasing loads of 3, 9, 16 and 20 kgms, from these, the respective radii of the circles of contact can be measured. Hertz has shown (1881) that in the case of isotropic elastically deforming materials, there should be proportionality between the cube of the radius of the circle of contact and the corresponding load applied (see Chapter 1). Fig.117 shows a graph of the cube of the radius against the load for the four pairs of values mentioned above. It is seen that near the origins this is approximately linear but that it increasingly curves away from linearity for larger loads. This non-linearity may be due to the anisotropy of the diamond but is more likely due to the onset of non-elastic deformation in the tungsten carbide ball.

The deformation of the ball for the impact experiment has been described in section 10.4, where it is shown conclusively that not only has the tungsten carbide ball elastically deformed on impact, but that it has by no means recovered - considerable plastic deformation having occurred at the tip, over a region nearly twice as large as the maximum area of contact attained in the test (the radii of the circular areas being approximately 0.1 mm. and 0.075 mm. respectively). The only explanation that can be given for the lines detected on this tip microscopically, is derived from the fact that

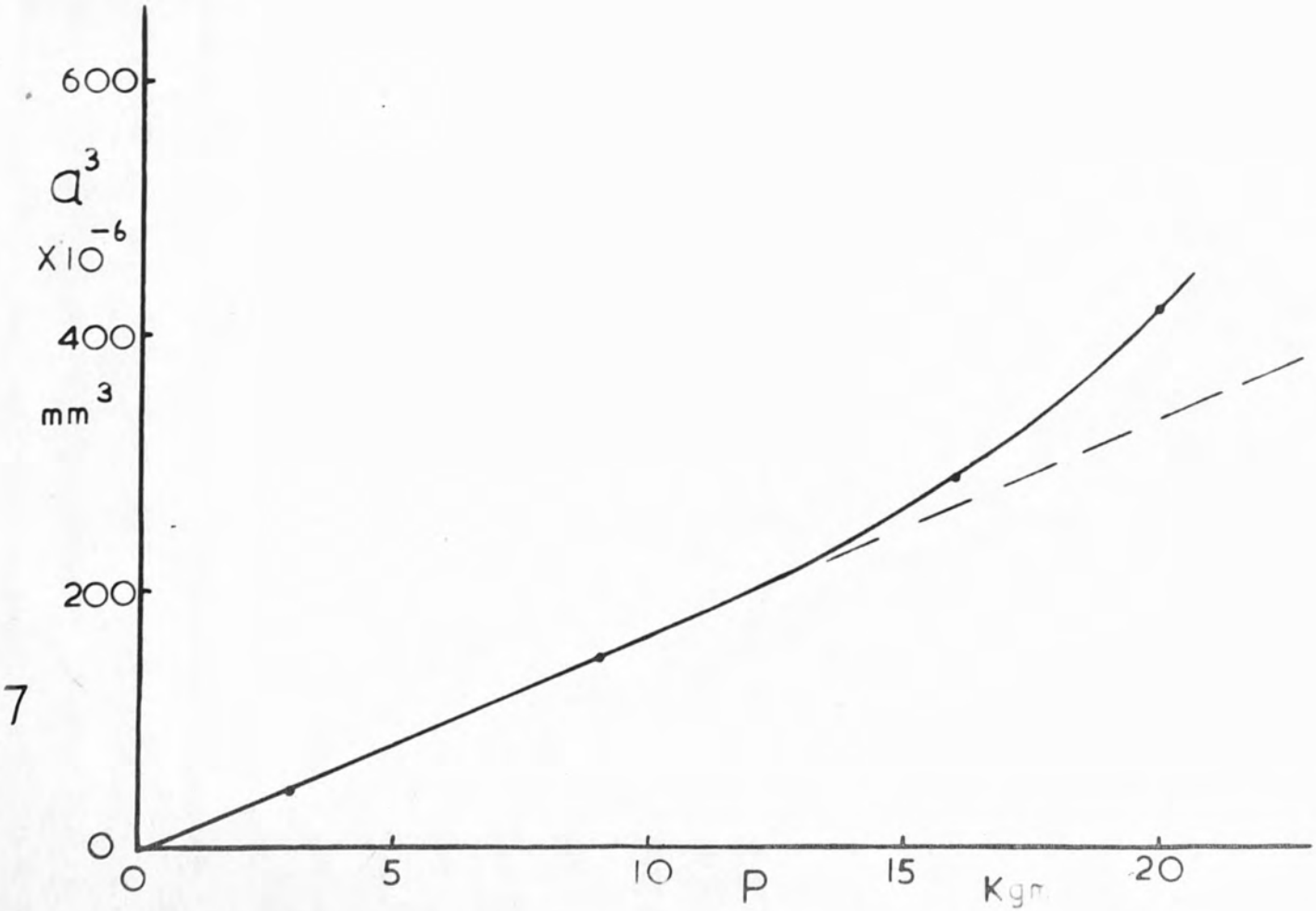


Fig 117

four of them occur approximately along four sides of a hexagon; it is possible that at the initiation of the cracks on the diamond face, the edges of the cracks, which are elevated above the surface when the ball has been removed (as indicated by the fringe patterns) press upwards violently onto the surface of the ball, thus marking the flattened region with lines forming an approximate outline of the crack figure. This is suggested tentatively, and does not explain the other two straight lines clearly seen on the face of the ball.

## 10.7 The Three Types of Internal Disruption

Finally there remains the three types of internal disruption; two of these have been discussed fully in Chapter 5 for the earlier impact tests done on the Octahedral face. The three dark shadows opposite three alternate sides of the hexagon pressure figure have been explained as cleavage crack developing along (111) planes going down into the crystal at an angle of $70^{\circ}\ 32'$ to the surface away from the region below the pressure figure. It is to be noted that this explanation is reinforced by the observation that when the last shadow area finally developed to the extent of the other two, a distinct crack sound was heard. In addition, it can be seen in Fig.100 that for each crack line occurring along each of these three sides, there is a separate and distinct shadow area. Thus for the shadow-area-side on the left of the photograph there are three distinct areas,

these can be correlated with a side of the pressure figure with three edges; the first crack that formed has developed most and deepest, the second is above this in the crystal and can be seen within it in extension, the third dark area has spread from the last crack to initiate, and has progressed least, being above the other two in the body of the crystal: the section for just this side of the pressure crack is shown schematically in Fig.118.

The irregular sets of curving line cracks seen in the body of the crystal running approximately parallel to the other three sides of the hexagon figure have been explained as non-crystallographic shock fracture cracks - analogous to the hackle marks found on the conchoidal fracture surfaces of glass and other brittle materials. This leaves the third type of internal cracking shown clearly in Fig.100, where it is seen to occur opposite the set of alternate sides of the hexagon where the dark shadow regions do not occur. These crack lines appear to be crystallographic as can be seen in Fig.105 where they are represented schematically.

It is thought that these lines indicate interrupted cleavage cracks. It has already been shown (Chapter 5) that the three sides marked C in Fig.105, represent intersections of cleavage planes (111) with the surface which go down and away from the hexagon into a region where the tensile stress is likely to be high (according to Hertz),

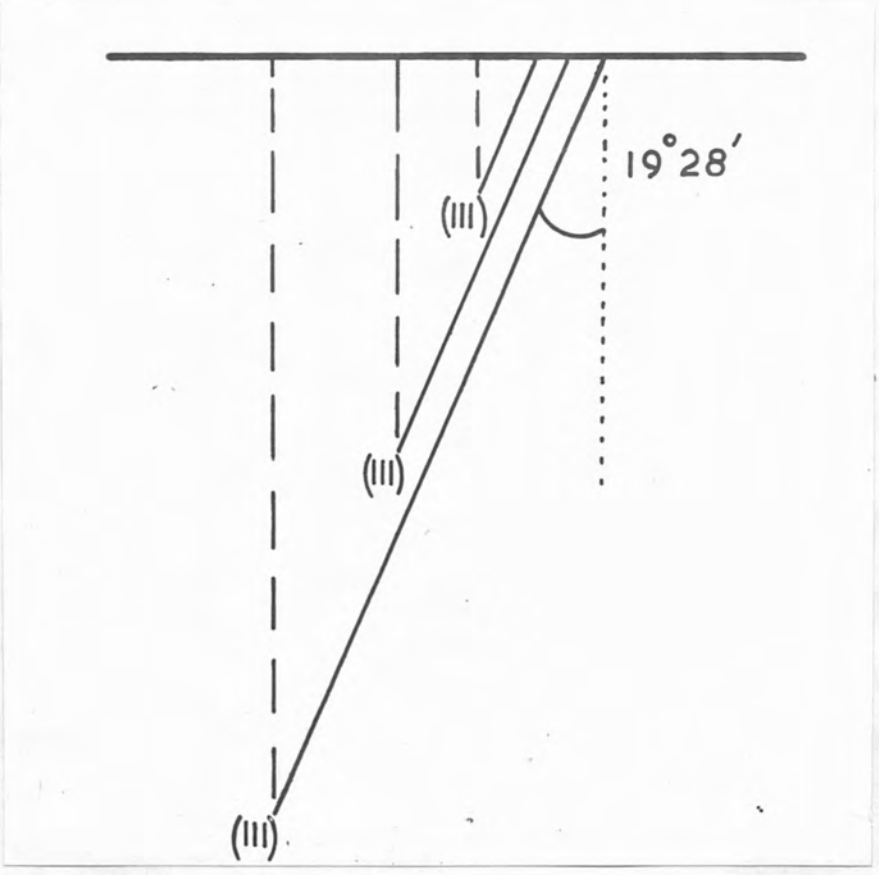


Fig 118

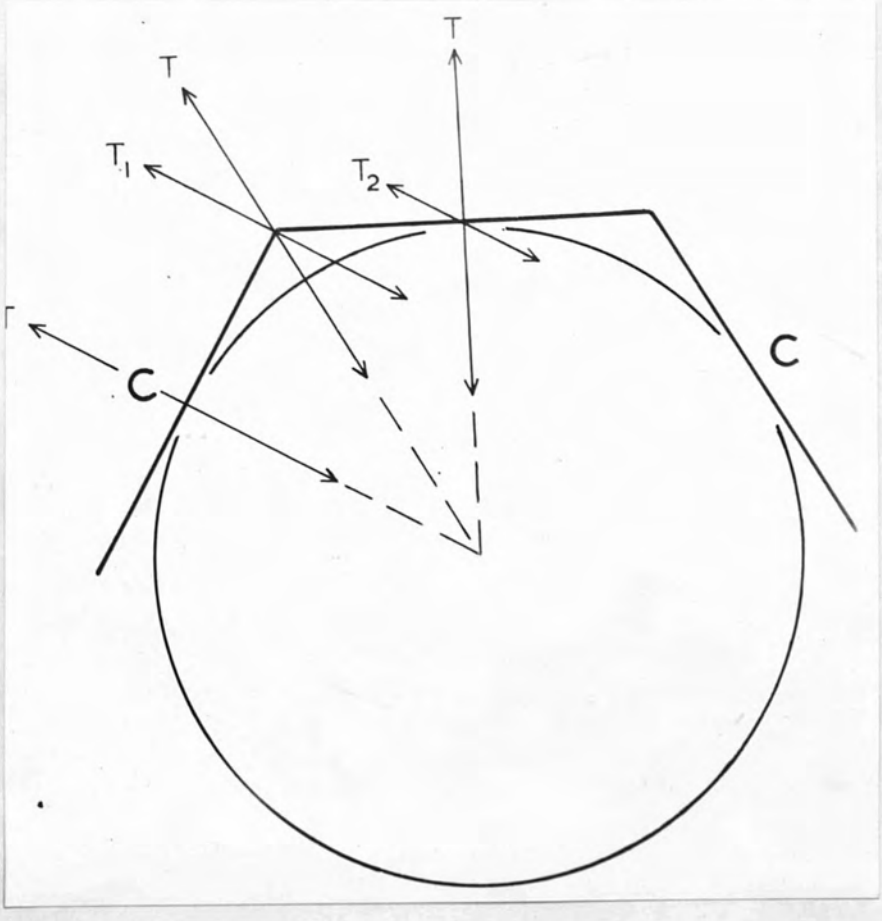


Fig 119

whereas the other three sides represent intersections of (111) planes with the face, which go down and inwards towards an axis passing vertically through the centre of the hexagon, into a region where tensile stress is rapidly decreasing. Outside the hexagon on these three sides, there is high tensile stress acting normal to the tangent of the circle of contact (i.e. along the radii from the centre) but no convenient cleavage. Now suppose for a load P the tensile stress acting normal to the hexagon edges at sides C in Fig.105 is T; as the load is increased a critical value is reached when the stress T becomes equal to the critical stress $T'$ (which has component perpendicular to the cleavage plane equal to the cleavage stress), and then cracking developes from these sides. The stress T exists all the way round the circle of contact but there are no appropriate cleavage planes for the other three alternate sides. However, for these sides, the stress T does have components normal to the adjacent sides C of the hexagon - which are lines of intersection of the two cleavage planes meeting the face. These components vary from a maximum of $T_1 = T \cos 30^\circ$ at approximately the ends of the sides, to a minimum of $T_2 = T \cos 60^\circ$ at the centre (see Fig.119). If upon cracking the stress release is so great that $T \cos 30$ becomes equal to $T'$ then secondary cleavage will start inside the crystal in the regions of both ends of the side at points such as a in Fig.105. The cracks will spread

in the directions (a b) parallel to the two adjacent C - sides, and will meet at (b) before they have had much opportunity to spread in depth. Once they meet the two cracks will spread no farther in these directions - and will become inhibited ,forming a 'V' shaped crack with vertex pointing away from the side. The mechanism will be repeated forming another 'V' shaped crack deeper in the body of the crystal and further away from the hexagon, in the direction where the tensile stress decreases least rapidly from the maximum value. In this way it is proposed that a whole series of these pairs of cracks are formed when the violent stress release occurs at the initiation of cracking. Each pair will occur one after another in quick succession forming a whole series of 'V' shaped cracks with the apices pointing away from the side, and the whole process is operating simultaneously for all three alternate sides where no dark shadows appear.

The cracks themselves seem to be localized cleavages, extending straight in ⟨110⟩ directions to where they intersect , but having very little depth, although what there is, is in (111) cleavage planes. However, the surfaces, within the crystal, containing these secondary cracks are not necessarily crystallographic, but are disposed in accordance with the complicated stress field existing beneath an octahedral crystal face on which a sphere is being pressed. In general, these surfaces will follow the directions in which the tensile stresses decrease least rapidly from the

maximum value which is found around the perimeter of the circle of contact; which means that they will be in directions going away from the hexagon figure and down into the crystal. These surfaces are not necessarily planes, but may be curving surfaces similar in shape to a segment of a Hertzian cone found in the equivalent problem for glass.

This phenomena, described as interrupted cleavage or crystallographic shatter may be actually localized micro slip occurring at successive cleavage planes as the cracking extends into the crystal, shattering where it cannot cleave in one plane. Whatever this phenomena really is (the explanations given are only tentative), it completes the internal disruptions going into the crystal from around the perimeter of the circle of contact on the surface. Together with the pure cleavage cracking extending from the other three alternate sides, these two types of disruptions give for impact on the Octahedral face of diamond, the equivalent of the Hertzian cone developing from the surface ring crack found for impact on glass.

In conclusion it is to be noted that there is an important observational difference between the two types of internal disturbances discussed above. The pure cleavage cracking is visibly reversible, the crack closing up when the load is removed, the dark shadows disappearing (the crack of course, has not joined up but only closed up). The interrupted cleavage cracks, however, are equally visible

with and without load, no change in disposition occurring as load is removed. The process of shatter, by which they are produced, is an irreversible process.

# CHAPTER XI

# CONCLUSIONS

## 11.1 Introduction

In each of the Chapters describing the experimental work done a discussion of the results obtained has been included at the end.

This Chapter attempts to give a full summary of the conclusions, which can be drawn for the various branches of the research, and their significance in the particular field of physics concerned.

## 11.2 Ring Crack Phenomena on Glass

It has been seen that for the well known Hertzian ring cracks formed on glass by static impact tests, there are accompanying surface distortions which have not been previously detected. These distortions have been measured quantitatively and for a primary ring crack extend to a height of the order of 1000 A above the undisturbed surface, the corresponding volume displaced above the surface being dependant upon the size of the ring crack, i.e., the size of the impacting sphere (for the experiments described this volume was of the order of $10^{-9}$ cc.). For multiple ring cracks the distortion characteristically repeats itself at each crack, and for dynamic impacts just producing a ring crack, the distortion has a height of the same order.

The significance of these surface distortions is that they would seem to indicate a micro-plastic flow of glass at room temperatures (both the pile up around the crack and the critical depression found for multiple cracks indicate this). The material having elastically deformed under pressure has been unable to recover after the stress release formation of cracking. The mechanism of this irreversibility has been clearly seen to be dependant upon the stress release, since complete recovery does take place if the stress is small enough, the crack becoming invisible on release of load. This micro-flow of glass is to be compared with that found by Taylor (1949) in micro indentation experiments: with very small loads Taylor formed perfect pyramid indents on glass, and it was suggested in the discussion on another of his papers (1950) that there may be a type of viscous flow occurring. It may be that the mechanism mentioned above is due to a sudden local temperature rise occurring upon initiation of a ring crack with the consequent stress release.

If a ring crack does not form until the applied stress is very large, then it has been seen that there is a probability of complete fracture occurring from the region of the local ring crack. This occurs violently and the familiar 'hackle' marks, associated with fractured glass, have been observed on the extensions of the Hertzian cone surface which are obtained on fracture.

It has already been noted in Chapter 4 that the preferential etching occurring at invisible ring cracks on glass throws light upon initial etching phenomena occurring on natural octahedral faces of diamond.

## 11.3 The Study of Ten Types of Optical Glass

The study of ring crack phenomena on these different glasses has been seen to give information on both their fracture-strength properties and their elastic properties. It is seen that indentation hardness measurements obtained by Taylor conform with the elastic properties of the glasses whilst surface hardness measurements by abrading, conform with the fracture strength properties.

It is seen, in comparisons, that some glasses (BSC and HC) are good in both of the above properties whilst others are low in both (DEDF and DF). Also, other glasses (MBC, TF and ELF) are good in one of the properties but bad in the other. These results are obviously of importance when it comes to choosing a glass for a particular use.

In the Appendix, a method of measuring surface hardness by abrasion is described. The determination of the Surface Hardness Value $(1/\lambda)$ gives further information as to the respective wear-characteristics of the different glasses. The values obtained are empirical because of the large number of constants for the apparatus which are involved; however they do illustrate relative differences in glasses

where the variations in hardness are comparatively small.

This method of measuring surface hardness has been used on other materials including thin electro platings of different thickness.

11.4 Pressure Figures on Diamond faces

Pressure crack figures, equivalent to ring cracks on glass, have been produced under controlled conditions on the Octahedral, Dodecahedral and Cubic faces of diamond. The accompanying internal and superficial distortions have been fully investigated.

On the Octahedral face, perfectly formed hexagon cracks were obtained, the shape and the accompanying surface distortion of which were very similar to those of some natural features found on naturally occurring Octahedral faces. This completely substantiates the conjecture made by Tolansky and Halperin (1954), following from the investigation of ring cracks on glass by Tolansky and Howes (1954), that the observed features are in fact pressure or percussion marks.

Pressure figures formed on Cubic faces, of which no evidence has been reported before were squares; while those produced on Dodecahedral faces were hexagons, one pair of sides of which were less perfect than the other sides. The shapes and orientations of the figures, formed on all the diamond faces impacted, conform with the lines of inter-

section of crystallographic {111} planes with each face; and it has been shown for the octahedral and the truncated cubic face the cracking has actually occurred along these {111} planes, in a form of localized cleavage.

The mechanism of the production of these cracks is seen to be a compromise between, the fracturing under maximum tensile stress occurring around the perimeter of the circle of contact proposed by Hertz (1881) for ring cracks on isotropic brittle materials, and the cracking along existing preferential easy cleavage {111} planes obtained in the case of anisotropic brittle crystals. Thus a crack figure is formed on a diamond face around the perimeter of the area of contact during impact but the directions of cracking conform to the crystal structure of the diamond.

The study of the surface distortions accompanying the pressure crack figures shows that these are very similar to the disturbances found on the surface of glass around ring cracks. There is a smooth rise of the material up above the undisturbed level towards the crack from the outside, a discontinuity occurring at the crack to zero level or a depressed level over the central area of the crack figure. The smoothness of this rise of the pile up strongly indicates a micro-plastic flow; this smoothness is seen particularly clearly in the interferograms showing profiles of sections lieing just outside the crack figures. No evidence has

yet been found for micro-slip on the surface in the pile up regions. Further evidence for micro-plastic flow in diamond is found in the existence of distinct depressions of the level within the central area of multiple crack figures produced which have been detected, there has been no detection however of any curvature of this central surface, even where the depression is considerable. Also it has been described how the diamond ball, on being damaged by the formation of a pressure crack figure on its tip, was found to have been flattened slightly, the radius of curvature at the tip being larger than it was previously - another indication of plastic flow.

This indication of micro plastic flow in diamond is an unexpected conclusion, and if correct, clearly has an important bearing upon both the abrading and the wear characteristics of diamond and upon its technological use as a lathe cutting-tool. Another point of technological importance is the establishment of the possibility of forming cracks on diamond using impactors of material considerably weaker than diamond; so far this has been achieved only on the Octahedral face but it is hoped that similar results will be obtained on the other two faces in subsequent experiments with a spherical impactor of even smaller diameter than that already used.

## 11.5 Quantitative Results for Diamond

The numerical data derived from the experiments on

diamond are collected together in Table 4.

Considering real stresses, from the Tungsten Carbide ball experiment, it is seen that the Octahedral face has a resistance some five times greater than glass, for which the critical average stress under identical conditions, is in the order of 200 - 250 kgm/sq.mm. Also it is to be noted that for tests using the diamond ball, the resistance of the truncated cubic face to cracking is approximately two and a half times that for the natural Octahedral face.

Considering nominal stresses, which are less reliable quantitatively, it may be taken that Octahedral faces are least resistant to cracking, and that the truncated two point dodecahedral face is more resistant than the truncated girdle cubic face. The natural cubic face seems more resistant, but this was a boart stone, full of inclusions, and its face may not be representative of natural cubic faces.

It was found experimentally that the more resistant the face, the more the disruption when cracking did finally occur, due presumably to the greater stresses involved. In the case of the Tungsten Carbide ball and diamond ball tests on the Octahedral face however, it was found that the former caused much greater disruption than the latter, although the real critical average stress at cracking was lower (1.1 x 10" dynes/sq.cm. compared with 1.4 x 10" dynes/sq.cm.) This has been discussed in Chapter 10 and it is concluded

TABLE 4

| Face of Diamonds and Type of Stone | Spherical Impactor Used and diameter | Load for different cracks formed in kgm. | Circular area of contact at cracking x $10^{-6}$ sq.cm. | Area of the Crack Figure x $10^{-6}$ sq.cm. | Average Stress x $10^{8}$ dynes/sq.cm. REAL .Load at first crack applied: Circular area of contact. | Average Stress x $10^{8}$ dynes/sq.cm. NOMINAL Max.Load applied: Greatest surface crack area |
|---|---|---|---|---|---|---|
| Octahedral face of Octahedral Stone | Diamond 0.78 mm. | primary crack at 5 | 35 | 44 | 1.4 | 1.1 |
| " " | " | primary crack at 3.5 increased up to 12 | 25 | 87 | 1.4 | 1.3 |
| " " | Sapphire 1.0 mm. | - | - | 55 | - | - |
| " " | Tungsten Carbide 1.0 m. | primary crack at 16 increased up to 30 | 142 | 261 | 1.1 | 1.1 |
| Dodecahedral face of Octahedral Stone | Diamond 0.78 mm. | 7-10-13-24-24 | - | 46-51-80 196-131 | - | 1.8 |
| Cubic face of Cubic Stone after polishing | " | 20-26-30-30 | - | 108-119-140-161 | - | 2.0 |
| Cubic face of Octahedral Stone | " | 29 | 86 | 210 | 3.3 | 1.4 |

that the greater disruption is probably due to the greater stress release, once cracking is initiated, due to the release of the potential energy stored in the elastically deformed tungsten carbide ball. The diamond ball, elastically deforming very little, reaches a higher stress at a much lower load and there is less potential energy to be released after cracking is initiated.

This does not explain why the critical stress in the later test was less than that found using the Diamond ball. However it is noteable that the second pressure figure is very much bigger than the first and this may indicate that the strength of the surface, found experimentally, depends upon the scale of the experiment (analogous to the strength-area relationship well known in strength of glass testing). It has already been seen in Chapter 6 that the hexagonal pressure figures formed on the Octahedral face are initiated from one point - which thus must be weaker than surrounding points on the surface; and in the discussion in this Chapter it was tentatively concluded that there may be localized weaknesses over the surface (analogous to the Griffith cracks for glass) due to vacant-surface-sites in the crystal lattice or possibly due to the surface manifestation of sessile dislocations on the crystal.

This leads to a theoretical aspect. In the Introduction of Chapter 1 there is given a determination of the theoretical

value of the critical average stress for initiation of a pressure crack figure on an octahedral face of diamond. This is only a very approximate determination as many assumptions are made, however the value comes out to be $2.1 \times 10^{13}$ dynes/sq.cm; as compared with the value of $1.4 \times 10^{11}$ dynes/sq.cm. found in the experiments using the diamond ball impactor. Thus for the formation of a crack figure of approximately $3 \times 10^{-5}$ sq.cm. in extent, the experimental value of stress required is about 150 times less than the approximate theoretical value of the strength.

It is seen above, that there are three points which indicate a distribution over the diamond octahedral surface of some type of localized weakness.

## 11.6 The Internal Disruptions for Diamond

Three types of internal disturbance occur during the formation of a pressure crack figure on diamond and the consequent cracking into the material. There is the pure cleavage cracking which occurs along crystallographic $\{111\}$ planes meeting the impacted surface. This goes down into the crystal away from the region below the surface crack figure, and is observed experimentally as dark shadow areas. These shadow areas (three or four as the case may be) do not however always develop symmetrically, some spread quicker and farther than others - again due presumably to local variations in strength. It is clearly seen in the experiment on the

octahedral face where a multiple pressure figure was formed using a tungsten carbide ball that, from the three alternate sides at which the shadow areas occur, there is a separate shadow area developing from each surface crack, forming the multiple crack,on these sides.

The irregular sets of curving line cracks seen in the body of the crystal are described as non-crystallographic shock-fracture cracks occurring as a shock wave passes through the crystal. They are most clearly seen for the pressure figure produced on the truncated cubic face but are quite distinct also, surrounding the multiple figures formed on the octahedral face. Unlike the cleavage cracking the mechanism here is irreversible, the crack lines being easily detected within the crystal after the load has been completely removed. They occur in those regions where cleavage cracking does not occur.

The third type of internal disorder has only been detected for the regions surrounding the hexagonal figure formed on the Octahedral face by the impact of the tungsten carbide ball. Similar to the other type of line cracks, this type is irreversible and occurs opposite the other three alternate sides of the hexagon figure as opposed to the three sides at which cleavage cracking occurs. It is distinctly crystallographic in origin occurring in short straight lines orientated parallel to the directions on the surface of the intersections of $\{111\}$ planes with the

surface; and the possibilities have been mentioned of interrupted cleavage or localized micro-slip, occurring at successive cleavage planes. The mechanism has been discussed tentatively, but at length, in Chapter 10. In connection with the possibility of micro-slip, it is seen that there is strong contrast between the damage produced finally on the diamond ball impactor and that produced on the sapphire ball. In the former case a pressure figure was formed on the surface with no sign of external slip, while for the latter it was quite clear that multiple slip had occurred extensively.

It seems probable that a fourth type of internal disturbance has occurred for the pressure crack figures formed on the natural cubic boart stone. Here and nowhere else, it is found in measuring the surface distortions, that the volume of the central area depression is greater than the volume-amount of the surrounding 'pile up'. This stone was quite opaque being full of inclusions and cracks, and it is concluded that there was a localized crushing of the material beneath the crack figure, at the stress release upon initiation of cracking - so that the material in this region was compressed into a smaller volume.

Finally, it is to be emphasised that there is a very large scale magnification in the vertical direction for the profile sections obtained, which means that the surface distortions recorded here are indeed only micro-effects.

Thus it is noteable that what may at first be thought to be an insignificant surface defect, turns out to have associated with it a considerable volume of internal damage. These observations clearly have an important bearing on the failures which occur when diamonds are used as lathe-cutting tools.

## 11.7 Further Work

This completes an investigation of pressure cracking phenomena on glass and diamond. But there are several avenues of possible research extending from this study.

It would be interesting to see whether any of the characteristic properties of diamond, such as absorption, X-ray and Counting properties, alter locally for regions where a pressure crack figure has been formed on the surface.

When the diamond stones used are no longer needed intact, then some will be etched to study the characteristics of etching in regions containing crack figures on the different diamond surfaces, others will be impacted to complete fracture if possible, so that a study may be made of the resulting fracture surfaces.

It is hoped in the future, to make an electron microscope study on the surface distortions under high lateral magnification, obtainable with this instrument.

Finally, impact phenomena on further crystalline materials may be studied. Some preliminary experiments

have already been done on Quartz, where static impact cracking occurs not by cleavage, but by twinning in crystallographic directions.

# APPENDIX A

## A METHOD OF MEASURING SURFACE HARDNESS

### A.1 The Abrading Method

The method followed is that first used by Chalmers (1941) of dropping particles of abrasive onto the surface under examination, through an orifice of constant diameter and down a tube of fixed size. In essence, it is a statistical effect - a large number of minute indents being made on the surface layer-analogous to the well known indentation methods for bulk hardness of metals. The principals of this type of abrading are fully discussed in Chalmers paper, where he applies the technique to the measuring of the hardness of thin electro plating and of the surfaces of metals, which have been treated in many different ways.

The method was extended to plastics and glass by Starkie (1942) using the same technique but employing carborundum particles instead of the rounded silica-sand particles used by Chalmers for metals; this work was mainly on plastics. The method is empirical owing to the large number of constants of the apparatus used.

In the experiments carried out, a graded Carborundum powder was used, the particles of which had an average diameter of 0.4 mms. This powder was dropped down a vertical glass tube of diameter $\frac{1}{2}$" and length 100 cms., through an orifice at the top, of $\frac{1}{8}$" diameter. These conditions allowing for steady

downward flow of the particles as they emerged from the tube, although of course, they are still accelerating under gravity. The specimen was tilted at an angle of 45° to the vertical so that once the particles had impinged on the surface, they rebounded away from it and did not strike a second time. For each test, an elliptical abrasion area was obtained on the surface, and these appeared as can be seen in Fig.120 for glass (afterwards silvered) having had quantities of 100 - 150 - 300 - 600 gms. of Carborundum dropped upon it. Such areas of abrasion were examined microscopically, and their appearance can be seen in Figs.121, 122, 123, 124, 125 and 126, showing the different amounts of action for weights of carborundum dropped of 10, 20, 50, 100, 300 and 600 grammes respectively - all on glass which was silvered afterwards. It will be observed that the pits are irregular in shape,and that their number increases with increasing weight dropped; however for each test the action is seen to be quite even over the area considered.

A.2 The Optical Measurement

The method employed by both Chalmers and Starkie for measuring the effect of the abrasion on the surface, was to measure the decrease in the specular reflection or transmission. Chalmers used a null method for obtaining the value of the specular reflection by balancing out the current from two photocells, one of which collected the reflected light from the

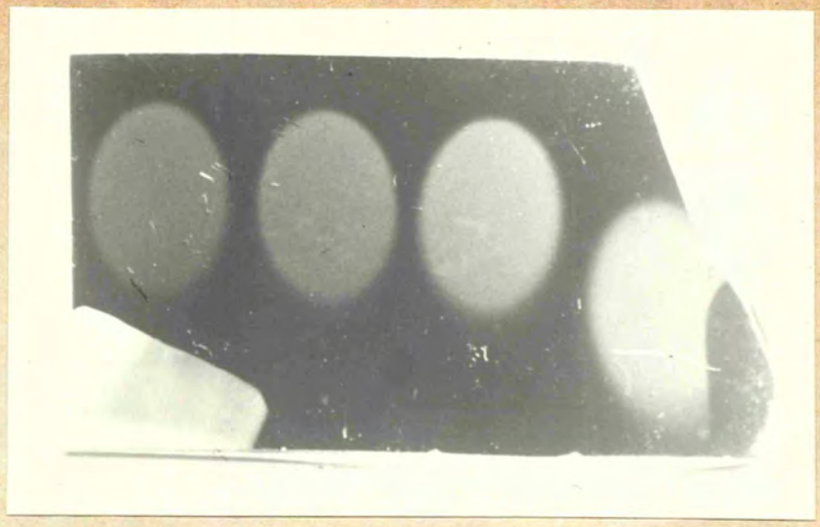

Fig 120 x 1

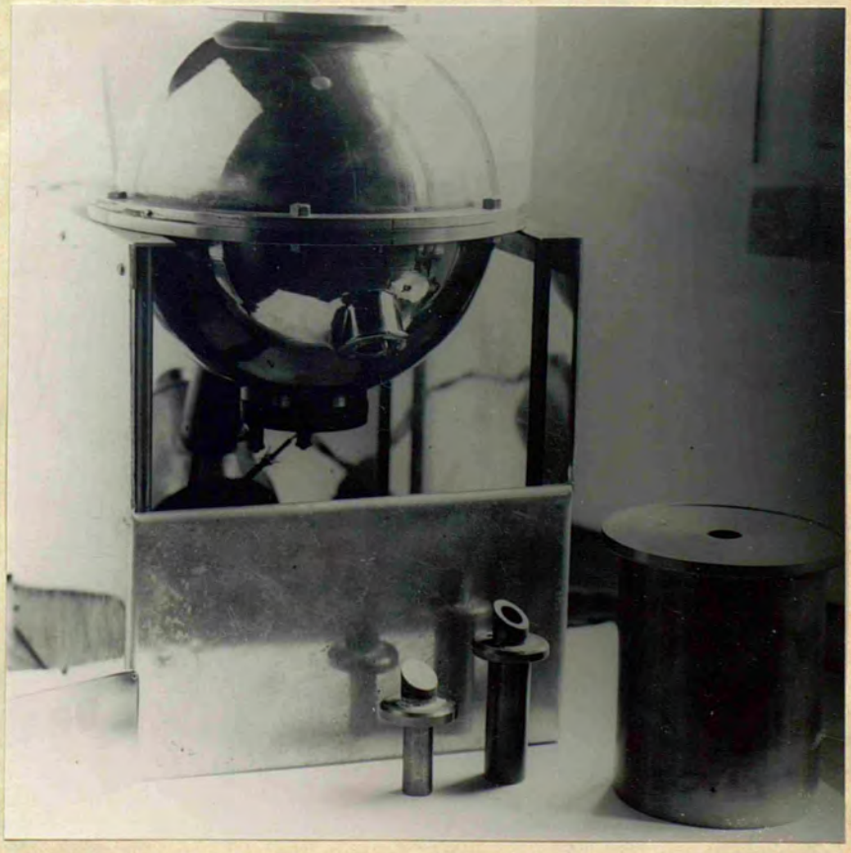

Fig 127 x $\frac{1}{4}$

Fig 121
X 220

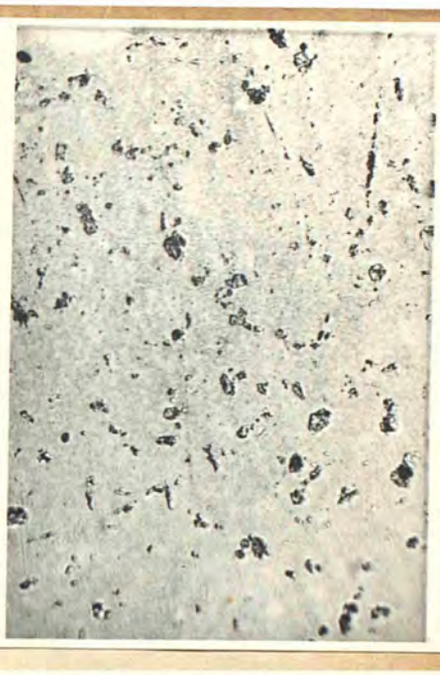

Fig 122
X 220

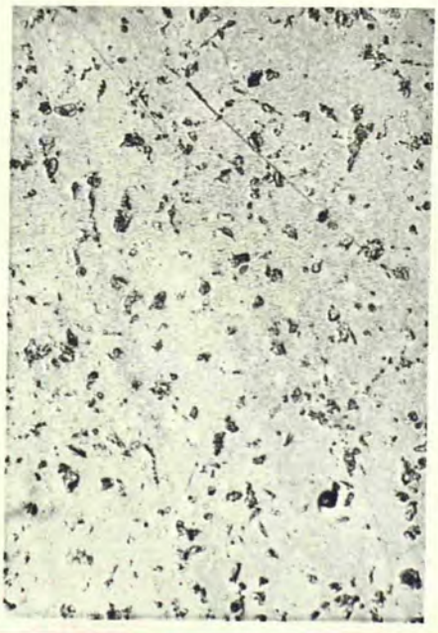

Fig 123
X 220

Fig 124
X 220

Fig 125
X 220

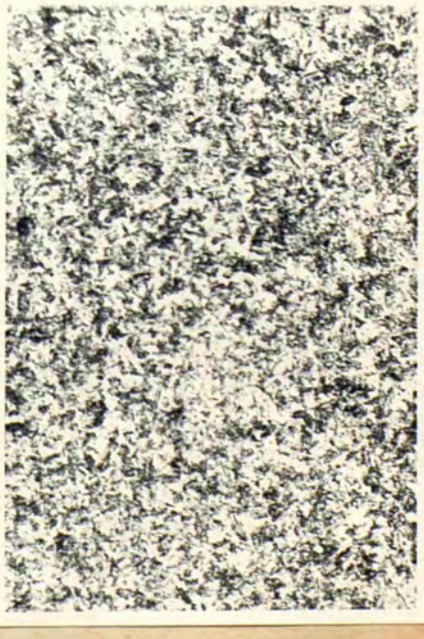

Fig 126
X 220

surface,originating from a constant light source. He measured the effect by finding the ratio of the specular reflection, after dropping a known weight of abrasive, to that of the unabraded surface; he took as a measure of the surface hardness, that weight of sand particles in grammes required to reduce this ratio to 0.5.

It was thought more accurate to measure the change in the diffuse reflectivity as well as that for the specularly reflected light, so as to obtain a ratio of the specular to the total reflectivity and measure the change in this quantity as the abrasion proceeded. To a first approximation, this ratio depends only on the smoothness of the surface, being independant of its colour or absolute reflecting power.

An integrating sphere optical smoothness meter was devised by Guild (1940) to measure this ratio; and the instrument used, in conjunction with the abrasion method of these surface hardness experiments described, was based upon Guild's instrument although made with some slight modifications. This is seen in Fig.127: and the design is shown diagrammatically in Fig.128. A is the lamp housing and optical system, from which a beam of light is directed onto the specimen surface placed at C - the filament of the lamp is approximately focussed on the specimen and the aperture iris diaphragm is exactly focussed at the place E. The lamp is supplied with a constant voltage from accumalators. B is the sphere (diameter 7") the interior of which was first electroplated with tin-nickel, then

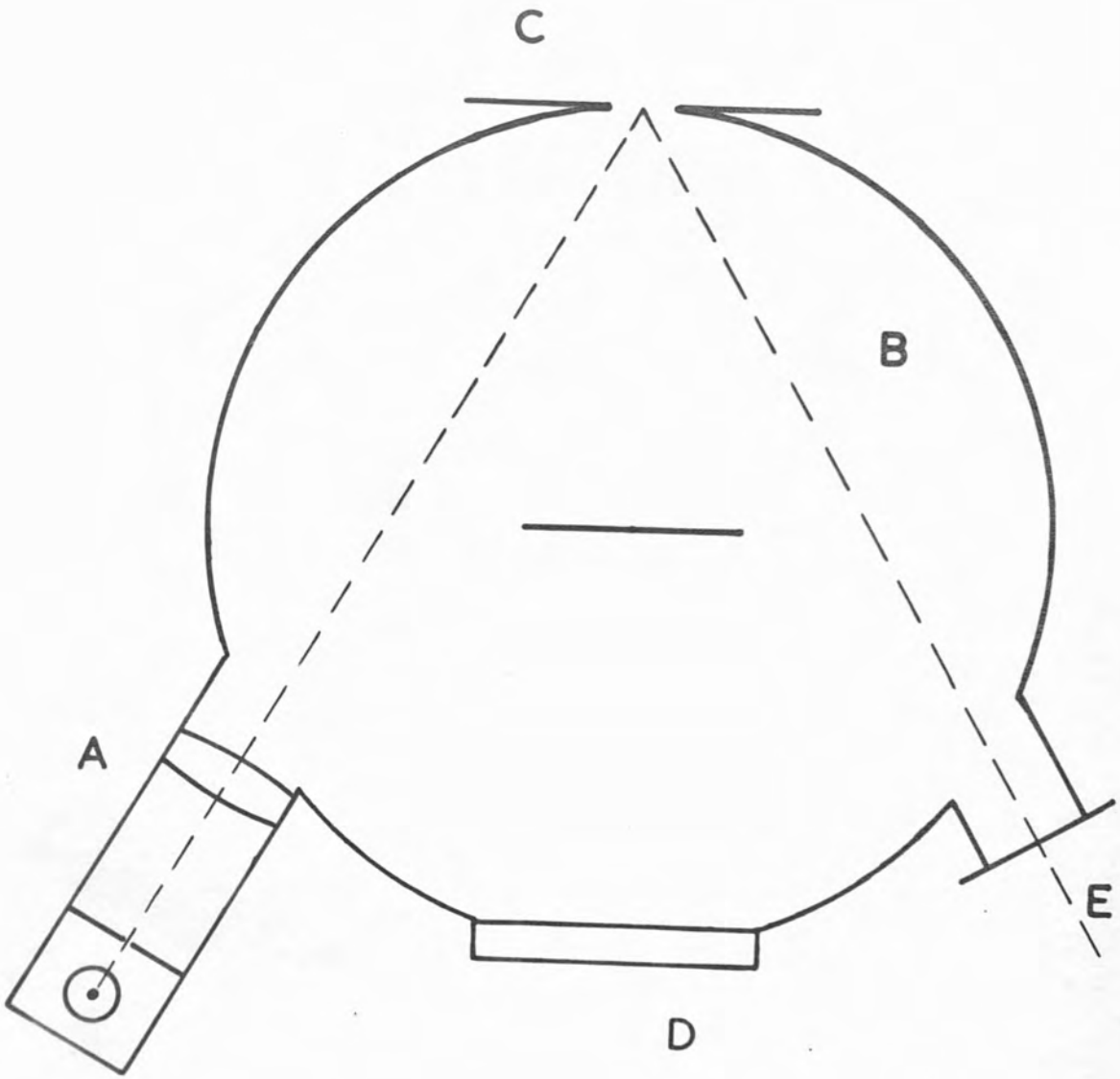


Fig 128

polished and coated with a smoked-on magnesium oxide film - which has effectively 100% diffuse reflectivity. In the centre of the sphere is a white disc to prevent direct illumination from reaching the photocell D - a barrier larger type connected to a Tinsley moving coil galvanometer, whose deflections give the value of the light intensity integrated onto the photocell by the sphere. C is the specimen table, the aperture over which the specimen surface is put, being 1.5 cm. diameter. E is the recieving aperture on the sphere, where the specularly reflected light from the plane specimen surface is recieved either by a magnesium oxide white disc, which scatters the light throughout the sphere so that it is integrated and thus measured, or by an efficient light trap placed at E so that the specular light is completely absorbed, the sphere then only measuring that light which has already been scattered on reflection at the specimen surface.

With this instrument, by replacing one of the fitments described above by the other (they are both seen in Fig.127) two readings are quickly obtained for the total and diffuse reflectivities of the surface placed on the aperture at C. From these readings, after applying some calibration corrections (including zero corrections using the big light-trap seen in Fig.127), a value is easily obtained for the ratio of the specular to the total reflectivities $(S/T)$ .

The instrument is very sensitive and will detect very small changes in surface structures which are quite

undetectable to the eye, it is particularly sensitive in the region of high reflectivities; which is the reason why in making measurements on abraded glass surfaces, these were first silvered.

A.3 Preliminary Experiments

The constants of the abrading apparatus taken as standard were chosen largely because of convenience. Providing the height of the tube is great enough to allow the stream of particles to spread out to the full cross section of the tube and to give a steady flow at the bottom, the tube can be of any length: 100 cm. was chosen. If the outlet orifice is too large a very uneven action is produced, $\frac{1}{8}$" was chosen which gave an even flow which did not last for an excessive time. Tests were done for variation of the angle of incidence of the falling particles on the surface, 100 gms. being dropped on a glass surface tilted at different angles. This was silvered, and the $(S/T)$ ratio of each patch measured by the integrating sphere instrument - the resulting graph of $(S/T)$ against angle is shown in Fig.129. It is seen that the effect of the 100 gm. of carborundum is very small for large angles (the $(S/T)$ ratio being still high), and increases as the tilt approaches the horizontal; however, as the horizontal is approached the rebounding particles tend to interfere with those still falling so that the increase in the effect falls off and the graph curves. The angle of 45° was chosen because, from the graph, it gives a considerable effect at a place

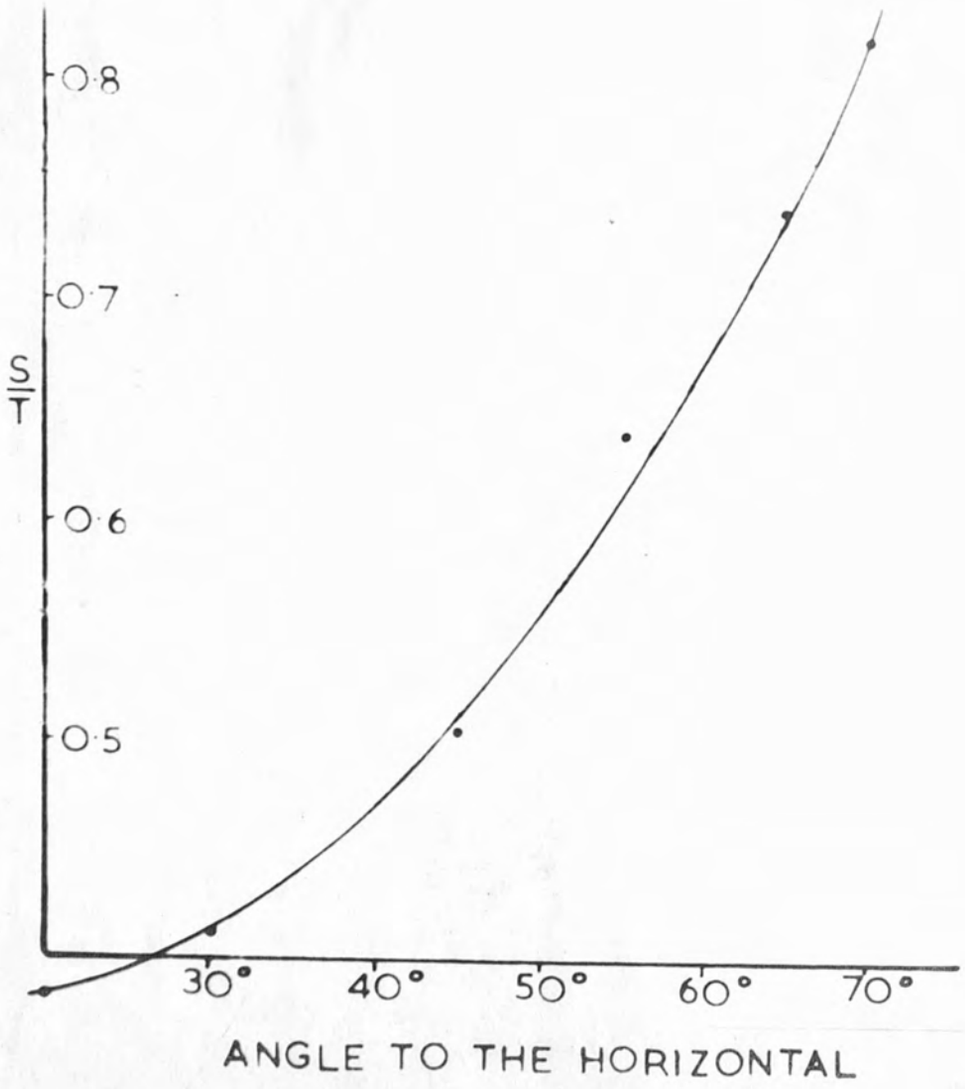


Fig 129

where the graph is still linear.

It was found after a large number of tests made with this apparatus, that there was a wearing effect on the carborundum particles used; these being found to be smaller on average after use on various materials such as steel, hard electro platings and different glasses. Thus the powder used should be changed at intervals over a period of testing - the interval depending upon the amount of use of the powder.

Finally in the preliminary tests, a series was done for different amounts of carborundum dropped on specimens of brass (4), glass (1 and 2), and an electro plating of speculum on brass (3). For each a graph was drawn of $(S/T)$ against weight dropped, and in the case of glass there are two graphs, one for measurements made on the abraded patches after the glass had been silvered (1), the other made before silvering (2). These graphs (1 2 3 4 ) are shown in Fig.130. It is noteable from the two glass graphs, that where the glass has been silvered the value of $(S/T)$ is greater at all points than for the unsilvered glass, which shows that the silver layer is smoother than the glass surface beneath, i.e., the laying down of a silver film does tend to reduce the roughness of the surface or the prominence of irregularities.

## A.4 Analysis of the Method

The theory of the abrasive action of dropping different amounts of abrasive particles onto a surface is given fully by Chalmers. Briefly, it can be seen that a given quantity

of abrasive should change a proportion, fixed for a given material, of the surface from its initial state to a final state. This condition, if it holds, leads to a logarithmic relationship.

The data for the graphs of Fig.130 are plotted logarithmically in Fig.131 (log $(10^{S/T})$ against weight dropped) where it is seen that the first part of all four graphs are linear, but that each curves away from the straight line, to flatten out for large amounts of carborundum dropped - this has been found to be the case in all tests made. Thus up to a critical value of the amount dropped (Wc) the logarithmic relation is seen to hold, while after that, deviation occurs due to secondary effects of saturation of the surface distortion, or possibly of work - hardening of the surface layer by the excessive abrasion.

From these graphs, it can be seen that in general :-

$$\log (10^{S/T}) = -\lambda W + K \qquad \text{providing} \quad W < W_c$$

thus $$\log (S/T)_1 / (S/T)_2 = \lambda (W_2 - W_1)$$

or $$\log (S/T)_0 / (S/T)_\omega = \lambda \omega = \log \sigma_\omega$$

where $\sigma_\omega = (S/T)_0 / (S/T)_\omega$ represents a measure of the change wrought by dropping w gms of carborundum on the abraded surface. Now the surface hardness (SH) will be a function of this quantity, the weight of carborundum dropped, and the constants of the abrading apparatus, so that with these remaining constant throughout all tests $SH = f(\sigma_\omega, \omega)$

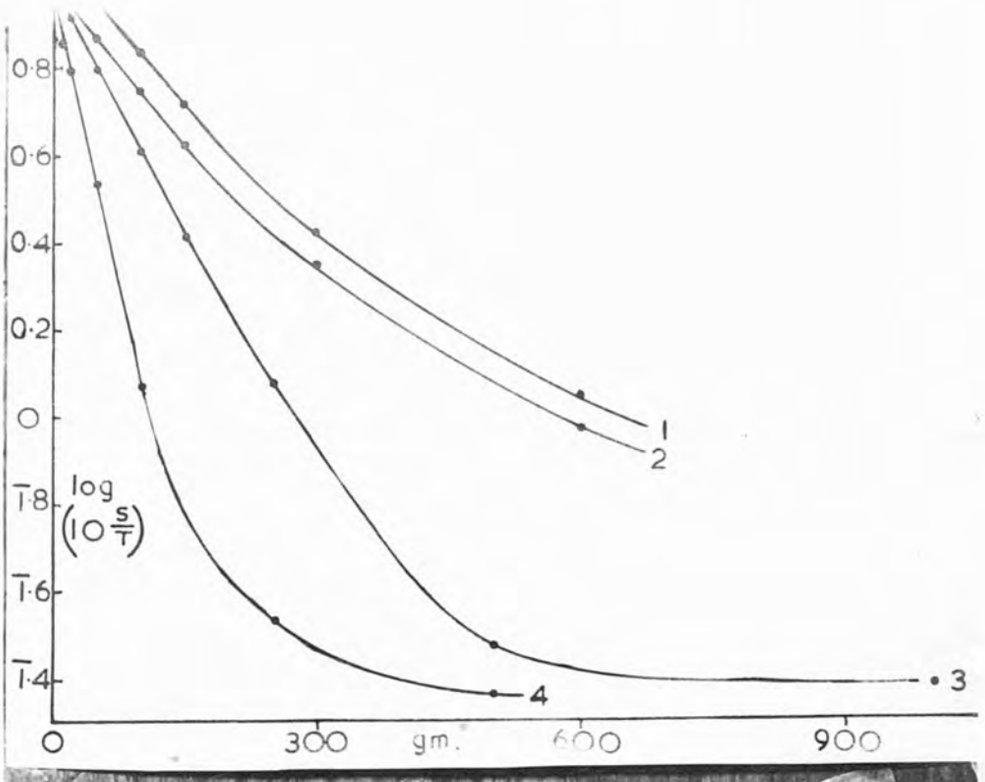


Fig 131

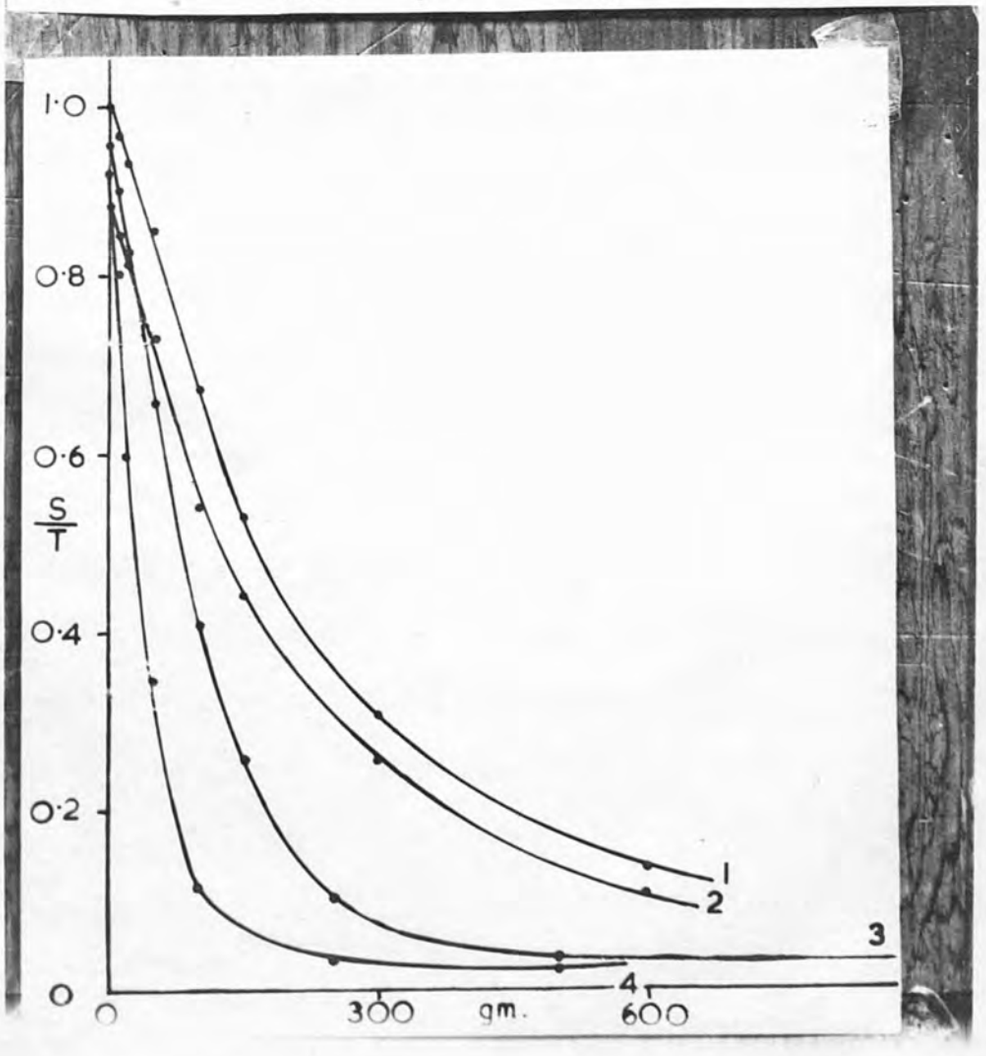


Fig 130

To obtain a measure of the surface hardness one could take a standard weight of carborundum dropped and then measure the different values of $\sigma_\omega$ for the different specimens. This is unsatisfactory however because for a very soft material the value of W appropriate for hard material, may give near-saturation of disruption on the surface, in which case for a slightly softer or harder material no measurable difference in the (SH) value would be obtained. It is a considerable improvement to have a surface hardness measurement which is independent of the load, and for this reason the value of $\log \sigma_\omega/\omega = \lambda$ is considered.

This is the slope of the straight line part of the graph of $\log (10^{S/T})$ against W, examples of which are seen in Fig.131. On inspection, it is seen that the surface hardness (SH) will be in some way inversely proportional to the value of $\sigma_\omega$ - hence it may be stated that :

$$(SH) \propto f(1/\lambda)$$

which is independant of the weight dropped (W) providing $W < Wc$. Thus a measure of the surface hardness property of any specimen considered is obtained by evaluating the quantity $(1/\lambda)$ and this value is taken as the surface hardness. It can be obtained from a minimum of two tests on the surface for different values of W (both less than Wc for the material of the surface), but is most accurately obtained by a series of tests and the plotting of the graph of $\log (10^{S/T})$ against W.

By this method the values of the surface hardness of brass, speculum electro plating, and the soft plate glass already used, are calculated from the graphs of Fig.131 as :-

| | | |
|---|---|---|
| $\left(\frac{1}{\lambda}\right)$ | Brass | 115 |
| $\left(\frac{1}{\lambda}\right)$ | speculum | 265 |
| $\left(\frac{1}{\lambda}\right)$ | glass | 450 |

the quantity is given as just a number, although dimensionally it is a weight. From the graphs for silvered and unsilvered glass it is seen that the slopes are the same within experimental error, which indicates that silvering does alter the hardness measurement, although it does slightly increase the $\left(\frac{S}{T}\right)$ values.

A.5 Results for Ten different types of Optical Glass

Ten different chemically composed glasses (from Chance Brothers Ltd. catalogue) were abraded and the abrasions were measured, the compositions of the glasses are in Table 1 found in Chapter 5 where the letter-symbols, by which reference is made to different glass are also found.

The values obtained for $\left(\frac{1}{\lambda}\right)$ for each glass are given below in order of 'surface hardness' :-

| Glass | $\left(\frac{1}{\lambda}\right)$ |
|---|---|
| BSC | 665 |
| HC | 625 |
| TF | 565 |
| ZC | 555 |
| MBC | 550 |

| | |
|---|---|
| ELF | 530 |
| BF | 480 |
| LF | 470 |
| DF | 445 |
| DEDF | 435 |

In considering these results the interest lies in the relative positions of the glasses in the hardness table and in comparing this table with tables giving results for other types of physical hardness and strength tests. Such comparisons are fully investigated and discussed in Chapter 5; it is only to be noted here that there is found better correlation between these results and those for the ring crack strength tests, than between these results and those for micro indentation hardness measurements - this indicating that for glass at least the abrasive action is more akin to cracking and chipping, than to micro-plastic deformation under impact.

The method of measuring the surface hardness described is also being used in connection with hard electro-platings of speculum and tin nickel of varying thicknesses. It has been shown that, in strong contrast to parallel experiments on measuring the micro indentation hardnesses of these electro-platings for varying small indentation loads, the surface hardness method is quite independent of the thickness of the plating.

## REFERENCES

Auerbach, F., Full Summary appears in Horestadt (1902) "Jena Glass" (Macmillan).

Bailey, J., (1939) Glass Ind. Jan - April.

Bennett, Jupnik, Osterburg and Richards,(1951) "Phase Microscopy" (J.Wiley & Sons).

Bhagavantam and Bhimasenacher,(1945) Proc.Roy.Soc.A 187,381.

Bragg, W.H. and Bragg, W.L., (1913) Proc.Roy.Soc. A 89,277.

Brossel, J. (1947) Proc.Phys.Soc. 59,224.

Chalmers,B.(1941) J.Inst.Met. 67, 295.

Champion, F.C. (1953) Proc.Roy.Soc.A 220,1143.

Griffith,A.A. (1920) Phil.Trans.Roy.Soc. A 221, 163.

Guild,J. (1940) J.Sci.Inst. 17, 178.

Hamy,M. (1906) J.Phy.Radium. 5, 789.

Harkins,W.D. (1942) J.Chem.Phy. 10,268.

Haward,R.N. (1949) "The Strength of Plastics and Glass" Cleaver-Hume).

Hertz, H. (1881) English translation of Miscellaneous Papers (Macmillan 1896).

Holden,J. (1949) Proc.Phy.Soc. B 62,405.

Inglis,C.E. (1913) Trans.Inst.Naval Archit. 55 pt.I,219.

Kuhn,H. (1951) Rep.Prog.Phy. 14,64 (The Physical Society).

Mohs,F. (1822) "Grundriss der Mineralogie" (Dresden).

Omar,M., Pandya,N.S., and Tolansky,S. (1954) Proc.Roy.Soc. A 225,33.

O'Neill,H.(1934) "The Hardness of Metals and its Measurement" (Chapman & Hall).

Orowan,E. (1948-9) Rep.Prog.Phys. 12, 185. (The Physical Society).

Pandya,N.S. and Tolansky,S.(1954) Proc.Roy.Soc.A 225,40.

Preston,F.W.(1926) J.Soc.Glass Tech.10, 236.

Preston,F.W. (1945) J.Am.Ceram.Soc. 28,145.

Raman,C.V. (1920) Nature 104, 113.

Raman,C.V. (1926) J.Opt.Soc.Amera. 12, 387.

Ramaseshan,S. (1946) Proc.Ind.Acad.Sci. A 24 No.1, 114.

Robertson,R., Fox,J.J. and Martin,A.E. (1934) Phil.Trans.Roy. Soc. A 232, 482.

Schmaltz,G. (1936) Tech.Oberflachenkunde (Berlin).

Schubnikow,A and Zinserling,K (1932) Zeits.f.Krist 83,243.

Schuler,M. and Dimpker,A. (1935) Zeits.f.Inst.55,63.

Smekal,A. (1927) Ann.Phys.Lpg. 83, 1202.

Smekal,A.G. (1953) Acta Phy. Austriaca 7 No.1, 110.

Starkie,D. (1942) J.Soc.Glass Tech. 26, 130.

Taylor,E.W. (1949) J.Sci.Inst. 26 No.9, 314.

Taylor,E.W. (1950) Trans.Soc.Glass Tech. 34, 69.

Timoshenko,S. (1934) "Theory of Elasticity" (McGraw-Hill).

Tolansky,S. (1944) Phil.Mag. 35, 120 and 175.

Tolansky,S. (1945) Proc.Roy.Soc. A 184, 51.

Tolansky,S. (1946) Proc.Roy.Soc. A 186, 266.

Tolansky,S. (1948) "Multiple Beam Interferometry" (Oxford).

Tolansky,S. (1951) Z.Electrochemie 56, 263.

Tolansky,S. and Halperin,A. (1954) Proc.Phy.Soc.B 67, 473.

Tolansky,S. and Howes,V.R. (1954) Proc.Phy.Soc.B 67,467.

Tolansky,S. and Howes,V.R. (1955) Proc.Roy.Soc. In print.

Tolansky,S. and Omar,M. (1953) J.Sci.Inst. 30, 337.

Wilks,E. (1952) Ph.D. Thesis, London University.

Williams,A.F. (1932) "The Genesis of Diamond" (Benn).

Willott, W.H. (1950) Trans.Soc. Glass Tech. 34, 77.

Zenicke,F. (1934) Physica 1, 689.

ACKNOWLEDGEMENTS

I wish to express my thanks to Professor S.Tolansky F.R.S. my supervisor, for his interest, advice and encouragement throughout the course of this work. Thanks are also due to my colleagues for helpful discussion and assistance from time to time, and particularly to Dr.A.R.Verma for valuable criticism in the preparation of the M.S. I also wish to thank the laboratory staff for their considerable help in the construction of apparatus used in the research.

I am indebted to the London County Council for a maintenance grant for the first year and to the Department of Scientific and Industrial Research for a grant for the two following years which enabled the work to be carried out.

The glass specimens used were kindly given by Chance Brothers Ltd. and by Dr.E.W.Taylor, and I am grateful to the Industrial Diamond distributors for the supply of diamonds. The diamond ball used in the main experiments on diamond was prepared by Mr.P.Grodzinski of Industrial Diamonds (Sales) Ltd.